Recrystallization Textures in HCP Metals

Thesis submitted in partial fulfilment

of the requirementsfor the degree of

Doctor of Philosophy

in

Metallurgical and Materials Engineering

by

Surjyakant Panda

(Roll Number: 512MM1005)

based on research carried out

under the supervision of

Prof. Santosh Kumar Sahoo

and

Prof.Subash Chandra Mishra

December, 2016

Department of Metallurgical and Materials Engineering

National Institute of Technology Rourkela

Metallurgical and Materials Engineering
National Institute of Technology Rourkela

December 20, 2016

Certificate of Examination

Roll Number: *512MM1005*
Name: *Surjyakant Panda*
Title of Thesis: *Recrystallization Textures in HCP Metals*

We the below signed, after checking the thesis mentioned above and the official record book(s) of the student, hereby state our approval of the thesis submitted in partial fulfilment of the requirements of the degree of *Doctor of Philosophy in Metallurgical and Materials Engineering* at National Institute of Technology Rourkela. We are satisfied with the volume, quality, correctness, and originality of the work.

Subash Chandra Mishra Co-Supervisor	Santosh Kumar Sahoo Principal Supervisor
Ashok Kumar Mondal Member (DSC)	SyedNasimulAlam Member (DSC)
Alok Satapathy Member (DSC)	External Examiner
SudiptaSen Chairman (DSC)	Subash Chandra Mishra Head of the Department

Metallurgical and Materials Engineering
National Institute of Technology Rourkela

Santosh Kumar Sahoo

Assistant Proffessor

Subash Chandra Mishra

Professor

December 20, 2016

Supervisor's Certificate

This is to certify that the work presented in the thesis entitled *Recrystallization Textures in HCP Metals* submitted by *Surjyakant Panda*, Roll Number *512MM1005*, is a record of original research carried out by him under our supervision and guidance in partial fulfilment of the requirements of the degree of *Doctor of Philosophy in Metallurgical and Materials Engineering*. Neither this thesis nor any part of it has been submitted earlier for any degree or diploma to any institute or university in India or abroad.

Subash Chandra Mishra
Professor

Santosh Kumar Sahoo
Assistant Professor

Dedication

This thesis is dedicated to my parents; the reason of what I become today, thanks for your continuous support and intensive care, and to my beloved wife for her advice, encouragement, and faith.

This honorable work is a symbol of my love to you.

Surjyakant Panda

Declaration of Originality

I, Surjyakant Panda, Roll Number 512MM1005 hereby declare that this thesis entitled "Recrystallization Textures in HCP Metals" represents my original work carried out as a doctoral student of NIT Rourkela and, to the best of my knowledge, it contains no material previously published or written by another person, nor any material presented for the award of any other degree or diploma of NIT Rourkela or any other institution. Any contribution made to this research by others, with whom I have worked at NIT Rourkela or elsewhere, is explicitly acknowledged in the dissertation. Works of other authors cited in this thesis have been duly acknowledged under the section "References". I have also submitted my original research records to the scrutiny committee for evaluation of my thesis.

I am fully aware that in case of any non-compliance detected in future, the Senate of NIT Rourkela may withdraw the degree awarded to me on the basis of the present dissertation.

December 20, 2016 *Surjyakant Panda*

NIT, Rourkela Roll Number- 512MM1005

Acknowledgement

I sincerely thank my supervisors, Prof. Santosh Kumar Sahoo and Prof.Subash Chandra Mishra for guiding me into this research field and for their constant help, encouragement, and endless support on my research work. Their care and enlightenment strengthen every progress in this work.

I would like to express my profound gratitude to Prof.Upendra Kumar Mohanty for his valuable suggestions in several occasions during my research work. I would like to acknowledge the Metallurgical and Materials Engineering Department, National Institute of Technology (NIT), Rourkela for providing me various facilities throughout my research work. I would also like to acknowledge texture laboratory, Department of Metallurgical and Materials Engineering, NIT, Rourkela for providing me texture measurement facilities.

Special thanks should be given to Prof. Satyam Suwas at Indian Institute of Science (IISc), Bangalore, for his enriching ideas and fruitful discussions. This research work was partially funded by the Department of Science and Technology (DST) (Grant No. SR/FTP/ETA-0029/2011 dated 08/05/2012) and UGC NRC-M of IISc, Bangalore, which is greatly acknowledged.

I am grateful to Materials Science Engineering Department, IISc, Bangalore, for providing rolling and texture measurement facility also to several members of the department. Specifically thanks go to Dr. Rama KrushnaSabat for his guidance and assistance during my research work.

I am deeply indebted to Prof.IndradevSamajdar at Indian Institute of Technology (IIT), Bombay, for his valuable suggestions and guidance in several occasions during my research program. I would also like to thank Prof.Prita Pant for helping nanoindentation measurement at Department of Metallurgical Engineering & Materials Science., IIT Bombay.

All the members of OIM & Texture Laboratory, Department of Metallurgical Engineering and Materials Science, IIT, Bombay, are greatly acknowledged for allowing

me to use texture measurement facility. My hearted thanks go Dr.Gulshan Kumar and Mr.ParthaBiswas for their kind help and assistance to running the EBSD/OIM facility.

During my Ph.D work, I am very much grateful to my friends especially BibhuduttaBishoyi, BikashRanjanParhi and HimanshuSekharMaharana for their kind care, selfless help, and the deep friendship. I did extremely enjoy working with them all.

Finally, I wish to express my hearted appreciation to my family. Their deep love, understanding, constant support and encouragement over the years are the great impetus to my study.

December 20, 2016 *Surjyakant Panda*

NIT, Rourkela Roll Number. 512MM1005

Abstract

Recrystallization texture developments and their importance in relation to mechanical properties of commercially pure titanium (cp-titanium), pure magnesium and pure zinc have respectively been investigated in the present study.

CP-titanium plates were subjected to unidirectional-rolling (rolling), accumulative roll bonding (ARB) and cross-rolling followed by annealing at 600^{o}C for a large range of soaking time starting from 10 s to 30 min. The samples were seen to develop almost similar texture when annealing was carried out beyond 5 min of annealing time. The initial $(11\bar{2}5)<1\bar{1}00>$ texture present in the deformed structure got strengthened during annealing of the samples under investigation. Further, $[11\bar{2}5]$ fibre texture was observed in the samples at higher annealing times (> 10 min). It was further observed that the hardness of the grains close to basal orientation was higher compared to non-basal orientations and the estimated bulk mechanical properties of cp-titanium had a direct relationship with the volume fraction of basal grains/orientations.

Pure magnesium was subjected to cold (cross-) rolling and hot rolling of 90 % reduction in thickness. Cold rolled samples were then subjected to annealing at 200°C for a range of soaking times staring from 10 s to 30 min. A dominant basal texture was observed in the samples. It was also observed that pure magnesium had lower grain size, grain orientation spread, grain average misorientation and volume fraction of basal orientations when cold (cross-) rolled and annealed, compared to the hot rolled condition. It was further observed that an increase in deviation from basal orientation decreased the hardness of an orientation and magnesium with higher volume fraction of basal orientations had higher hardness.

As-cast pure zinc was subjected to cryo-rolling of 90% reduction in thickness. The rolled samples were then annealed at 50^{o}C for different soaking times of 5 min, 10 min, 20 min and 30 min respectively. A dominant $<11\bar{2}0>$ fiber texture was observed in both rolled and annealed samples. Also $\{10\bar{1}2\}$ type compressive twins were observed in the samples and these twinning was found to be significant in all the samples. The Vickers hardness of the samples was increased till 10 min of annealing time followed by decreased in hardness on further increasing the annealing time.

Contents

List of Figures

List of Tables

Chapter 1

Introduction

Understanding of recrystallization or annealing texture is very important as annealing, the process of recrystallization texture developments in materials, is the final forming operation for many industrial/structural materials. These texturesare accountable for the anisotropy in mechanical properties of the material and will in many cases control the properties of the end productto a large extent. In cubic materials, such recrystallization textures have been well documented in the literature although no general acceptable mechanism for such texture developments have been reported [1-9]. However, in hexagonal materials the examination of recrystallization texture is very much limited compared to cubic materials [1, 2, 10, 11]. As a general rule, it has been well accepted that the recrystallization texture development in a material primarily dependent on the cold deformation texture that exists in the material prior to annealing [4, 12-18]. Keeping this in mind the present study (primarily) aimed at finding out the recrystallization texture developments in hexagonal metals subjected to large strains and/or different strain-paths. The present study also aimed at correlating the evolved recrystallization textures of the hexagonal metals with the mechanical properties of these metals. The second objective was being targeted because of the nature of these metals which are highly anisotropic.

Three hexagonal metals were selected, based on their relative c/aratios, for the present study: (1) Commercially pure titanium (c/a= 1.587, which is lower than the ideal c/aratio of 1.633), (2) Pure magnesium (c/a= 1.623, which is nearly equal to the ideal c/aratio) and (3) Pure zinc (c/a= 1.856, which is greater than the ideal c/aratio). Both titanium and magnesium are widely used as structural materials for their excellent mechanical properties [19-22]. However, zinc is widely used in galvanizing iron and steel products because of its superior corrosion resistance [23, 24]. These materials have been subjected to large strains and/or different strain-paths using a laboratory rolling mill, before annealing. Care has been taken to change/weaken the initial cold rolling texture wherever possible. For example, commercially pure titanium (cp-titanium) was cold rolled through accumulative roll bonding (ARB) as well as multi-step cross rolling (MSCR). ARBprocessing generallyincreases the initial strain level and hence increases the

colddeformation texture component in the material [25-27]. Whereas, MSCR can change the initial deformation texture in the material [28-31].

It has been well understood that mechanical properties of hexagonal materials can be regulated through texture control in these materials. Although this is valid for other materials also, but this has been widely exploited in hexagonal materials [32-36]. For example, pure titanium single crystals as well as polycrystalline titanium showed a decreasingYoung's modulus and shear modulus with increasing deviation fromexact basal orientations [37].In the present study, this has also been attempted to correlate the annealing texture developments with the mechanical properties of the hexagonal metals such as titanium and magnesium.

1.1 Objectives

a) ***Recrystallization texture in cp-titanium:***Plastic deformation of cp-titanium through cold rolling, ARB processing and cross-rolling to impose large amount of deformation as well as to modify the deformation texture before annealing. Annealing of the deformed samples at 600 ^{o}C for different soaking times to investigate the recrystallization texture developments in the material. Subsequently, a systematic micro-macro correlation of mechanical properties w.r.t orientations/textures of cp-titanium has been proposed through tensile testing, nanoindentation, X-ray diffraction (XRD) and electron back scattered diffraction (EBSD).

b) ***Recrystallization texture in pure magnesium:***Plastic deformation of pure magnesium through cold (cross-) rolling followed by annealing at 200 ^{o}C for different soaking times. Investigation of recrystallization texture developments in the material after annealing. Hot rolling of pure magnesium at 200 ^{o}C to compare the texture developments in the hot rolled and annealed samples. Exploitation of mechanical property of pure magnesium from orientation perspective.

c) ***Recrystallization texture in pure zinc:***Plastic deformation of pure zinc through cryo-rolling (rolling at liquid Nitrogen temperature) as pure zinc gets annealed at room temperature deformation. Annealing of the cryo-rolled samples at 50 ^{o}C for different soaking times. Investigation of textures in the samples after cryo-rolling

and subsequent annealing. The orientation dependent mechanical properties has not been proposed in this case as the structural application of pure zinc is limited as well as the experimental difficulties might be occurred because of low annealing temperature of pure zinc.

1.2 Framework of the Thesis

The present thesis has been divided into eight (8) chapters followed by references. Chapter 1 provides an introduction to the work of the thesis followed by main objectives of the thesis. In chapter 2, an extensive literature review has been provided. This chapter starts with the introduction of the materials used in the present work. Then the theory of recrystallization texture and the reported mechanisms of recrystallization texture developments have been provided. Subsequently, the recrystallization texture developments in hcp metals such as titanium, zirconium, magnesium and zinc have been reported. *Zirconium is an important structural material, extensively used in nuclear industries. This has also a c/a ratio of 1. 593 and is close to that of titanium. It has been believed that the thermo-mechanical processing behaviour of zirconium is equivalent to titanium and hence, this has not been used in the present thesis. However, the available literature on recrystallization texture developments in zirconium has been provided for the readers of this thesis.* Finally, chapter 2 ends with the available literature on orientation dependent mechanical properties of HCP (Hexagonal Close Packed) metals used in the present thesis. Chapter 3 explains the experimental details including the materials used, sample preparation and characterization techniques used in the present thesis. Chapter 4, 5 and 6 respectively provide the recrystallization textures observed in cp-titanium, pure magnesium and pure zinc with discussion of the recrystallization texture developments in these metals followed by conclusions. The orientation dependent mechanical properties of cp-titanium and pure magnesium have been provided in Chapter 7. Finally the work has been summarized in Chapter 8 which follows the scope for further research and the list of publications (in international journals and international/national conferences) published/communicated from the present work.

References

[1] F. Haessner, *Recrystallization of Metallic Materials*, Rieder-Verlag, Stuttgart, 1978.

[2] M. Hatherly and W. Hutchinson, *An Introduction to Textures in Metals*, Chameleon Press, London, 1990.

[3] M. Holscher, D. Rabbe and K. Lucke, Materials Technology, 62 (1991) p.567.

[4] S. H. Hong and D. N. Lee, Materials Science and Engineering A,351 (2003) p.133.

[5] T. Kamijo, A. Fujiwara, Y. Yoneda and H. Fukutomi, Acta Metallurgica, 39 (1991) p.1947.

[6] K. Lucke and M. Holscher, Textures and Microstructures, 14-18 (1991) p.585.

[7] Y. B. Park, D. N. Lee and G. Gottstein, Acta Materialia, 46 (1998) p.3371.

[8] I. Samajdar and R. D. Doherty, Acta Materialia, 46 (1998) p.3145.

[9] O. Engler and V. Randle, *Introduction to Texture Analysis Macrotexture, Microtexture, and Orientation Mapping*, CRC Press, New York, 2010.

[10] R. D. Doherty, Progress in Materials Science, 42 (1997) p.39.

[11] Y. N. Wang and J. C. Huang, Materials Chemistry and Physics, 81 (2003) p.11.

[12] N. Bozzolo, N. Dewobroto, H. R. Wenk and F. Wagner, Journal of Materials Science, 42 (2007) p.2405.

[13] R. J. Contieri, M. Zanotello and R. Caram, Materials Science and Engineering A, 527 (2010) p.3994.

[14] A. Etter, M. Mathon, T. Baudin, V. Branger and R. Penelle, Scripta Materialia, 46 (2002) p.311.

[15] X. Chen, L. X. Wang, R. Xiao, X. Y. Zhong, G. J. Huang and Q. Liu, Journal of Alloys and Compounds, 604 (2014) p.112.

[16] D. N. Lee, Scripta Metallurgica, 32 (1995) p.1689.

[17] Y. B. Park, D. N. Lee and G. Gottstein, Materials Science and Technology, 13 (1997) p.289.

[18] F. Wagner, N. Bozzolo, O. Van Landuyt and T. Grosdidier, Acta Materialia, 50 (2002) p.1245.

[19] G. Lütjering and J. C. Williams, *Titanium*, Springer-Verlag, New York, 2003.

[20] R. Boyer, G. Welsch and E. W. Collings, *Materials properties handbook: Titanium alloys*, ASM International, Materials Park, OH, 1993.

[21] H. Friedrich and B. L. Mordike, *Magnesium Technology: Metallurgy, Design Data, Applications*, Springer-Verlag, Berlin, Heidelberg, 2006.

[22] B. L. Mordike and T. Ebert, Materials Science and Engineering A, 302 (2001) p.37.

[23] X. G. Zhang, *Corrosion and Electrochemistry of Zinc*, Springer Science & Business Media, Berlin, 1996.

[24] A. Stwertka, *"Zinc". Guide to the Elements*, Oxford University Press, Oxford, 1998.

[25] Y. Saito, H. Utsunomiya, N. Tsuji and T. Sakai, Acta Materialia, 47 (1999) p.579.

[26] D. Terada, S. Inoue and N. Tsuji, Journal of Materials Science, 42 (2007) p.1673.

[27] S. Chowdhury, V. Srivastava, B. Ravikumar and S. Soren, Scripta Materialia, 54 (2006) p.1691.

[28] M. Rout, S. K. Pal and S. B. Singh, Cross Rolling: A Metal Forming Process in *Modern Manufacturing Engineering, Materials Forming, Machining and Tribology*, Springer International Publishing, New York, 2015, p.41.

[29] S. Suwas and N. P. Gurao, Development of Microstructures and Textures by Cross Rolling in *Comprehensive Materials Processing*, Elsevier Ltd., Amsterdam, 2014, p.81.

[30] X. Li, T. Al-Samman and G. Gottstein, Materials and Design, 32 (2011) p.4385.

[31] A. Bocker, H. Klein and H. J. Bunge, Textures and Microstructure, 12 (1990) p.103.

[32] U. F. Kocks, C. N. Tomé and H. R. Wenk, *Texture and Anisotropy: Preferred Orientations in Polycrystals and Their Effect on Materials Properties*, Cambridge University Press, Cambridge, 2000.

[33] B. Hutchinson, Materials Science and Technology, 31 (2015) p.1393.

[34] E. Merson, R. Brydson and A. Brown, Journal of Physics: Conference Series, 126 (2008) p.12.

[35] G. Nayyeri, W. Poole and C. Sinclair, Investigation Of The Local Mechanical Properties in Pure Mg Using Nanoindentation in *Mg2012: 9th International Conference on Magnesium Alloys and their Applications*, Vancouver, 2012, p.1325.

[36] B. Verlinden, J. Driver, I. Samajdar and R. Doherty, *Thermo-Mechanical Processing of Metallic Materials*, Elsevier Ltd., Amsterdam, 2007.

Chapter 2

Literature Review

This chapter has been divided into following three important sections to provide an extensive background for the readers.

i) A brief introduction of the materials used in the present study, namely Titanium (Ti), Magnesium (Mg) and Zinc (Zn): This includes the physical metallurgy of these materials along with their properties and applications for different components.

ii) Recrystallization texture developments: Reports on recrystallization texture developments in hexagonal metals are limited. Such texture developments and related mechanisms have been discussed first, and subsequently available literature on recrystallization texture developments in hexagonal metals has been discussed. As mentioned earlier, recrystallization texture developments in hexagonal Zirconium has also been included in this section.

iii) Finally, the role of texture/orientation on mechanical properties of the materials has been discussedfrom the available reports.

2.1A brief Introduction to Hexagonal Materials

2.1.1 Titanium (Ti)

2.1.1.1 Metallurgy of Titanium and its Alloys

Titanium was first discovered by W. Gregor in 1791 [1] and later in 1795 by M. H. Klaproth [1,2]. Titanium was first extracted by W.J. Kroll [3] who produced titanium from its ore by the non-vacuum process. This process involves the reduction of titanium tetrachloride with magnesium in an inert gas atmosphere. The commercial interest of titanium rises due to its low density, high strength, and excellent corrosion resistance. Titanium has been mostly used in aerospace industries [4-8] and structural works where strength to weight ratio is crucial [2,4,8,9] and also in corrosion resistance areas such as chemical industries [2, 8, 10].

Pure titanium has hcp (Hexagonal Close Packed) crystal structure (α-titanium) at room temperature which transforms to bcc (Body Centred Cubic) β-titaniumabove 882.5^{o}C [8, 11, 12]. The hcp unit cell of room temperature α-phase and β-phase along with the most densely packed lattice planes and parameters are shown in figure 2.1 [11]. The c/a ratio of α-titanium is 1.587 which is lower than the ideal c/a ratio of 1.633. Some alloying elements are added to pure titanium to alter the allotropic phase transformation [8, 12-15]. These alloying elementsare commonly known as alpha and beta stabilizers. The α-stabilizers increase the β-transformation temperature whereas β-stabilizing elements lower the β-transformation temperature. The most common α-stabilizers are aluminium (Al), oxygen (O), carbon (C) and nitrogen (N). The β-stabilizers are distinguished into, β-isomorphous types (molybdenum (Mo), vanadium (V), tantalum (Ta) and niobium (Nb)) and β-eutectoid types (iron (Fe), chromium (Cr), manganese (Mn), cobalt (Co), nickel (Ni), copper (Cu), silicon (Si) and hydrogen (H)) [8,15].There are also some other elements exits for example, zirconium (Zr) and tin (Sn), which behave more or less neutral or slightly decrease the transformation temperature.

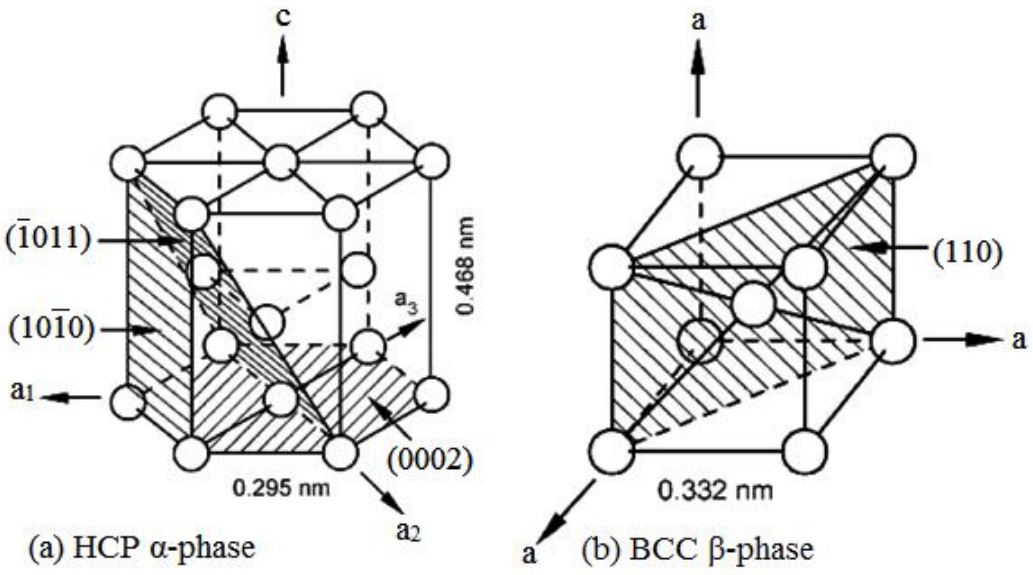

Figure 2.1: HCP unit cell of α-phase and BCC β-phase of titanium [11].

Titanium is usually deformed by the combined effect of slip and twinning [8, 11, 16-19]. The various slip systems observed in hcptitanium is schematically shown in figure 2.2 [8]. However, the dominant slip systems in α-titaniumare prismatic $\{10\bar{1}0\}<11\bar{2}0>$ followed by pyramidal $\{10\bar{1}1\}<11\bar{2}0>$and basal $(0002)<11\bar{2}0>$ with an <a> type

Burgers vector [17]. The maximum critical resolved shear stress (CRSS) is required for slip with <c+a> type Burgers vector [17,20,21]. The slip modes usually observed in β-titaniumare {110}<111>, {112}<111> and {123}<111> [22]. Figure 2.3 shows the schematic representation of twin systems observed in titanium [19].

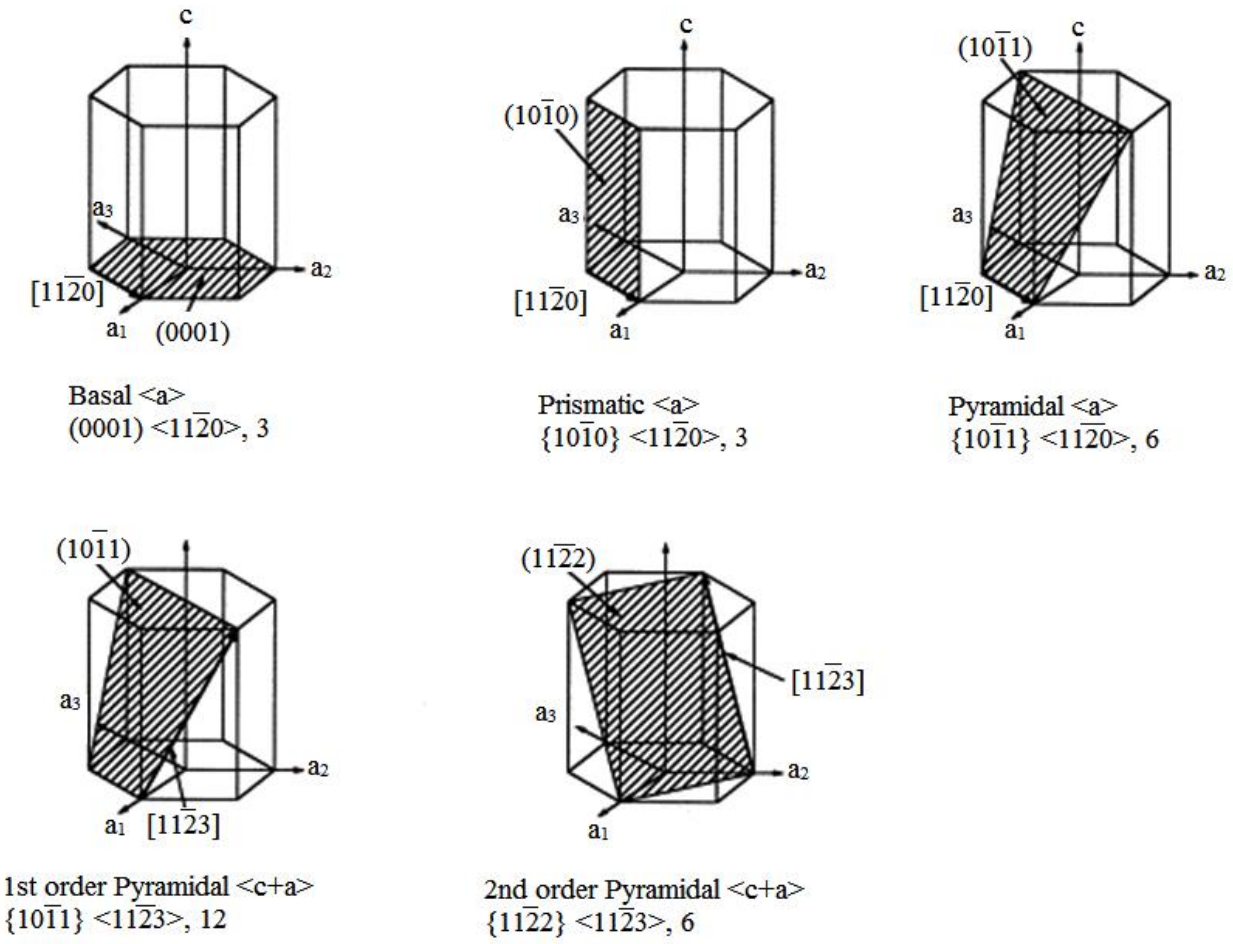

Figure 2.2: Schematic presentation of slip systems of hcp titanium [8].

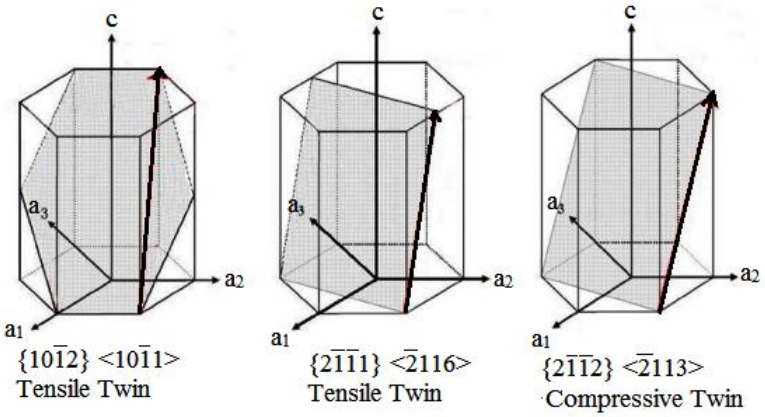

Figure 2.3: Schematic presentation of twin systems in hcptitanium [19].

2.1.1.2 Classification of Titanium Alloys

Titanium alloys are usually classified as; α-alloy, α+β alloy, β-alloy, and transition structure near-α and near-β alloy [8, 11, 15, 23, 24]. The titanium alloys composed of Al, O, N and C which are α-stabilizers are considered as α-alloys. The most common of the α-alloys is commercially pure titanium (CP-Ti) [25]. There are several commercially available grades of CP-titanium and they differ in physical and mechanical properties depending on their chemical compositions [2, 11, 26]. The alloying elements like C, O, N and H are added to titanium for increasing the strength of the alloy. The pure titanium contains about one weight percentage of these interstitial elements. Figure 2.4 shows the typical microstructure of cold rolled and annealed pure titanium [27].

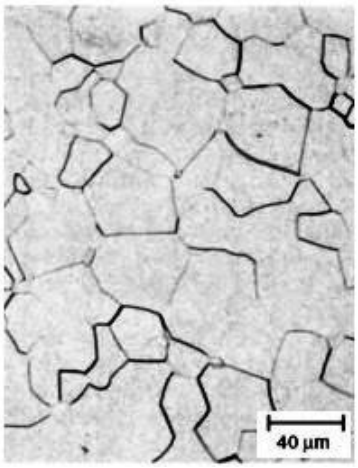

Figure 2.4: Microstructure of cold rolled and annealed high-purity unalloyed titanium sheet [27].

The *α+β alloys* have sufficient amount β-stabilising elements [5, 23, 25]. As the name implies, the titanium alloys that have a structure of partly alpha phase and partially beta phaseare α+β titanium alloys. The addition of V, Ta, Mo and Nb to pure titanium tends to promote room temperature existence of beta phase. The most important α+β titanium alloy is Ti-6Al-4V alloy; it is very useful and most available, strongest among all the Ti alloys[28]. The α+β alloys are also considered as precipitation-hardening alloys. The phase transformation of α+β alloy occurs at the temperature of 955^{o}C [25]. The typical microstructures of theTi-6Al-4V alloy are shown in figures 2.5 and 2.6. The microstructure of the Ti-6Al-4V alloy in annealed condition is shown in figure 2.5 [29]. Figure 2.6 shows microstructures of dual phase Ti-6Al-4V alloy after hot working and heat treatment [30]. The microstructure consists of martensitic, globular, necklace, lamellar, bi-modal grains.

The *β- alloys*are produced by adding large amounts of V and Mo to make the β-phase stable at room temperature. A typical β-phase alloy has a composition of 13% V, 11% Cr, and 3% Al. The β-phase alloys are typically employed in the aerospace sector for landing gear applications [24]. The microstructure of annealed *β-alloy*, Ti-3Al-8V-6Cr-4Zr-4Mo,is shown in figure 2.7.

*Near-α alloy*is entirely alpha phase with a small amount of β-phase dispersed through the alpha phase as illustrated in figure 2.8. Such alloys are obtained by adding small amounts of Mo and V [13, 28].

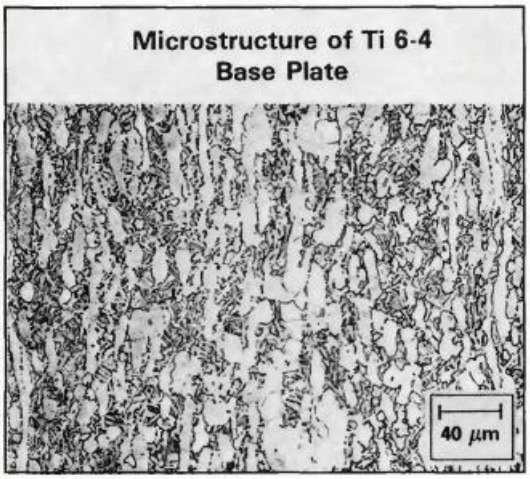

Figure 2.5: Typical microstructure of Ti-6Al-4V in annealed condition [29].

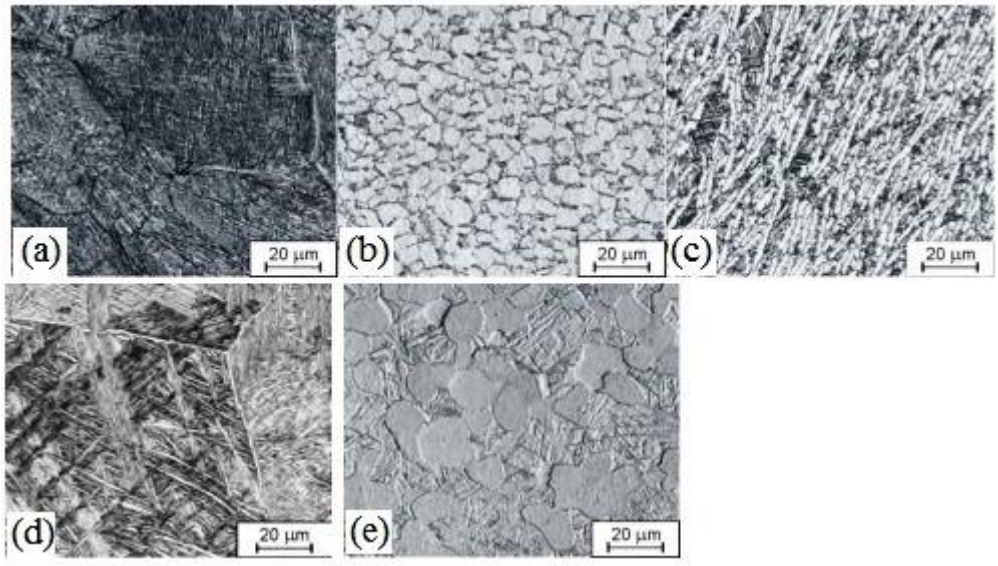

Figure 2.6: Microstructure of α+β phase Ti-6Al-4V alloy: a) martensitic, b) globular, c) necklace, d) lamellar, e) bi-modal [30].

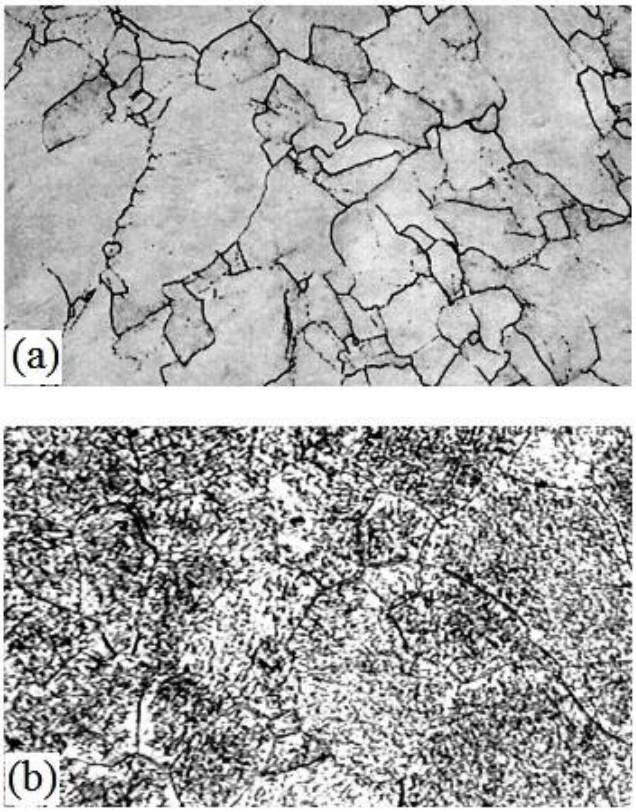

Figure 2.7: Microstructure of β- titanium alloy, Ti-3Al-8V-6Cr-4Zr-4Mo: (a) Annealed at 816˚C for 30 min. followed by air cooling, (b) Annealed at 816˚C for 15 min. followed by air cooling and then heated at 566^{o}C for six hr. &air cooled[9].

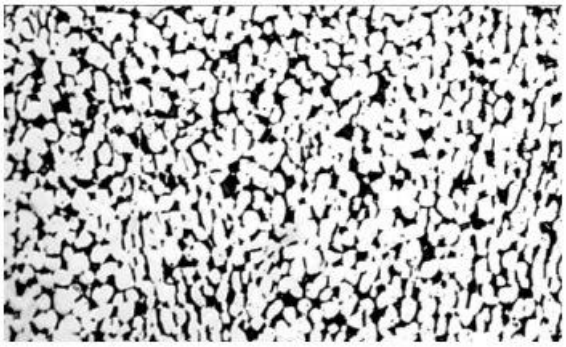

Figure 2.8:Microstructures of Ti-6Al-2Sn-4Zr-2Mo-Si (near alpha alloy) during as forged condition[9].

2.1.1.3Properties and Applications of Titanium Alloys

Titanium has light weight, high fatigue strength, high-temperature resistance to creep and highly ductile in nature. It has good thermal conductivity (20 W/m-K), high specific heat capacity (523 J/kg-K), very high yield stress (116 GPa), low specific gravity (4.5) and excellent resistance to corrosion [11, 13, 15]. Due to these exceptional properties titanium and its alloys are widely used in structural industry for making of structural components and in the aerospace industry as engine components and airframes. Titanium has superseded steel alloys for use in the small and intermediate pressure compressor assemblies of gas turbine power plants [5,15]. With advanced high-temperature stability,near-α titanium alloys competewith nickel alloys for usein the hot-end high-pressure compressor stages of the Rolls-Royce Trent 700 and RB211 engines [23]. In non-aerospace application [10] category titanium has popularly used in sports and racing car parts, bike frames, wrist watches, tennis racquets, underwater craft, golf clubs and general industrial equipment [13,15]. Due to its high corrosion resistance [13,32] to sea water, titanium and its alloys havebeen used in petrochemical industries [13,25]. Titanium is non-toxic for which it has been employed in biomedical applications like artificial bone and joint replacement [28] and pacemakers, and often used for corrosion problems in handling foods. Titanium is also used as the coating of welding rods [13,25] and also in the production of chlorine [11,25,28]. Although theproduction cost limits its applications,the usage of titanium and its alloysiscomparable to other structural materials like aluminium and steel.

2.1.2 Magnesium (Mg)

Magnesium is the lightest structural material among all the engineering materials [33]. It was discovered in 1808 by Sir Humphrey Davy [34]; earlier in 1755, it was identified as an element. However, it was not commercially used before 1920 [33]. Magnesium has started to receive attention in the mid-nineteenth century in Germany, and its primary application was for aircraft and military applications [33, 35]. Magnesium is a relatively common metal in the Earth's crust and is a principal constituent of dolomite. However, magnesium is relatively expensive to produce, because it is hard to extract from its mineral ores. A number of commercial processes are used for the production of magnesium [33, 35-37]. The electrolysis process was the one of the primary magnesium extraction processes [36]. The electrolysis process primarily involves plating of magnesium out of a molten bath of magnesium chloride.

Magnesium has a hexagonal closed pack structure with lattice parameters of a = 0.32094 nm, c = 0.52108 nm and c/a = 1.623 at room temperature. The c/a ratio is nearly equal to the ideal c/a ratio of 1.633. At room temperature, the basalslip is the primary slip system, as the CRSS (critical resolved shear stresses) of non-basal slip systems such as prismatic slip and pyramidal slip systems show much higher values at room temperature than thatof basal slip system. However, prismatic and pyramidalslip systems are activated at higher temperatures [38-41]. Figure 2.9 shows the different slip and twin systems in magnesium [42]. Table 2.1 shows the axis-angle relationships for different twin systems in magnesium [41, 43-45].

As a pure metal, magnesium is very weakand hence, it has been alloyed with different elements for engineering applications. The primary alloying elements are Al, Mn and Zn [33, 35-37]. Less common elements such as thorium (Th), Zr and rare earth elementsare also used [35-37]. For many years, magnesium was primarily used as an alloying element in Al industries and desulphurisation of steel; with very limited use of wrought products.Magnesium alloys are usually classified into two categories as:(a) casting alloys and (b) wrought alloys. Three types of cast magnesium alloys are available; aluminium – zinc – manganese (AZ) series, aluminium – manganese (AM) series and aluminium – silicon – manganese (AS) series [35,46]. These series of alloys possess excellent casting characteristics;develop high strength and having large stable properties at elevated temperatures.

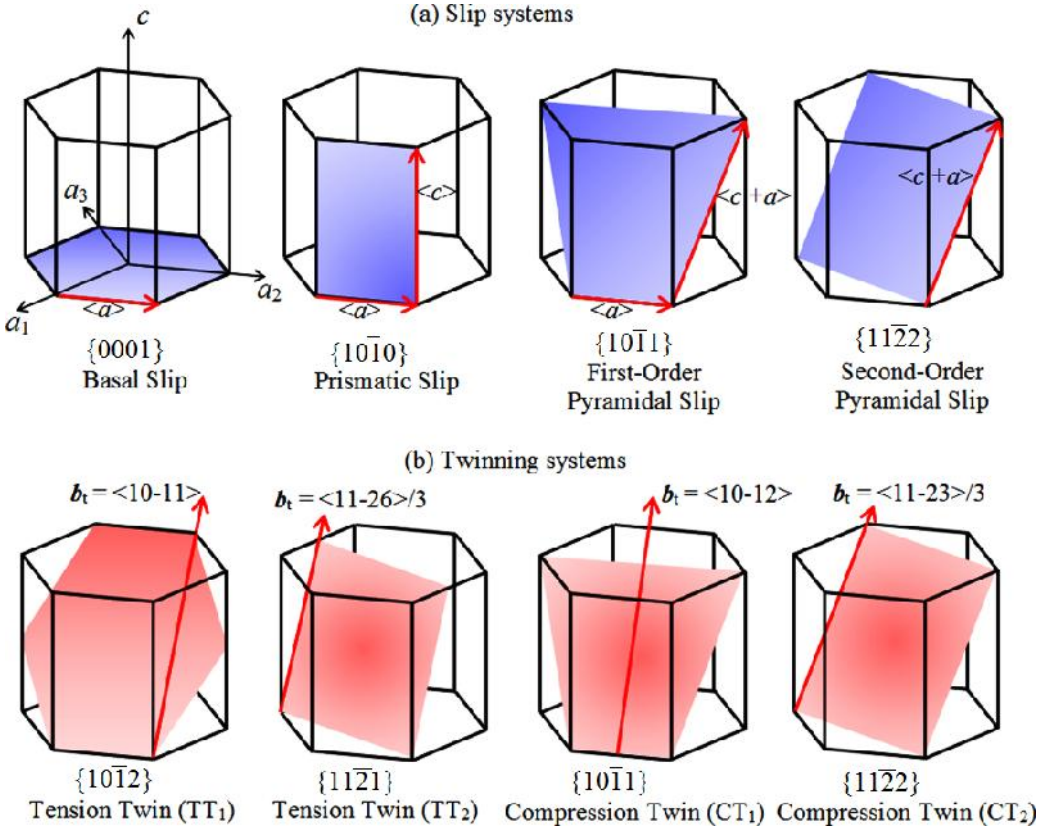

Figure 2.9: Schematic presentations of slip and twinning systems in magnesium arrow heads represent the Burgers Vector [42].

Table 2.1: Axis-angle relationship for different twin systems in magnesium [41,43-45].

Twin Type	**Misorientation angle/axis**	
{10$\bar{1}$2}	$86^0 < 1\bar{2}10 >$	Tensile Twin
{10$\bar{1}$1}	$56^0 < 1\bar{2}10 >$	Compressive Twin
{10$\bar{1}$3}	$64^0 < 1\bar{2}10 >$	Tensile Twin
{10$\bar{1}$1} - {10$\bar{1}$2}	$38^0 < 1\bar{2}10 >$	Double Twin
{10$\bar{1}$3} - {10$\bar{1}$2}	$22^0 < 1\bar{2}10 >$	Double Twin

The magnesium alloys having Al as a principal alloying element are; AZ63A, AZ81A, and AZ91C. AZ63A magnesium alloy has high yield strength and maximum toughness. AZ81A magnesium alloy is used where high ductility and high yield strength is required [47]. AZ91C magnesium alloy is most important and useful alloy where pressure tightnessand good weldabilityare required [48]. The common, rare earth and Zr containing magnesium casting alloys are; EK30A, EK41A, and EZ33A. All these three alloys provide high-pressuresolid castings and possess excellent creep strength at a temperature up to 260^{o}C [33]. HK31A and HZ32A are alloys containing Th as principal amount. These are useful forhigh-temperature applications. The two alloys, ZH62A and ZK51A, containing Mn, Zn and Zr provide almost same mechanical properties suchasgood creep strength, fatigue strength and good pressure tightness.AM100A comes under AM series of magnesium casting alloys containing Al and Mn as main alloying elements.It is only used in permanent mould castings. This alloy has excellent mechanical properties [35].

The most common magnesium wrought alloys are AZ31B, AZ31C, AZ61A, AZ80A, ZK60A, ZK60XB, ZK60A, ZK60XB and M1B [33, 35, 49]. AZ31B magnesium alloy is the most widely used and possessesexcellent forming characteristics withgood ductility and strength [37]. Alloy AZ31C has almost similar characteristics like AZ31B but having higher impurities. AZ61A and AZ80A possess excellentstrength while elongation is higher in ZK60A. ZK60XB and ZK60A alloys have almost similar characteristics while ZK60XB has maximum properties in large extrusions [49]. The M1A magnesium alloy has low strength and low ductility andit is used where strength and ductility are less concerned. From all the magnesium alloys the AZ31 series alloys received most attention because of its excellent properties as comparable to other light metals like aluminium and steel.

Due to the low density of magnesium, it is used in the automobile industry to increase the fuel efficiency of the vehicles [50]. The crankcases and the transmission housing system of Volkswagen car were the first application of die-cast magnesium alloys in automobile industry [38]. Recently magnesium and its alloys are popularly used in heavy body components such as dashboard supports, gearbox housings and engine blocks, samsonite luggage, military aircraft and space industries [35, 36, 38]. However, in automobiles industries, the application of magnesium and its alloys are still very limited [37]. The fundamental cause of this limitation is the poor room temperature formability.

2.1.3 Zinc (Zn)

Zinc was identified by Andreas Sigismund Marggraf in 1750, but it was used centuries before discovered in the metallic form. It was named from the German word *Zinke*, by the alchemist Paracelsus [51, 52]. Zinc has never been found in its pure form naturally. Zinc was found as a mineral in the earth's crust, usually associated with other base metals such as copper and lead. Zinc is extracted from its carbonate or sulphide ores by the cold electrolytic procedure [53]. In the metallurgical process, the ores are first melted, and the obtained zinc oxide is reduced to wrought zinc.

Zinc has c/a ratio of 1.858, which is greater than the ideal c/a ratio (1.633) of the hcp crystal structure. Slip occurs by (0001) basal plane in the direction of $< 11\bar{2}0 >$. Plastic deformation also accommodated by the prismatic and pyramidal slip systems along with the mechanical twinning [54] as shown in figure 2.10. Due to the presence of twinning,pyramidal slip and basal slip cannot be activatedeasily. In zinc, twinning is favoured by compression parallel to the c- axis and tension normal to the c-axis as shown in figure 2.11. It is also observed that low testing temperature and high strain rates increase the tendency for the development of twinning in zinc [55].

Zinc has restricted solid solubility with other elements due to hcp crystal structure. The main alloying elements of zinc are Al, Cu, Pb and Cd for increasing itsfabricability. Brass, an alloy of zinc and copper, is the most important alloy of zinc [56]which is stronger and more ductile than copper [57]. It has superior corrosion resistance and is widely used in marine hardware, water valves, instruments and communication equipments [58]. Other alloys of zinc are solder (zinc – tin - lead), prestal (zinc - aluminium), german silver, typewriter metal, spring brass and nickel silver [52, 57]. Among the alloys zinc-bromide and zinc-nickel power cells are commonly used in batteries now.

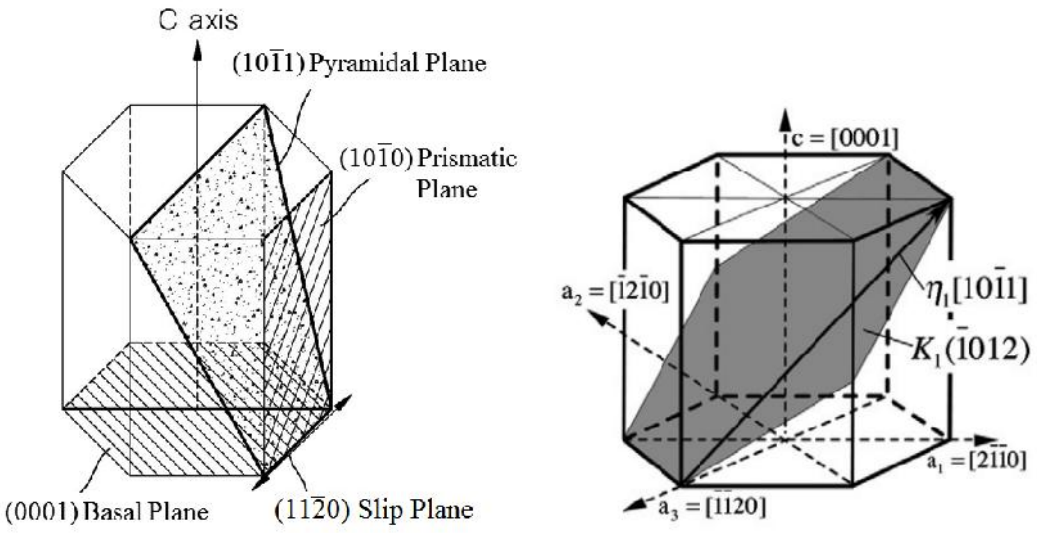

Figure 2.10: Zinc crystallographic unit cell showing the slip planes and tensile twin in the direction of $<10\bar{1}\,\bar{1}>$ [18].

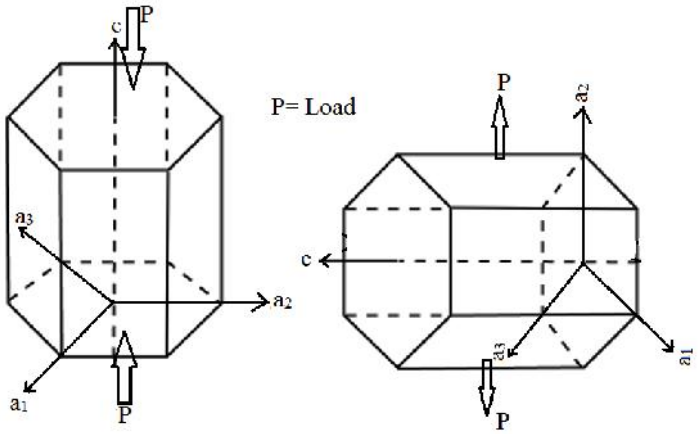

Figure 2.11: Schematic presentation of nature of twin development in zinc.

According to ASTM [57] specification, commercial use of zinc was divided into two categories; as die cast parts and coatings for corrosion resistance. ASTM B86 series, AG 40A and AG41A alloys are commonly used die-cast zinc alloys for industrial applications. AG 40A alloys have excellent impact strength and good dimensional stability. The AG41A alloy has better castability and higher strength. The main advantage of zinc diecasting is that the casting operation is done at a very low temperature as compared to other materialslike aluminium, magnesium and copper alloys. By this

significant advantage zinc die castings are used in submerged plunger machines and give long cavity life [59, 60].

Zinc coating is very popular in industries due to its very low corrosion rate [51, 52, 61]against the atmosphere. In the whole world more than 50% of zinc utilised for corrosion resistance coatings [52] as shown in figure 2.12. In steel industries, zinc coatings are used for protecting the steel from the atmospheric corrosion for many years. Zinc coatings are also applied before a painting of many automobile body parts and in structural parts [52].

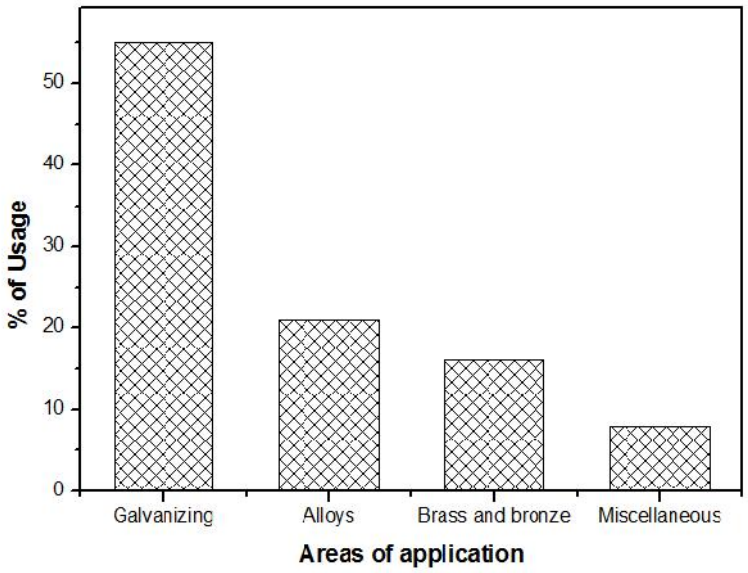

Figure 2.12: Most of the useful industrial applications of zinc in different areas.

2.2 Introduction to Recrystallization Texture

When a cold deformed material is annealed, the deformed grains gets recovered, recrystallized and then growth of the grains occurs. During the processes of recrystallization and subsequent grain growth, the initial cold deformation texture will change [62-65]. The texture so-formed is known as recrystallization texture or annealing texture [62, 66]. The important factors which govern the recrystallization texture are; initial grain size [67-70], alloying element [67,71-73], presence of precipitates/second phase particles [74-77], deformation mode [63,67,78], strain rate [63,67,79,80] and the deformation temperature [63,81]. Except the above parameters, there aresome other the

factors which also control the recrystallization texture such as energy stored during deformation [63,82-86], the orientation and the location of the new grains [63,87].

The initial grain size: Afiner initial grain accelerates the process of recrystallization and recrystallization texture of the single crystal as well as polycrystalline materials [63, 67, 68, 88, 89]. According to C. S Barret [90], aluminium with finer initial grain size recrystallizes fully on annealing at 350^{o}C, which was 6.6 times as fast as coarse grained aluminium. The size of original grain probably has significant effect on the rate of nucleation, since boundaries of initial grains are the sites for recrystallization nuclei to form. The stored energy of cold work, the driving force for recrystallization, is a function of grain size has been presented by Clarebrough *et.al.*[88].Copper of two different grain sizes was strained by various amounts and it was observed that the stored energy was greater in the fine grained samples than in the coarse grained samples. Also, therelease of stored energy wasmore rapid for fine grained samples than that for the coarse grained samples. The occurrence of either higher nucleation rate for fine grains where the growth rates are equal or a higher growth rate for fine grains when nucleation rates are constant [91]. Bhattacharjee *et. al.* [68] reported on the recrystallization textures in high purity nickel, showing significantly sharper cube texture in fine-grained starting material than in the coarse-grained starting material. Duggan and Lee [89] proposed the effects of prior grain size, rolling reduction and annealing temperature in 70:30 brass. After 92% reduction in thickness and subsequent low temperature (300^{o}C) annealing the texture of material changed from the {236} <385> (figure 2.13a) to {110} <110> (figure 2.13b) due to the increase in initial grain size. Whereas at high reductions and high temperature (600^{o}C) annealing led to the development of {113} <332> texture for small grain sized specimens (figure 2.13c). But at low reductions the {110} <112> and more general {110} <hkl> orientations were produced. For all grain sizes investigated (30–300 μm) the texture of heavily rolled material was {236} <385> after annealing at 300^{o}C, and {113} <332>after annealing at 600^{o}C. These results illustrate the importance of grain growth effects on annealing textures.

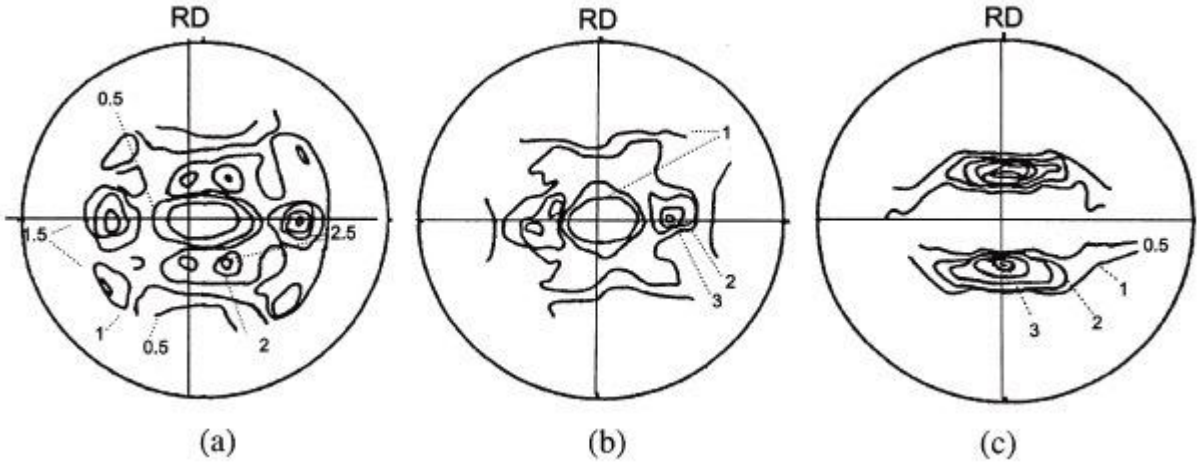

Figure 2.13: Effect of initial grain size on the recrystallization texture of 92% thickness reduction and annealed brass material, (a) 30 mm grain size, 18 hr at 300^{o}C, (b) 30 mm grain size, 18 hr at 300^{o}C, (c) 30 mm grain size, 1 hr at 600^{o}C [89].

*The alloying element:*The alloying additions strongly influence the rate of recrystallization [71-73,92-94]. The effect is specially marked in high purity metals on additions of only thousands or hundreds of an atomic percent of impurities. In less pure metals, the effect of alloying additions is weaker. For instance, theaddition of few percent of Mn, P and S to iron raises the temperature of recrystallization from 350^{o}C to 500^{o}C [92]. The addition of Tein copper lowers the rate of recrystallization [92]. Unfortunately, the available data on the separate effect of alloying additions on nucleation and growth are very scarce and mainly relate to the kinetics of growth rate. An analysis of the kinetics of growth of recrystallization nuclei in pure nickel and nickel alloyed shows that with additions of allying elements can increase the activation energy of grain growth [92]. Lucke [93] explained the total effect of alloying additions on the rate of recrystallization by their retarding effect on the growth of recrystallization nuclei. It is obvious that the sharp increase of the incubation period is also associated with the redistribution of dislocations during the formation of recrystallization nuclei. This is well confirmed by the results of separate determination of the activation energies of nucleation and grain growth in zone refined aluminium [94]. Minor additions of copper only slightly changed the rate of growth and sharply decrease the rate of nucleation. The alloying elements have agreat effect on the fcc materials as the recrystallization texture of pure copper (112) <111> texture component changed to (011) <211> texture component after addition of the alloying elements[95-98].Along with the major brass type (011) <211>texture component,

the alloying elements has the other minor components are goss (011) <100> and copper (112) <111> [95], as shown in figure 2.14. As the alloy content increases in copper, the strong cube texture component diminishes [96-98]. Figure 2.15shows the rolling and recrystallization texture components of Cu-1%P alloy, the transformation of brass texture to the goss texture after recrystallization due to the addition of P as an element in copper [99].

.

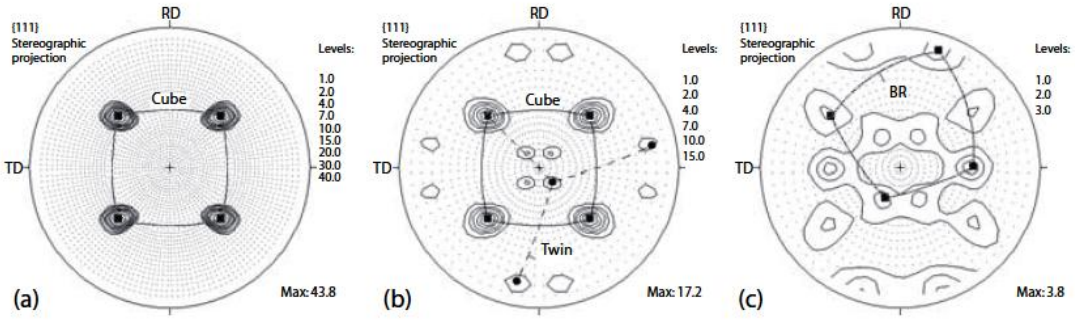

Figure 2.14: {111} pole figures of recrystallization texture componentsin rolled (a) aluminium, (b) copper,and (c) brass (Cu-37%Zn)[95].

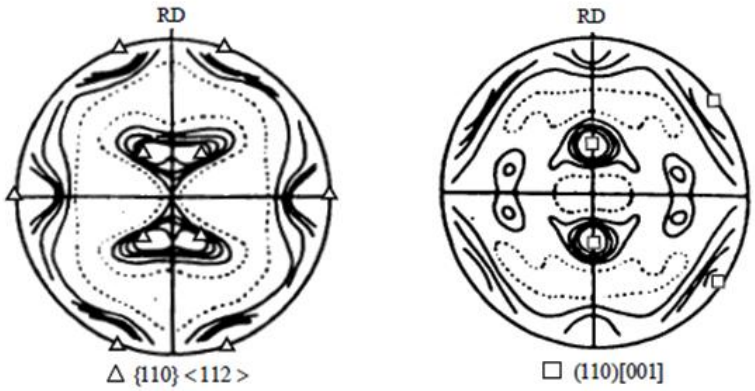

Figure 2.15: {001} pole figures of Cu-1%P alloy, shows the transformation of (a) {110} <112> brass rolling texture to (b) {110} <001>goss texture after recrystallization [99].

Engler[97] reported on the effect of Mnas an alloying element in copper. With the increase in Mn content in copper (figure 2.16), the presence of cube orientation decreases and finally vanishes. After complete recrystallization, the Cu-4%Mn shows the cube component, the Cu-8%Mn shows a small variation in cube orientation by {013}

<100>orientation and the Cu-16%Mn displays the complete alteration of cube texture and goss texture component [97].

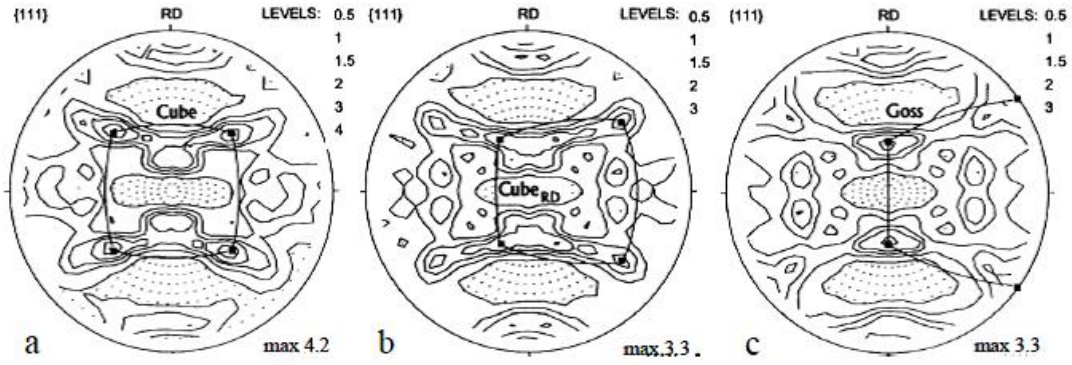

Figure 2.16: {111} pole figures of 97.5% rolled Cu-Mg alloys after complete recrystallization (a) Cu-4%Mn (b) Cu-8%Mn (c) Cu-16%Mn [97].

The presence of precipitates/second phase particles: The second phase particles already present in the structure before deformation also affects the development of the recrystallization texture [63, 67, 74, 75]. In the annealing of a material containing second phase particles, the interaction between precipitation and recrystallization controls the annealing mechanism [91]. Figure 2.17 shows a schematic diagram of the interaction between precipitation and recrystallization suggested by Hornbogen and Köster [75]. According to the figure 2.17, recrystallization occurs before precipitation at high temperatures, whereas precipitation takes place before recrystallization at low temperatures. Ryu*et. al.* [76] reported on the effect of precipitation on the evolution of recrystallization textures in an AA 8011 aluminium alloy. By annealing at a temperature of 275^{o}C, precipitation took place before recrystallization. This resulteda weak recrystallization texture consisting of {011}<122>, {001}<100>, and an RD rotated cube {hkl}<001>, among which the strong {011}<122> orientation formed near the large $FeAl_3$ particles and the {001} <122>orientation originated from the matrix was relatively weak. On annealing at 350 and 500^{o}C, the {001} <100>orientation developed strongly, while the {011} <122>orientation was weak because the driving force for the recrystallization of the matrix was higher than the dragging force of the precipitates.The development of recrystallization texture has been studied in the 6000 series Al-Mg-Si alloys used for automotive sheets with the effect of precipitation on recrystallization [77]. Coarse

constituent particles size larger than 1micron accelerate recrystallization process by enhancing particle stimulated nucleation (PSN) which leads to a very weak recrystallization texture. On the other hand, recrystallization process is retarded or completely inhibited by small (<1micron) and closely spaced particles [77].

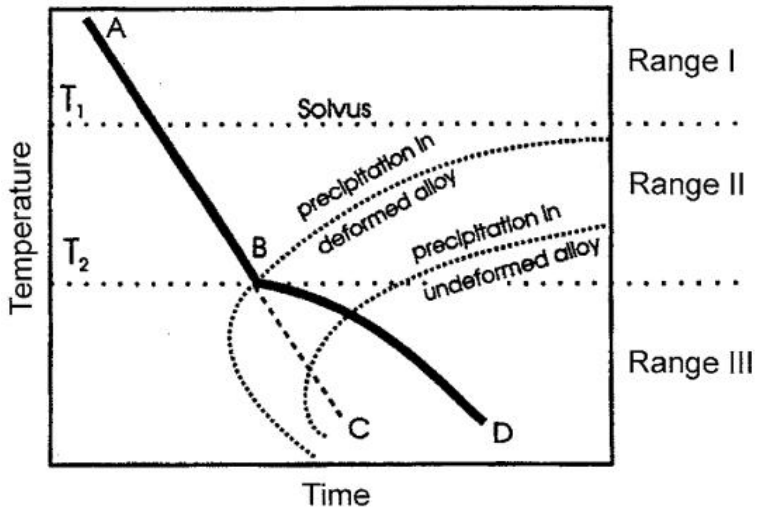

Figure 2.17: Schematic diagram showing interaction between precipitation and recrystallization [75].

The deformation mode: The mode of deformation also affects the recrystallization rate [62, 63, 78]. Mode of deformation can determine the alignment of dislocations and this subsequently determine the recrystallization texture developments of the materials after annealing. Single crystals deformed in a single glide, recover on annealing, but may not recrystallize because the dislocation structure does not contain the heterogeneities and orientation gradients needed to provide a nucleation site [63]. The best examples of this effect can befound in the hexagonal metals which deform by glide on the basal plane [63]. Wrobel*et. al.*[78] reported in his study on Cu and Cu-5%Al alloy that the recrystallization kinetics depends on upon the change in direction of the plastic flow during deformation. In copper with a changein the mode of deformation the crystallographic texture changes whereasin Cu-5%Al alloy the crystallographic texture does not alter. The recrystallization texture changed from (110) <001> to $(100)<1\bar{1}0>$ after changing the mode of deformation in a copper single crystal.

The effect of strain rate on texture development has been studiedin a variety of materials and deformation modes [63,67,100,101]. Increasing the strain rate during

deformation stimulates the recrystallization process and hence affects the recrystallization texture. The driving force for the process is provided by the high internal energy which is associated with the deformation state. The effect of strain rate is exemplified by the classic work of Rollett*et. al.*[63]. He reported on the development of texture in torsion and reversed torsion. In his study, a weak shear texture component was observed during change in net strain. Higginson *et. al.*[102] studied the effect of strain path in aluminium by the combinations of free compression and plane strain compression, the strain path changes in the direction of 0^o, 90^o, 120^o and 180^o. The starting material had a weak texture component and the samples subjected to 0^o and 180^o strain path changes also showeda weaktexture component after deformation, whereas in 90^o and 120^o strain path directed to a strong ND-rotated cube texture component and somewhat weaker cube texture. In anotherstudy Higginson *et. al.*[100] studied the development of texture as a function of roll pass schedule on through thickness in two pass hot rolling of aluminium. To visualise the difference in strain path some of the specimens were rolled by reversing the rolling direction between the first and the second rolling pass (FR) while the rest of the sample were rolled in the same direction in both passes (FF). There was a small textural differencewas observed in the surface of the slab. The FF-sample exhibited stronger ND rotated cube texture component as compared to the FR-sample. For the 10% and 50% reduction in sample thickness, no considerable texture differences were observed. Table 2.2 shows the summary of rolling texture and recrystallization texture in an aluminium alloy in five different ways [101]. (PS: plane strain texture; SH: shear texture; CUBE: cube recrystallization texture; RND: random recrystallization texture, SYM: symmetrical rolling; ASY: asymmetric rolling; L: lower contact ratio; H: higher contact ratio; WL: with lubrication; WOL: without lubrication)

The deformation temperature: In the view of the effect of the deformation temperature on the structure of the deformed materials it is to be accepted that the recrystallization characteristics of deformed metals will vary with the deformation temperature [63,103-105]. However, the number of specific quantitative investigations in this aspect of recrystallization is somewhat limited. Gindene*t. al.* [103] studied the effect of deformations in the range of 14% to 50% reduction in thickness at temperatures of -269^oC, -253^oC, -196^oC and 23^oC on the recrystallization process in 99.98% pure copper. They found that lowering the initial deformation temperature caused a decrease in both the temperature and the effective overall activation energy at the start of the recrystallization.

Similar findings have also been reported for aluminium [104]. In addition, Gindene*t. al.* [105] found that the largest recrystallized grain sizes occurred after low deformations at room temperature and that increasing the strain, and simultaneously reducing the deformation temperature which leads to a more uniformly distributed and finer grain size. These results are consistent with the general findings that a reduction temperature leads to an increase in the dislocation density, and strain energy with more uniform dislocation distribution as compared to room temperature deformation.

Table 2.2: Effect of different strain states on the rolling and recrystallization textures of aluminium alloy[101].

	Rolling Texture			**Recrystallization Texture**		
	s = −0.8	**s = 0**	**s = +0.8**	**s = −0.8**	**s = 0**	**s = +0.8**
SYM-L-WL		PS	PS		CUBE	CUBE
SYM-L-WOL		PS	SH		CUBE	RND
SYM-H-WOL		PS	SH		CUBE	RND
ASY-L-WOL	SH	SH	SH	RND	RND	RND
ASY-H-WOL	SH	SH	SH	RND	RND	RND

The stored energy is a most important driving force for recrystallization microstructure and texture in metals [63,81-87,106]. The stored energy may include energies due to vacancies, dislocations, grain boundaries, stacking faults and complex interactions between them and surface energies. For a given deformation mode, grains of different orientations are expected to develop microscopic defects at various rates. This leads to the variation of stored energy as a function of crystallographic orientation.Shin *et. al.* [107] reported the evolution of <100> preferred orientation as the recrystallization texture in deformed silver wire specimens during annealing. The texture evolution during recrystallization was a result of the release of the stored energy during deformation.

Rajmohan *et. al.* [84] reported on the comparison between orientation dependent stored the energy of cold rolled and stress relieved interstitial free steel and observedthat the release of stored energy in γ-fibre seems to be more uniform than in the α-fibre as shown in figure 2.18.

Figure 2.19 displays the variation of the critical recrystallization temperature as a function of stored energy.This exhibits even for equally deformed samples.The recrystallization activities still differ strongly from grain to grain, nucleation starts first in grains with the highest stored energy [85]. Ette*et. al.* [82] reported on the influence of the cold rollingreduction of stored energy in a Fe–53%Ni. This result proposes that the energy gap between the cube and the other main orientations increases for a cold rolling reduction greater than 80%. Such an increase promotes the cube orientation to grow faster during recrystallization by supplying the necessary driving force for cube grain boundaries migration into the surrounding matrix. For low reductions, no such energy gap change was observed and all orientations can grow instantaneously. The stored energy also plays a great role for the sharpness of the γ-fibre in Fe-steel sheet during recrystallization [108].

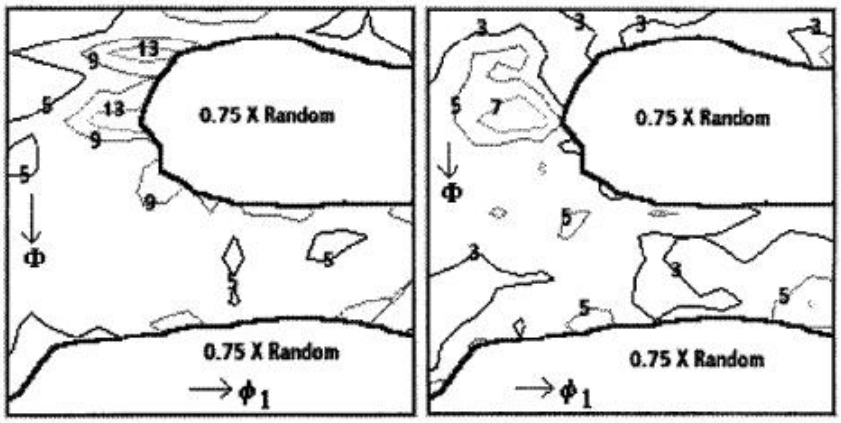

Figure 2.18: (a) ϕ_2=45º section of stored energy distribution function of 80% cold rolled IF steel (b) ϕ_2=45º section of stored energy distribution function of 80% cold rolled and stress relieved at 600°C for 5 minutes IF steel [84].

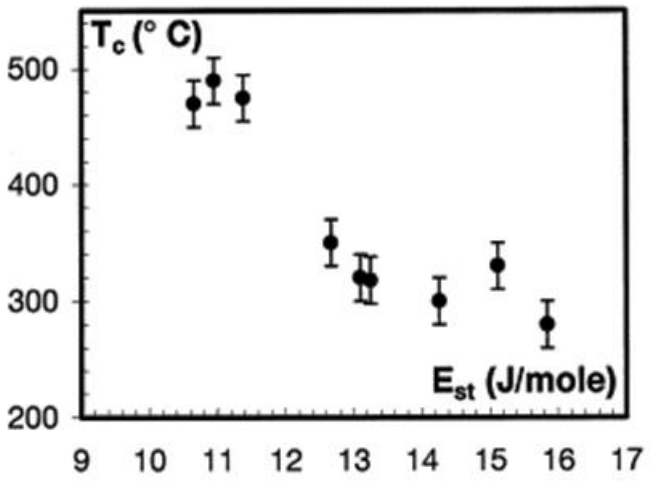

Figure 2.19: Variation of the critical recrystallization temperature as a function of stored energy [82].

The orientation of grain and the position of the new grains are the main factors of inhomogeneous recrystallization in the materials. This is because slip systems and strain path which operate during deformation are dependent on crystallographic orientation. The distribution and density of dislocations are also orientation dependent. Therefore, availability and feasibility of nucleation sites and growth rate of recrystallizing grains depend strongly on the orientation of grains [63]. The initial orientation and the 'orientation path' during deformation will affect the nucleation of grains inthe deformed matrix. Ferran*et. al.* [87] anticipated the effect of orientation of the new grains on the recrystallization texture of aluminium. The orientation nucleation was gained from the orientation relationships found between the new grains and surrounding matrix. In which there was a tendency for the rotation axis to lie closer to <111> or <100> than the rotation axis of a random polycrystal. Moreover, a tendency for rotation angles to have lower values than the rotation angles for a random polycrystal.

2.2.1 Theories of Recrystallization Texture

The evolutions of recrystallization texture in the metals are followed up profusely by two theories [64] i.e. the theory of oriented nucleation (ON) (provided by Burgers and Louwerse in 1931) and theory of orientated growth (OG) (provided by Barret in 1940 and Beck in 1954). The theory of oriented nucleation (ON) claims the origin of the recrystallized texture is in the preferred nucleation of deformed matrix. Whereas, the theory of oriented growth (OG) claims that, the source of the final texture lies in the

preferred growth of particular nuclei of a more or less random initial distribution of deformed matrix.

2.2.1.1Theory of Oriented Nucleation (ON)

According to ON theory, orientation is determined directly at the stage of formation of recrystallization nuclei as subgrains of a definite orientation which grow more perfectly during recovery before recrystallization. Burgers and Louwersehavebeen developed the oriented nucleation theory working on the compressed single crystal aluminum specimen. He concluded that on annealing a deformed crystal, the nuclei of the recrystallized grains have developed from the most heavily deformed grains which are already present in the deformed matrix [109-112]. The theory of orientated nucleation gives the useful information where deformation texture changes to a qualitative identical recrystallization texture. For example,the evolution ofgoss recrystallization texture in Fe-Si steel and cube recrystallization texture in aluminum [110-112].

Beck and Sperry [113] reported on nucleation mechanism through migration of pre-exiting high angle grain boundaries. Their observations based on optical microscopy and later Bailey [114-116] studied with transmission electron microscopy in Cu, Ni, Au, Ag and Al. In all these studies, the deformation of metals were less than 40%. This mechanism takes into account the migration of a pre-existing high angle grain boundary towards the center of a more highly strained grains [117] as shown in figure 2.20. The migration of a pre-existing high angle grain boundary was happened due to the favourable energy balance between the reduction of stored energy during the removal of defects initiated by the passage of the boundary, and the increase in total grain boundary surface during bulging [116].

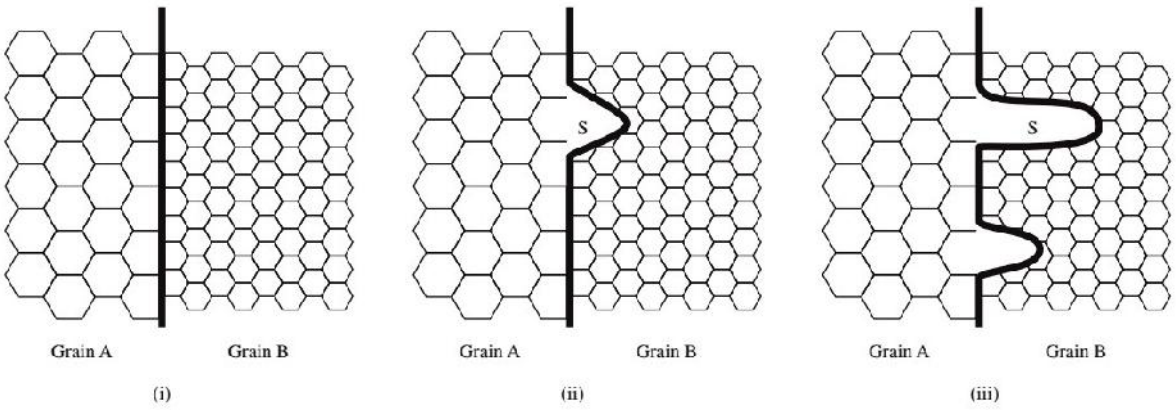

Figure 2.20: Schematic representation of nucleation by migration of boundaries induced by deformation [117].

2.2.1.2Theory of Orientated Growth (OG)

Barret[117] proposed that the evolution of recrystallization texture can be determined from the original orientation of the nuclei having the maximum growth in the deformed matrix. By this theory, it was confirmed that the development of recrystallization texture was associated with the grain boundary rotation. This theory is more successful than oriented nucleation theory. Later in 1966 by Beck and Hu [118] and in 1974 by Luke [119] confirmed that the evolution of cube texture component after recrystallization is formed by rotation of 40˚ about <111> axis[120,121]. With the help of this theory, the suggestion for the movement of the grain boundaries with the definite orientation relationships was established, and it concludes that the orientation of the recrystallization texture is separated from deformation texture differed by rotation of 30^o to 40^o about a common axis [122]. That is why the recrystallization texture in fcc metals differ by a rotation of 30^o to 40^o about <111> axes (figure 2.21), for bcc metals 30^o about <110> axes and 30^o about <0001> axes for hcp metals.

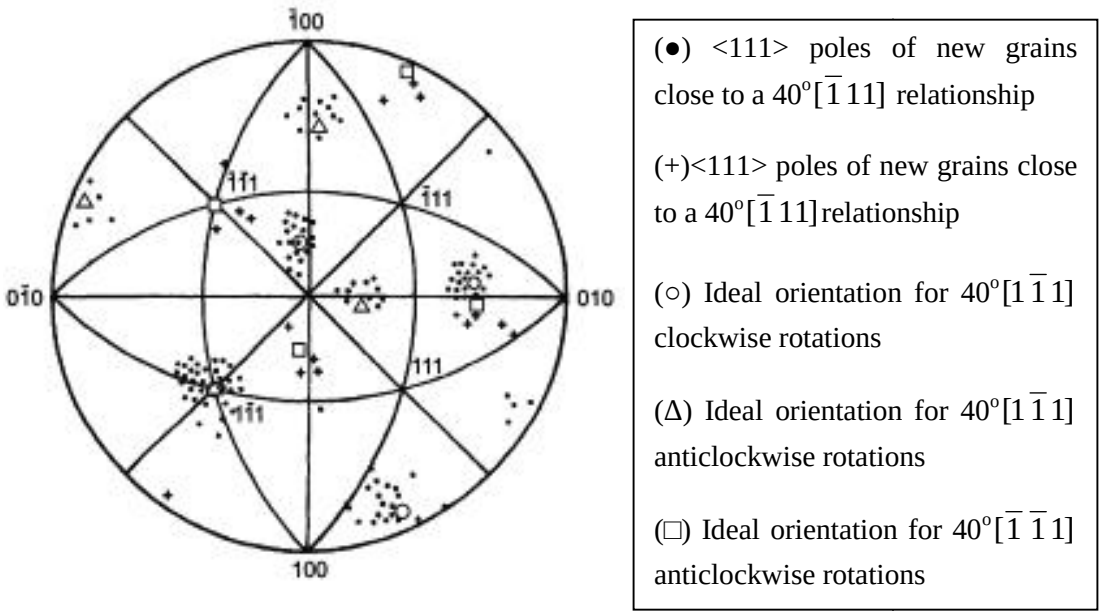

Figure 2.21: Rotations associated with nucleated grains and the deformed matrix of aluminium single crystal [122].

2.3 Recrystallization Texture Developments in HCP Metals

2.3.1 Recrystallization Texture of Titanium

The development of recrystallization texture in commercially pure titanium after cold rolling has been studied by number of authors [124-138]. The recrystallization texture component is directly depends upon the rate of deformation and annealing temperature. According to the annealing temperature, recrystallization texture components are divided into three categories [133]. When the annealing temperature is less than or equal to 500ºC, therecrystallization texture components are $(2\bar{1}15)<12\bar{1}0>$ and $(0001)<10\bar{1}0>$, ± 30º of transverse direction (TD) splitting which is similar to the rolling texture components. If the annealing temperature is in between 500ºC to 700ºC, the complete recrystallization of the crystals with grain growth starts to occur. The recrystallization texture components in this temperature range are $(0001)<12\bar{1}0>$ and $(0001)<10\bar{1}0>$, ±30º to TD. There will be grain growth if the annealing temperature is greater than 700ºC, and the recrystallization texture components are either $(10\bar{1}3)<12\bar{1}0>$ or $(\bar{2}025)<12\bar{1}0>$ and these are the components of $(0001)<12\bar{3}0>$, ±30º to TD orientation [133]. It is known that the texture component $(\bar{1}013)<1\bar{2}10>$ is recrystallization texture component which develops from cold rolled texture component $(\bar{2}115)<0\bar{1}10>$ through 30º rotation about c-axis. The resulting recrystallization texture component $(\bar{1}013)<1\bar{2}10>$ has centered on $\{\phi_1=0^o, \Phi=35^o, \phi_2=30^o\}$ angles in the Euler space [138]. Figure 2.22 shows a schematic representation of cold rolled and recrystallized texture components in a rolled titanium sheet.

Bozzolo*et. al*. [125] reported the development of recrystallization texture component due to grain growth in 80% cold rolled cp-titanium sheet. The development of recrystallization texture during annealing was done in two stages; the first one was due to primary recrystallization and the second one was due to grain growth. During primary recrystallization the texture developed was nearly equal to the deformed texture i.e. close to $\{\phi_1=0^o, \Phi=35^o, \phi_2=0^o\}$ and during secondary recrystallization main recrystallization texture component hasdeveloped due to grain growth and the orientation was nearly centered around $\{\phi_1=0^o, \Phi=35^o, \phi_2=30^o\}$ by 30º misorientation angle from primary recrystallization orientation. Figure 2.23 shows ODF at $\phi_1=0^o$sections with increasing mean grain size.

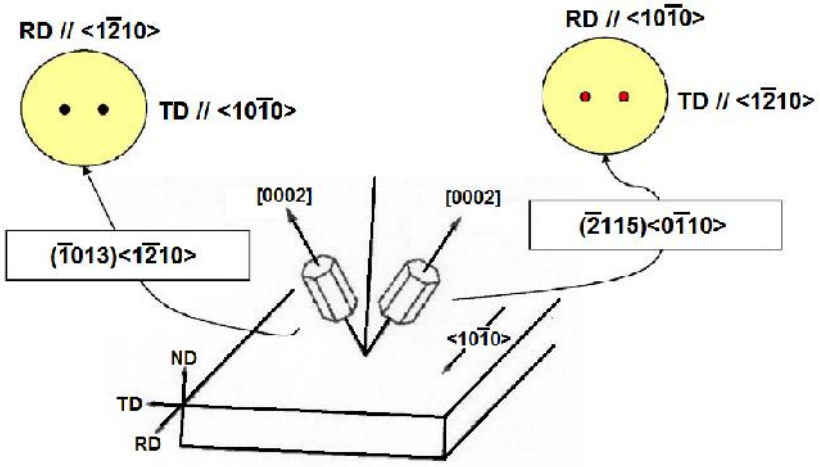

Figure 2.22: Cold rolled texture component and recrystallized texture component of a titanium rolled sheet [139].

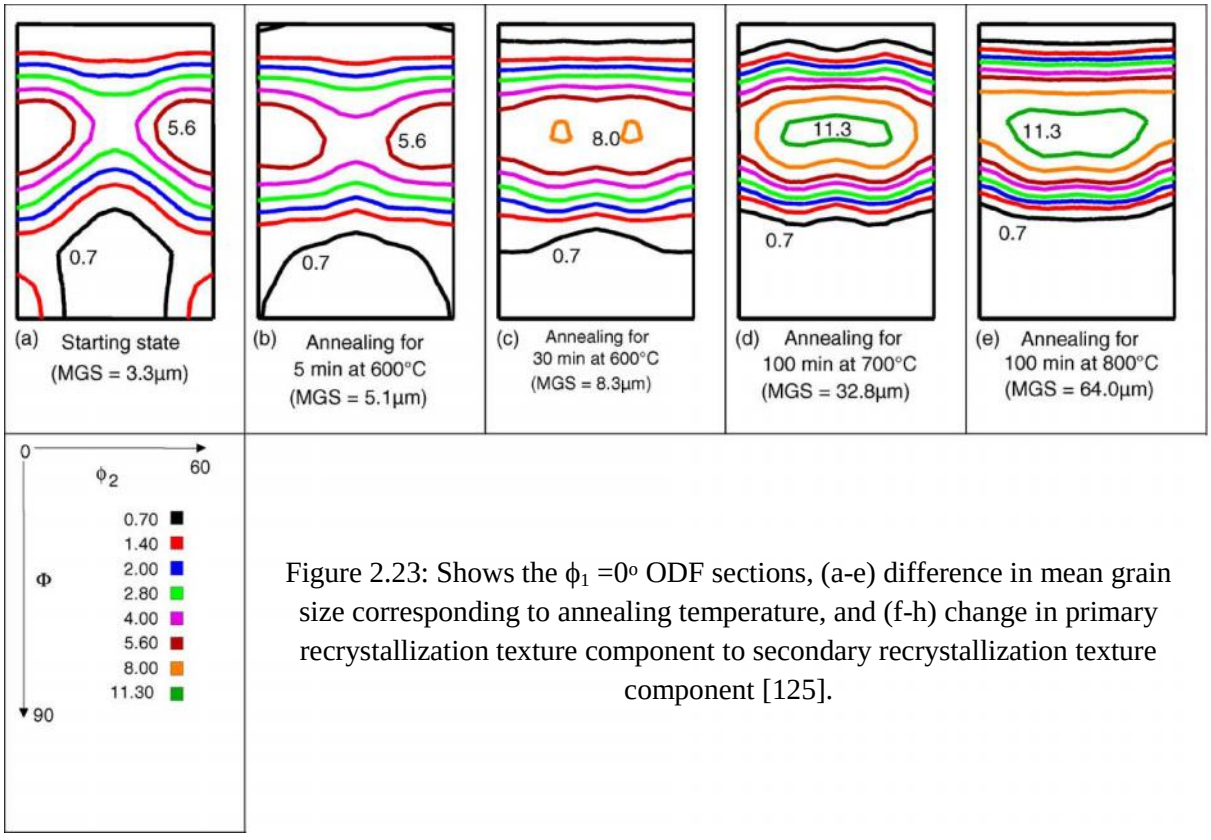

Figure 2.23: Shows the ϕ_1 =0° ODF sections, (a-e) difference in mean grain size corresponding to annealing temperature, and (f-h) change in primary recrystallization texture component to secondary recrystallization texture component [125].

Jing *et. al*. [130] studied the development of recrystallization texture of cp-titanium in two cases; in the firstcase, development of recrystallization texture is done in hot rolled plate and in the second case, the development of recrystallization texture in cold rolled

plate. In both the cases the recrystallization texture form with the basal pole tilted 30º - 40º away from normal direction towards transverse direction.After annealing, main recrystallization texture component $(10\bar{1}3)<5\bar{2}\bar{3}0>$ getting stronger with increase in annealing time and at the same time, the $(11\bar{2}5)<11\bar{2}3>$ cold rolled texture component diminishes which is in line with the findings of Bozzolo *et. a.l* [125]. The initial hot rolled texture were, pyramidal texture $(\bar{1}013)<5\bar{2}\bar{3}0>$ and $(\bar{2}021)<10\bar{1}5>$, basal texture $(0001)<2\bar{1}\bar{1}0>$ and stronger prism texture $(11\bar{2}0)$<0001>.After annealing at 500ºC for 30 min, the $(\bar{2}021)<10\bar{1}5>$ texture componentdiminishes, and development of $(\bar{1}013)<1\bar{2}10>$ and $(11\bar{2}5)<11\bar{2}3>$ new textures components were found in the initial hot-rolled plate. After cold rolling with a reduction of 60%, the most common $(11\bar{2}5)<1\bar{1}00>$ cold-rolled texture component was developed with a higher strength. In the case of annealing at 700ºC for 30 min, the recrystallization texture component $(\bar{1}013)<1\bar{2}10>$ was developed by inheriting the cold-rolled texture component. Again if the soaking time was increased (700ºC for 60 min), the recrystallization texture component $(\bar{1}013)<1\bar{2}10>$ strengthens by consuming the cold-rolled texture componentof $(11\bar{2}5)<1\bar{1}00>$.

Zhu *et. al*. [138] also reported the evolution of common $(\bar{1}013)<1\bar{2}10>$ recrystallization texture component by consuming the cold rolling texture component $(\bar{2}115)<0\bar{1}10>$ through 30º rotation about c-axis. The cp-titanium sheets are processed under normal cold rolling, annealing, hot rolling, cross rolling and phase transformation. The recrystallization texture component in low alloyed titanium (T40) [140] sheets was centred around $\{\phi_1=0^o, \Phi=30^o, \phi_2=30^o\}$ due to primary recrystallization and $\{\phi_1=0^o, \Phi=45^o, \phi_2=0^o\}$ due to complete recrystallization. Inoue and Inakazu [141] reported on the development of recrystallization texture at low and high-temperature annealing of pure titanium. The $(\bar{1}013)<12\bar{3}0>$ recrystallization texture component was developed during recrystallization of both straight and cross rolled pure titanium samples. For low-temperatureannealing, the recrystallization texture developed was different for both the samples. The $(02\bar{2}5)<21\bar{3}0>$ recrystallization texture component was found in unidirectionally rolled sample while the cross rolled sample retains the initial rolling texture component.

2.3.2 Recrystallization Texture of Zirconium

Vanitha*et. al*. [142]has reported on the development of recrystallization texture in single phase zircaloy 2 (figure 2.24 and figure 2.25). The origin of evolution of recrystallization texture has been categorised into three ways; one is due to strain localizations at the early stage of recrystallization about 10 – 20% recrystallization of grains. Second is due to deformed bands at the intermediate stage of annealing about 50 – 55% recrystallization of grains and lastly due to the recovering grains at the final stage of recrystallization about 85% of recrystallized. The development of texture due to strain localizations has equiaxed grains, smaller size, and strong textures. The recrystallized grains are orientated about $45^{o}$and $60^{o}$to the rolling direction. The grain orientations have filled with the negative textural softening. The texture developed due to deformed bands has random orientations, large grain size, and high aspect ratio and this texture component was developed due to the effect of orientation pinning. At the third stage of recrystallization, the development of texture was insignificant; these orientations were characterized by positive textural softening.

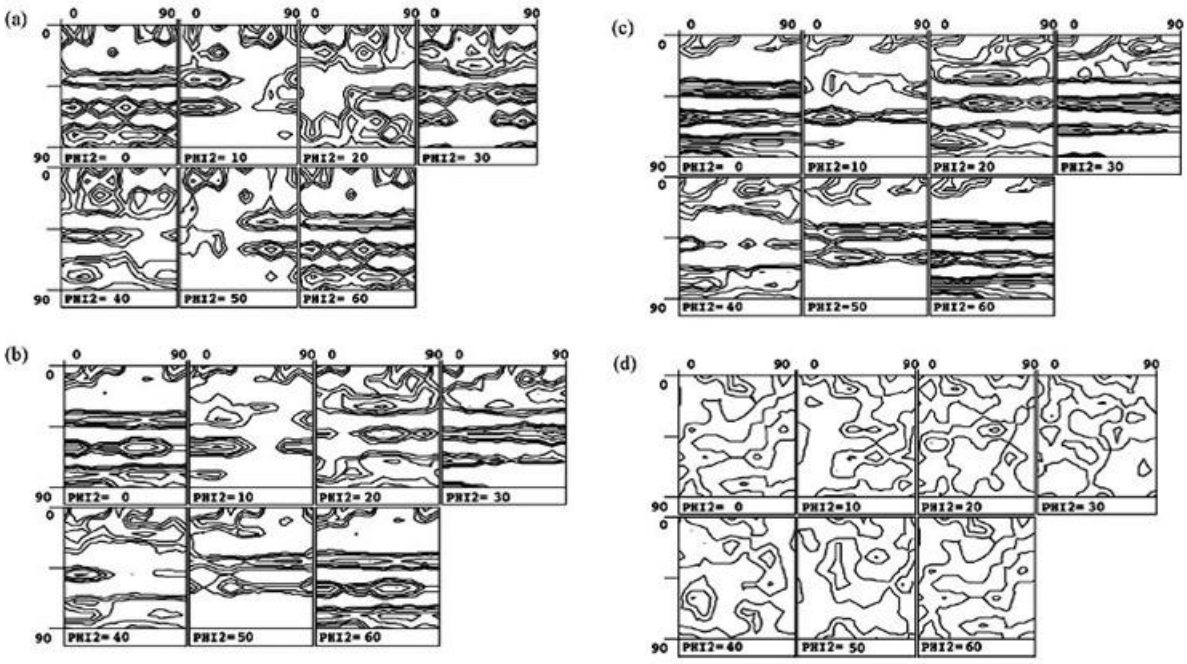

Figure 2.24: ODFs of 40% deformed material after recrystallization annealing at 710^{o}C and for (a) 12 min, (b) 24 min, (c) 48 min and (d) 60 min [142].

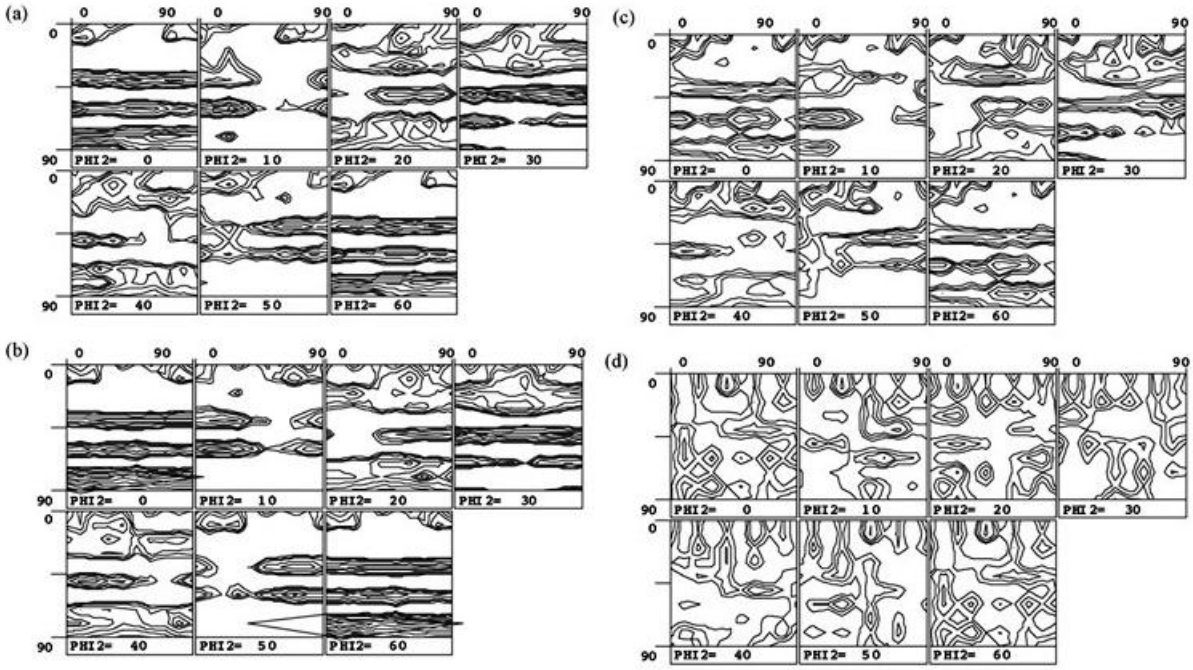

Figure 2.25: ODFs of 60% deformed material after recrystallization annealing at 710ºC and for (a) 12 min, (b) 24 min, (c) 48 min and (d) 60 min [142].

The evolution of recrystallization texture in low alloyed zirconium (Zr702) was studied after three different cold rolling reductions (SR- simple rolling, TR- transverse rolling, CR- cross rolling) [143]. The texture evolutions due to primary recrystallization in these cases are relatively different from each other (figure 2.26). These differences in recrystallization texture were due to the effect of local deformation structure and sharpness of deformation texture. Dewobroto*et. al*. [144] investigated the mechanism of recrystallization texture development in a low alloyed zirconium (Zr702). The mechanism associated with the development of recrystallization texture is mainly during grain growth, and the recrystallized component was centred around $\{\phi_1=0^o, \Phi=30^o, \phi_2=30^o\}$. During the primary stage of annealing, the initial deformation texture characteristics were retained.

Texture development in Zr-1.0Nb [145] alloy sheet during cold rolling and subsequent annealing was centred on $\phi_2 = 30^o$ with the orientation component of {0001} $<10\bar{1}0>$ fibre. The intensity of the texture component increased with increase in rolling reductions and annealing temperature. The principal mechanism related to the development of recrystallization texture was the mobility and the formation of high angle grain boundaries (HAGB). The main driving force for the development of the

recrystallization texture in Zr – 2Hf alloy is the difference in stored energy from deformation to recrystallization [146]. The mechanisms associated with the evolution of recrystallization texture areoriented nucleation and grain growth theory. For the rolling reductions 50% - 90% there were two partial fibre orientations called; deformation fibre (D_f) = {hkil} $<10\bar{1}0>$ and recrystallization fibre (R_f) = {hkil}$<11\bar{2}0>$and two main orientations called 'tilted' {0001} $<10\bar{1}0>$and 'tilted' {0001} $<11\bar{2}0>$texture components were developed. The basal poles {0001} were nearly 25^o away from the specimen normal direction (figure 2.27 and figure 2.28). After primary recrystallization and grain growth the intensity of the recrystallization fibre increases and at the same time the intensity of the deformation fibre decreases.

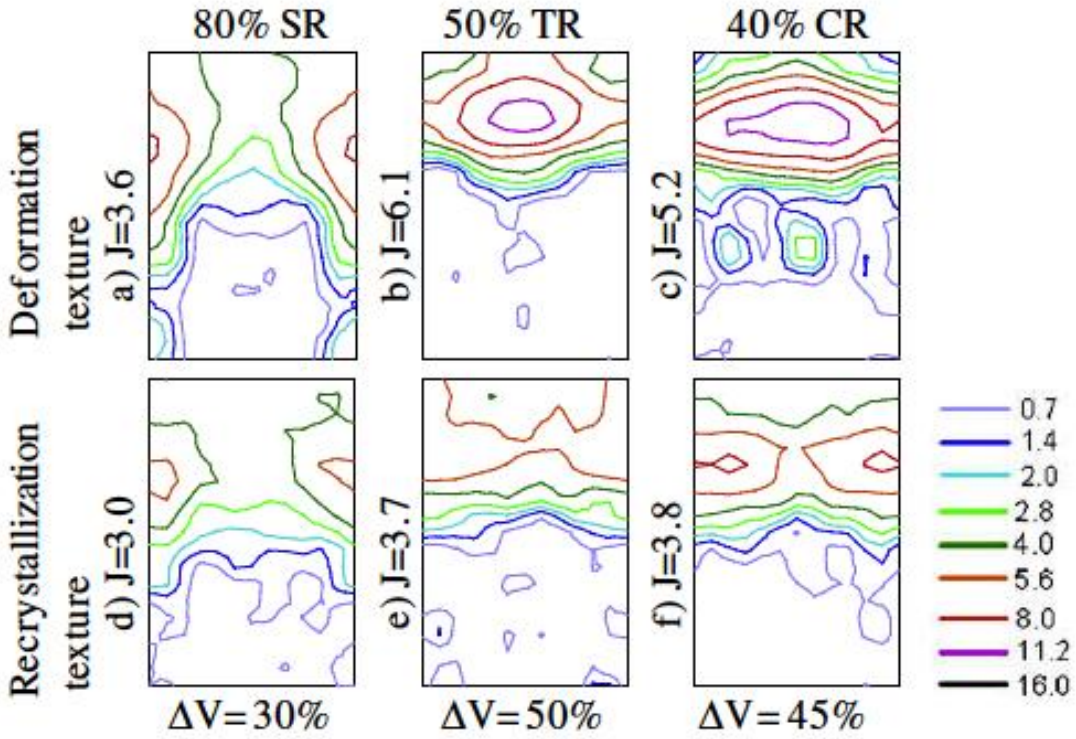

Figure 2.26: ODF figure atϕ_1=0^osection shows the change in texture development during deformation and recrystallization for three different cases [143].

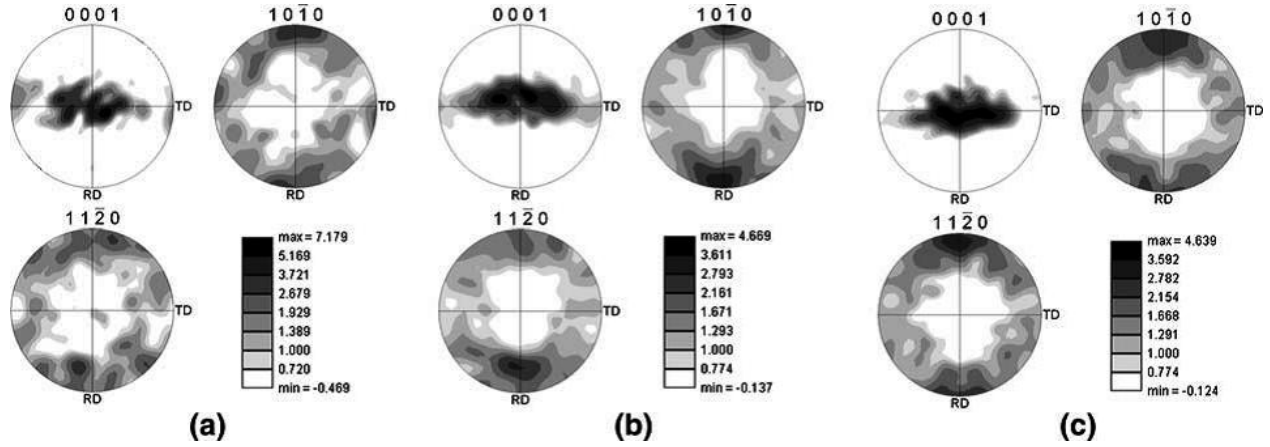

Figure 2.27: $\{0001\}\{10\bar{1}0\}$ and $\{11\bar{2}0\}$ pole figures of 50% deformed Zr – 2Hf alloy after recrystallization at 530°C for (a) 4 min, (b) 8 min, and (c) 180 min [146].

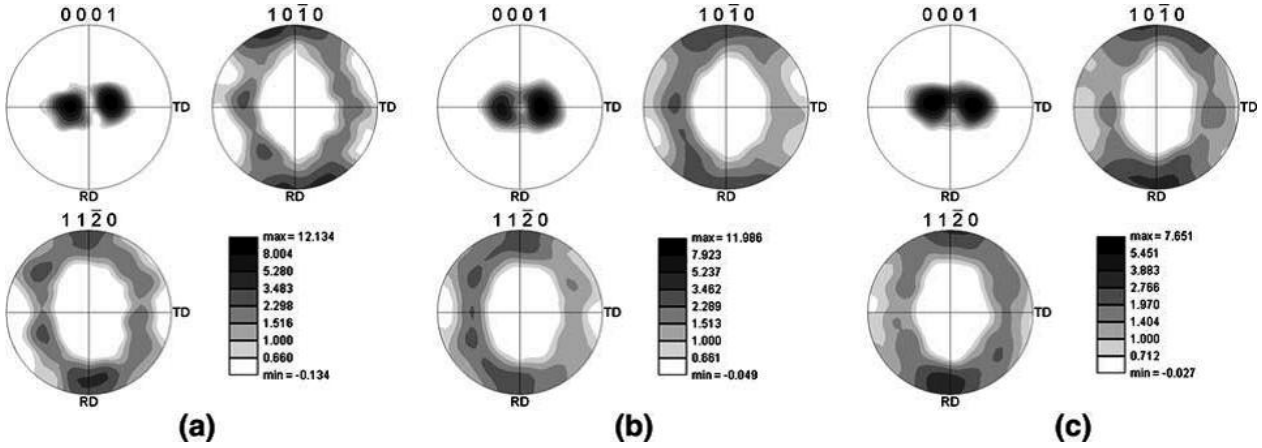

Figure 2.28: $\{0001\}\{10\bar{1}0\}$ and $\{11\bar{2}0\}$ pole figures of 90% deformed Zr – 2Hf alloy after recrystallization at 530°C for (a) 4 min, (b) 16 min and (c) 180 min [146].

The recrystallization texture in alpha zirconium (α-Zr) tubes was the predominantly $\{11\bar{2}0\}<10\bar{1}0>$ component. The misorientation angle between deformed orientation and recrystallized orientation grains depends on the annealing temperature and increases from 20° to 30° when passing from annealing temperature of 580°C to 600°C [147]. Perlovich [147] reported on the development of recrystallization texture in tube and sheet of α-Zr. The recrystallized texture is the well-defined (0001) component in the direction of $<21\bar{3}0>$ and $<11\bar{2}0>$. This recrystallization texture developed by the rotation of the basal axis about 30° to the deformed matrix. The rotation of the deformed

matrix after recrystallization of α-Zr is due to the favored contribution of prismatic slip in its plastic deformation.

Hirwarkar*et. al*. [148] studied the recrystallization texture and the mechanisms responsible for recrystallization in piligeredZircaloy – 4. Preferred nucleation and grain inhibition/pinning arethe mechanisms accountable for the recrystallization. While the former is active in the highly deformed region where stored energy is high, grain inhibition occurs in the non-deforming region and stimulates primary recrystallization.

2.3.3 Recrystallization Texture of Magnesium

In magnesium, generally basal texture component was reported due to the easy accommodation of basal slip systems [149-156]. The recrystallization texture of pure magnesium during symmetric and asymmetric rolling was conveyed by Beausir*et.al.*[157]. Basal texture component (0002) parallel to normal direction was the dominant texture component in symmetric rolling samples whilein the asymmetric rolling samples the basal texture component was rotated by 5-10^{o}anticlockwise from normal direction (figure 2.29). Dynamic recrystallization process was the main factor in the evolution of recrystallization texture component for both the samples.

Figure 2.30 shows the initial texture of AZ31 magnesium alloy. A strong basal fibre texture component for recrystallized sheet and random texture for squeeze cast bar were observed [149]. The texture component was centred on ±15^{o}rotation of basal pole from the normal direction to rolling direction. Perez-Prado *et. al*. [150] have reported the development of homogeneousprismatic $\{11\bar{2}0\}$ recrystallization texture component in magnesium AZ31 for the first time. The texture was measured through thickness gradient for AZ31 material. The basal texture component was present on the outer-surface, and $\{11\bar{2}0\}$ prismatic texture component was observed in mid-layer of the sheet, as shown in figure 2.31.

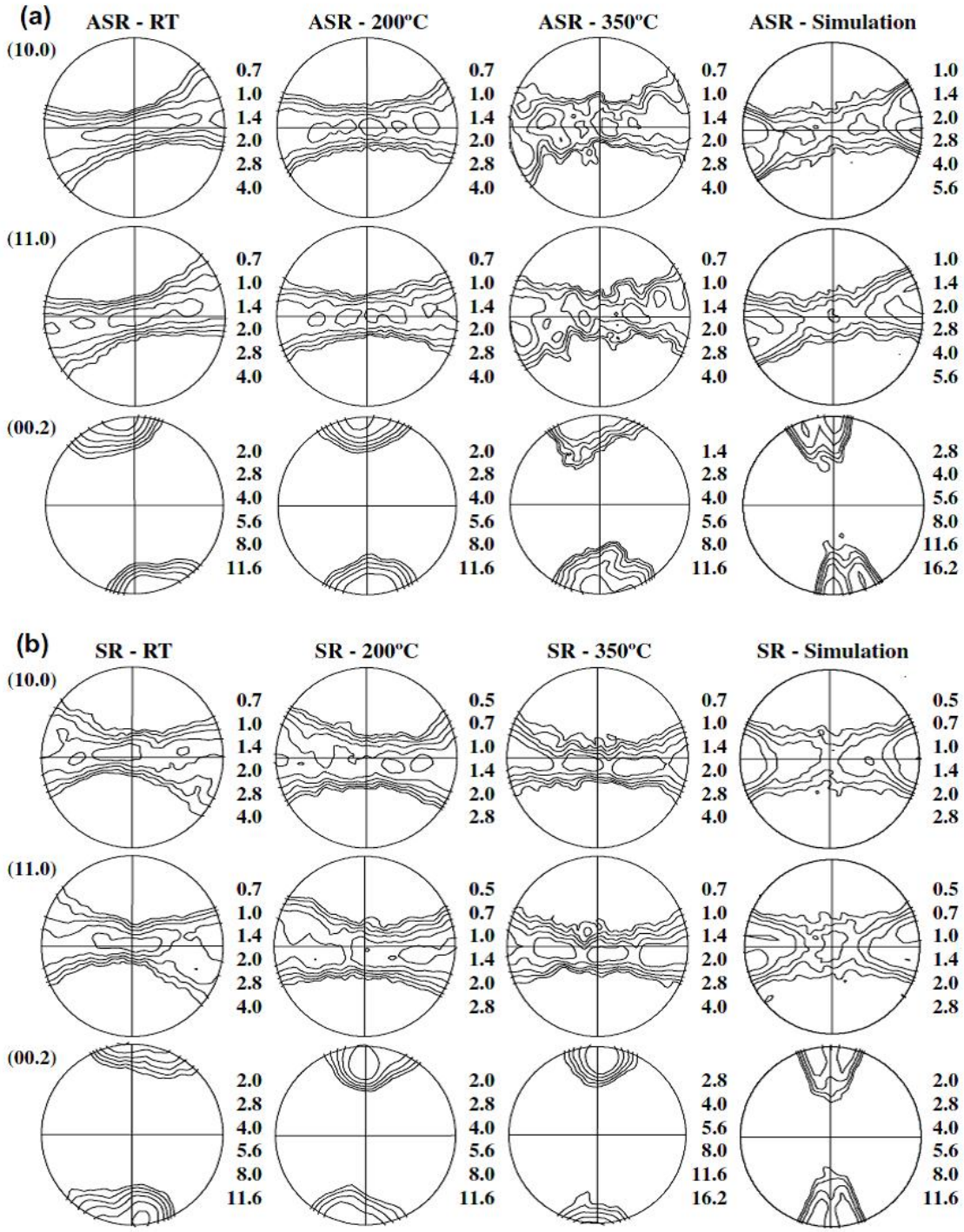

Figure 2.29: Experimental and simulated pole figures of pure magnesium sheets annealed at, room temperature (RT), 200°C, 350°C (a) asymmetric rolling (ASR), (b) symmetric rolling (SR) [153].

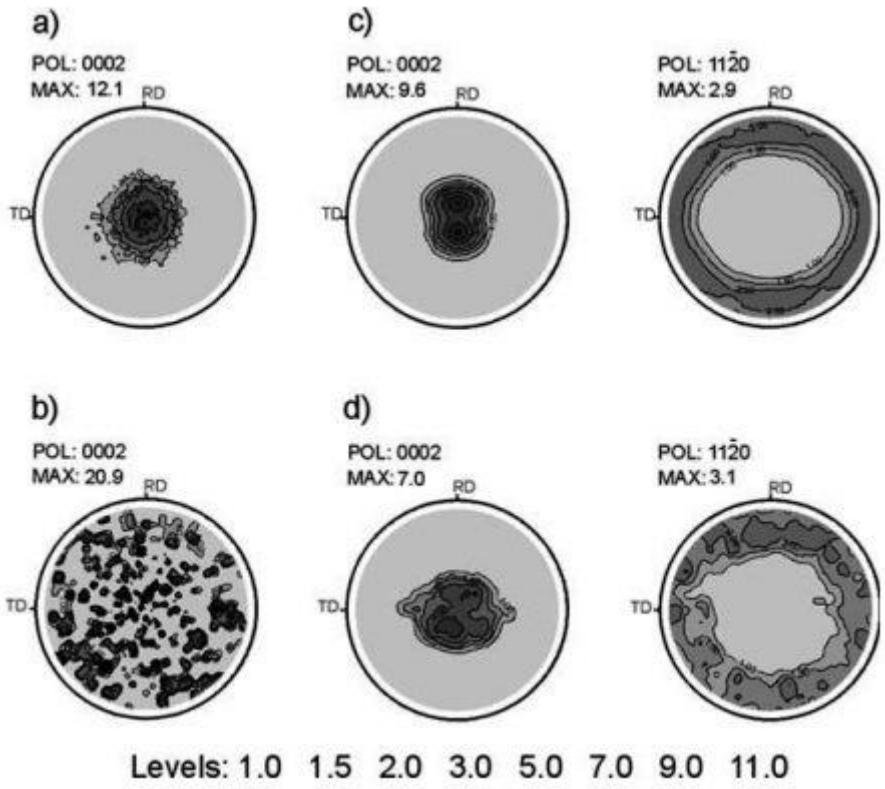

Figure 2.30: The initial texture of AZ31 (a) recrystallized sheet and (b) squeeze-cast bar. The cold rolling texture of (c) recrystallized sheet and (d) squeeze cast bar [149].

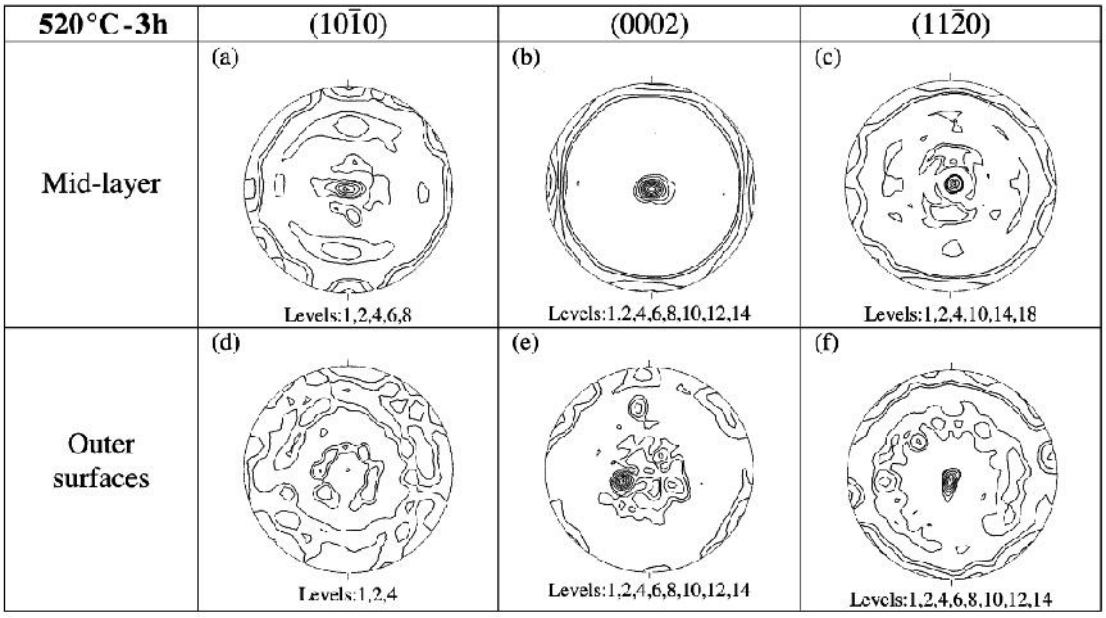

Figure 2.31: Shows the pole figures of mid-layer and the outer surface of the AZ31 alloy sheet annealed at 520^{o}C for 3hours [150].

Huang*et. al.* [154] reveal the development of double peak type texture formation with the basal planes tilted towards the rolling direction due to the activation of both basal and pyramidal slip systems duringto cold rolling (figure 2.32). Basal slip system was activated during hot rolling of AZ31 magnesium alloy. The basal texture (0002) component was the predominant during cold rolling and hot rolling.It is also revealed that annealing hadno major effect on the texture evolution.

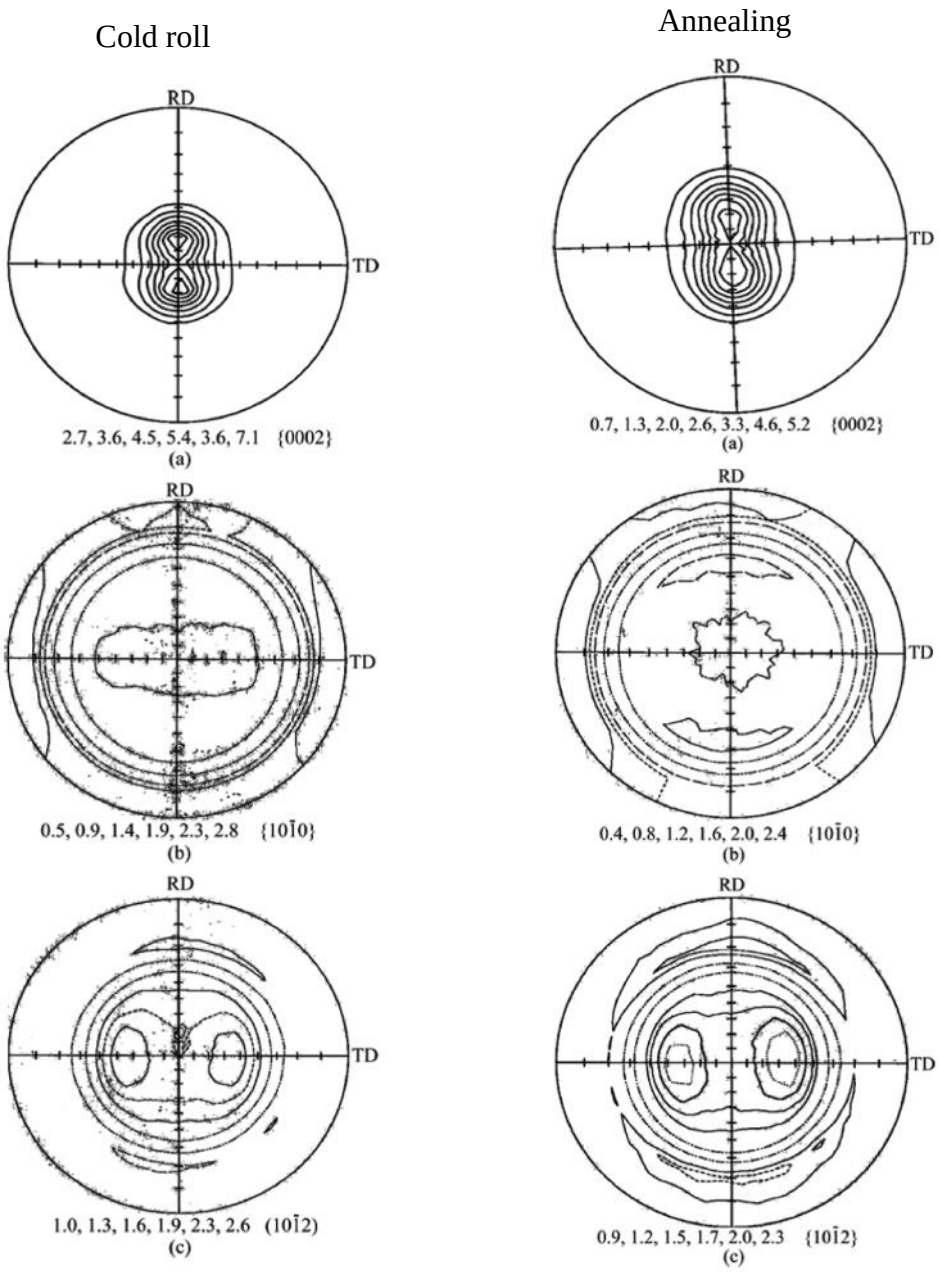

Figure 2.32: (0002), $(10\bar{1}0)$ and $(10\bar{1}2)$ pole figures of both cold-rolled and annealing samples (300^{o}C for 120 min after cold rolling) [154].

Barnett *et. al.*[155] studied the characterization of texture evolution of pure magnesium, Mg-3Al-1Zn, and Mg-0.2Ce magnesium alloy. The basal texture component was developed in all the samples (figure 2.33), while there was a significant increase in texture sharpness in Mg-0.2Ce magnesium alloy as compared to pure magnesium and Mg-3Al-1Zn alloy. The recrystallization texture of hot rolled pure magnesium sheets at a temperature below 230°C and above 230°C has been studied by Qiao *et. al.* [156]. When the pure magnesium sheet hot rolled below 230°C, the deformation texture with the basal plane (0001) perpendicular to the sheetplanes and the $<10\bar{1}0>$ direction parallel to the rolling direction has been observed due to incomplete dynamic recrystallization. However, when the sheet was hot rolled above 230°C the dynamic recrystallization hascompleted and the $\{0001\}\ <11\bar{2}0>$ texture was observedas shown in figure 2.34.

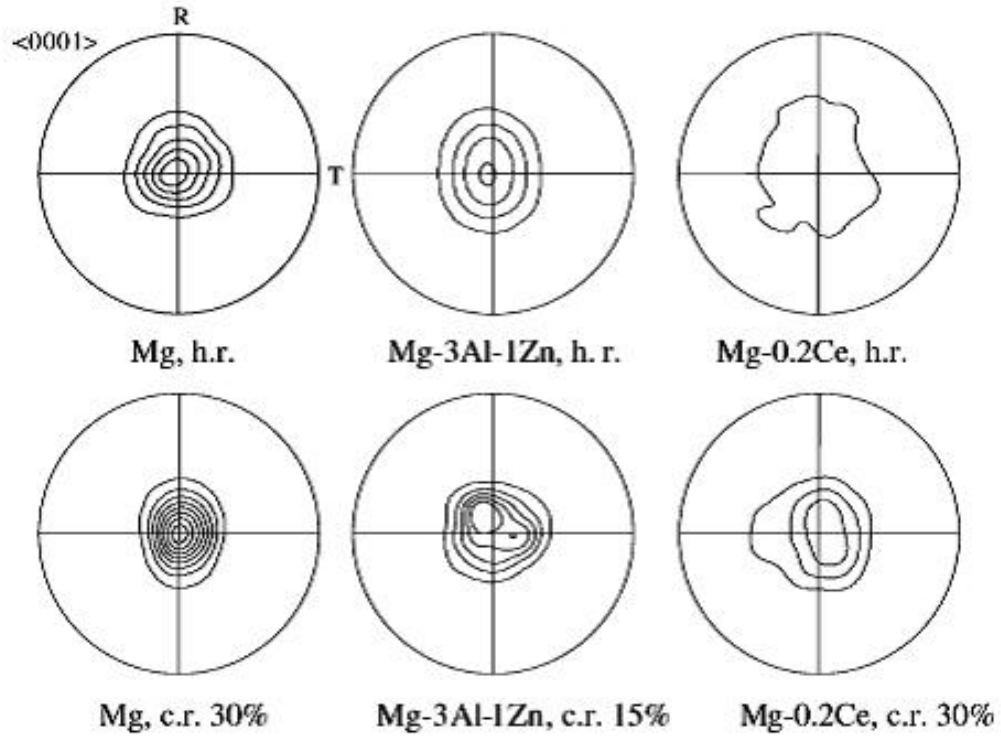

Figure 2.33: Hot rolling (h.r) and cold rolling (c.r) pole figure (0001) of pure magnesium, Mg-3Al-1Zn, and Mg-0.2Ce [155].

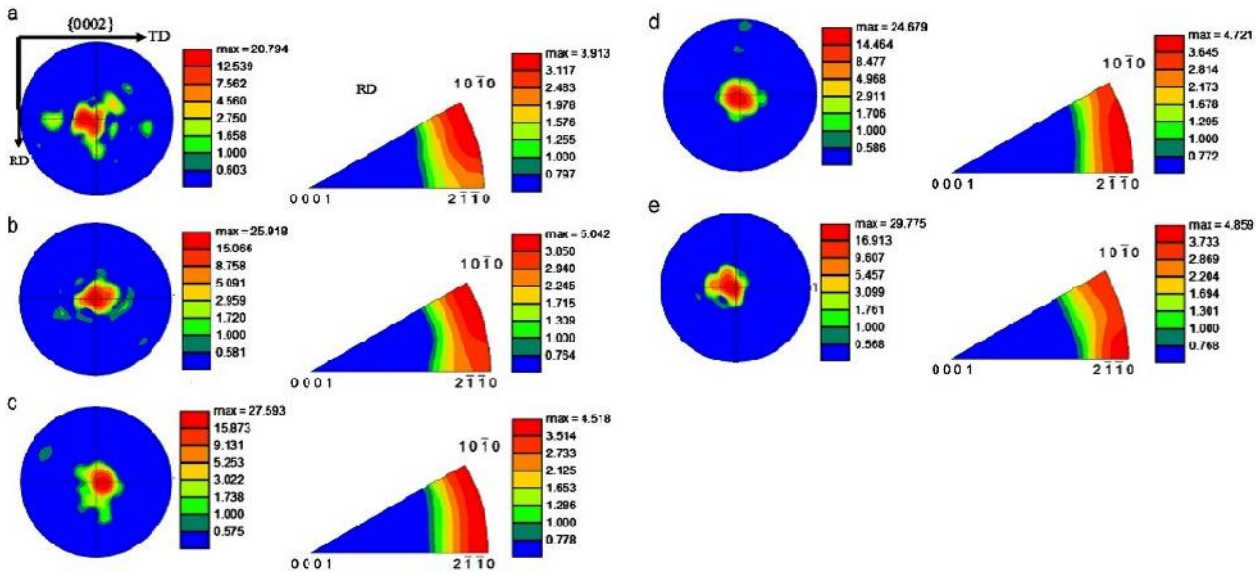

Figure 2.34: {0002} pole figures of AZ31 magnesium alloy with different rolling temperature (a) 180°C, (b) 210°C, (c) 230°C, (d) 240°C, (e) 250 °C [156].

Yue *et. al.* [158] infer that a strong wire texture was observed in AZ31 magnesium alloy perpendicular to compression axis due to dynamic recrystallization process. This texture component exists even after full annealing at high temperatures as shown in figure 2.35. He also studied the static recrystallization process in AZ31 magnesium alloy during isothermal annealing. A strong texture nearer to (0001) was developed, compared with those near $(10\bar{1}0)$ or $(11\bar{2}0)$ plane. The development of recrystallization texture was mainly controlled by grain growth without any change in texture.

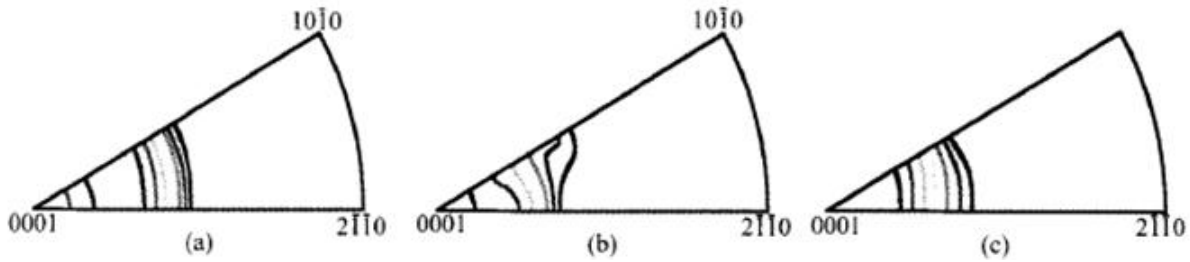

Figure 2.35: Inverse pole figures of AZ31 magnesium alloy (a) deformed at a strain rate of 1.2 and annealed at 573K, (b) deformed at a strain rate of 1and annealed at 473K, (c) deformed at a strain rate of 1 and annealed at 673K [158].

The figure 2.36 shows the development of textural components during hot rolling of AZ31 magnesium alloy at different strain rates. A strong basal $\{0002\}\ <10\bar{1}0>$ type texture was observed at low strain rates and c-axis of recrystallized grains tilts from the normal direction to the rolling direction. The double peak type basal texture was seenin the recrystallized grains with an increase in strain rate. At high strain rate, the intensity of basal $\{0002\}\ <10\bar{1}0>$ texture was decreased. A double-peak type basal texture was identified from the {0002} pole figure. The two peaks are tilted towards RD and the opposite direction of RD respectively [159].

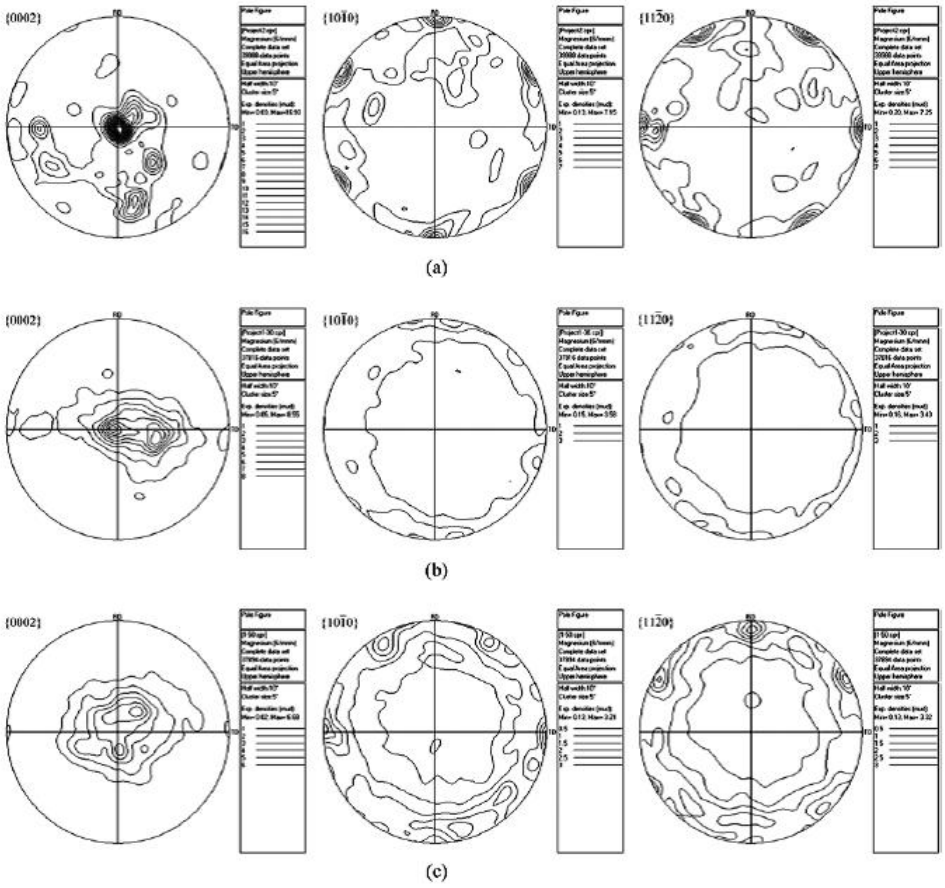

Figure 2.36: $\{0002\}$, $\{10\bar{1}0\}$ and $\{11\bar{2}0\}$ pole figures of hot rolled AZ31 magnesium alloy (a) 20% rolled, (b) 30% rolled, (c) 50% rolled [159].

Chao *et. al.* [160] observed a double-peak type basal texture and the basal pole was titled about ±10° to the normal direction of the (0002) $<10\bar{1}0>$ orientation, which is in line with the findings of Fei*et. al.* [159]. With the increase in annealing time and

temperature, a new texture component was found in the $<11\bar{2}0>$ direction parallel to the drawing plane and the intensity of the new texture component has increased with the extensiveness of recrystallization.

Li *et. al.*[161] reported on the texture and micro-texture evolution in ME20 magnesium alloy and the role of slip and twinning during hot rolling of differently orientated samples. A consistent basal texture persisted during all stages of deformation. At low strain rates the texture was a combination of two components: the initial prismatic texture component $\{12\bar{3}2\}<\bar{1}\,\bar{1}22>$ and a new off-basal component $\{10\bar{1}1\}<10\bar{1}0>$. For medium to high strain rate, the basal texture and the basal pole elongates towards rolling direction as shown in figure 2.37.

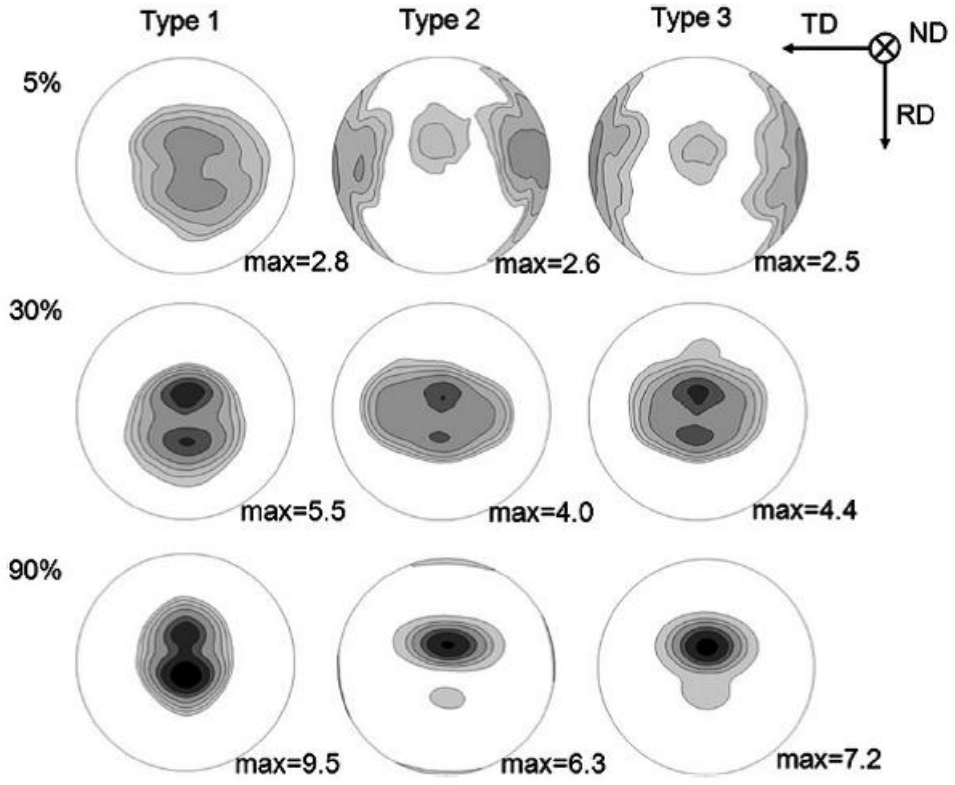

Figure 2.37: {0002} pole figures of hot rolled ME20 magnesium alloy at different rolling reductions for (a) type-1 sample, (b) type-2 sample, and (c) type-3 sample [161].

2.3.4 Recrystallization Texture of Zinc

The crystallographic texture component developed in zinc sheets is c-axis 15^o-20^o tilted away from normal direction towards rolling direction in both deformed and annealed conditions [162-167]. Some researchers also reported basal fibre component as the main texture component in zinc sheets [67]. Phillip *et. al.* [162] were the first to report on the development of deformation texture and recrystallization texture of zinc-copper-titanium and zinc-copper alloys. The development of two new fibre components centred at $\phi_1 = 90^o$, $\Phi = 90^o$, $\phi_2 = 30^o$,and $\phi_1 = 270^o$, $\Phi = 90^o$, $\phi_2 = 30^o$with c-axis 20^o away from ND towards RD.Figure 2.38 shows the development of texture during cold rolling of zinc-copper-titanium alloy and zinc – copper alloy [162]. The pole figure shows two peaks with c-axis at 20^o to ND in the ND-RD plane and two peaks with c-axis in RD. After the cold rolling of 80% reduction, the texture component observed was c-axis in RD and was developed due to the activation of pyramidal slip (pyramidal <c+a>) and/or $\{10\bar{1}2\}$ twinning mechanism. After the completion of primary recrystallization, the intensity of the cold rolling texture component along the c – axis towards RD was reduced (figure 2.39a). The cold rolling texture component in Zn-Cu alloy hadtwo peaks only, along the c-axis at 30^o to ND in the ND-RD plane (figure 2.39b).

The change in the crystallographic texture of polycrystalline zinc during deformation and recrystallization were studied by Solas*et.al.* [163]. After the deformation process at 125°C, the texture component was developed around the c-axis and tends to be oriented along the compression direction (i.e. the ND), but there are also some secondary grains orientated around c-axis close to the TD (figure 2.40a). The basal component close to the ND is rotated about 20° towards the RD. The $\{10\bar{1}0\}$ pole figure shows the uniform distribution of oriented grains in the RD-TD plane (figure 2.40b). After complete recrystallization, it has been observed that the basal component near the TD was vanished (figure 2.40c), whereas the change in texture of the prismatic pole was insignificant (figure 2.40d). During the recrystallization process the grains with the c-axis close to the TD vanishes.

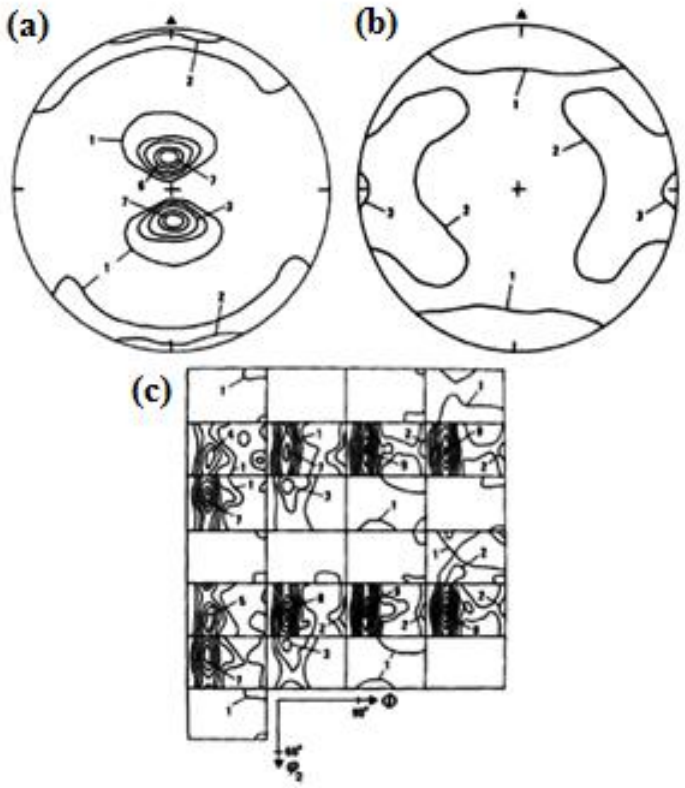

Figure 2.38: Pole and ODF figure of 80% cold rolled ZnCuTi alloy; (a) (0002) pole figure (b) (0001) pole figure and (c) ODF figure with ϕ_1= constant [162].

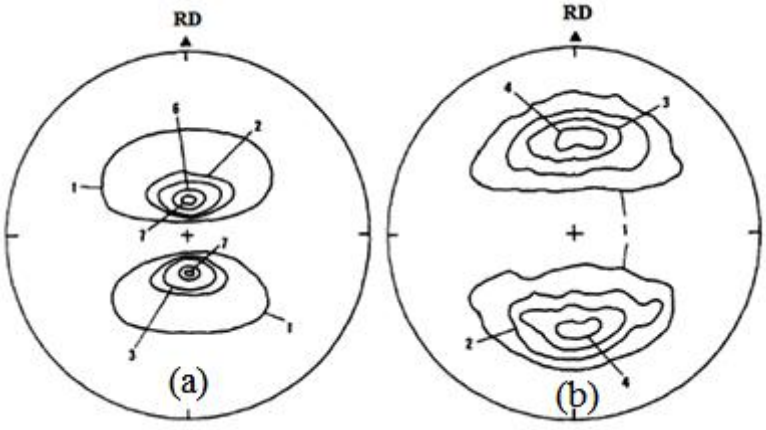

Figure 2.39: (0002) pole figures of (a) ZnCuTi recrystallized for 10 min at 80^{o}C after 80% cold roll (b) ZnCu alloy after 80% cold roll reduction [162].

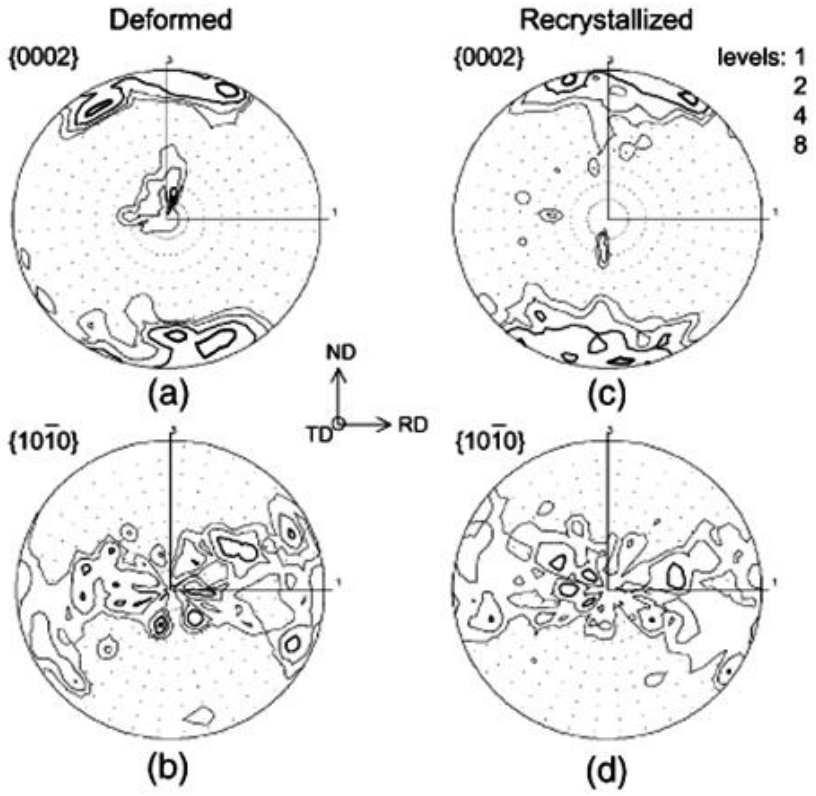

Figure 2.40: $\{0002\}$ and $\{10\bar{1}0\}$ pole figures of the deformed and recrystallized zinc [163].

2.4 Orientation Dependant Mechanical Properties of HCP Metals

It has been well accepted that 'many material properties are texture specific' [168,169]. In fact, it has been found that, in many cases, 20% – 50% values of the material properties are dependent on the texture of the material [169]. In the present study the orientation or texture dependent mechanical properties of hexagonal metals (CP-titanium and magnesium) has been investigated owing to that fact that hexagonal materials are inherently anisotropic [168-171]. In this section, the available literature on the mechanical properties of hexagonal materials pertaining to their texture or orientation has been discussed.

Hexagonal metals have fewer easy glide systems than cubic metals and possess greater crystal anisotropy [168-174]with more potential for texture strengthening. So texture control in hexagonal materials is more important in recent years [175]. Attempts

have been made to improve the mechanical properties of hexagonal metals by controlling the texture [169,170,175-180].

Zhu *et. al.* [178] investigated the relationship between texture control processes and mechanical properties in titanium sheets processed by cold rolling, cross rolling and phase transformation. Their results showed that after cold rolling and annealing, titanium sheet exhibits a strong anisotropy of mechanical properties due to the development of sharper $(\bar{2}115) < 0\bar{1}10 >$ and $(10\bar{1}3) < 1\bar{2}10 >$ pyramidal textures. During cross-rolling processes, a basal type texture or a near basal type texture was developed. The phase transformation process proved to be the best texture control process by which the $[\bar{2}110]$ and $[\bar{2}117]$ parallel to ND fibre textures were formed and the isotropic planar mechanical properties are achieved.

In pure titanium single crystals, Young's modulus and shear modulus decreases with increase in deviation from the basal orientation [176,178]. Lutjering *et. al.*[11] also obtained similar results for polycrystalline titanium. Nasiri-Abarbekoh*et. al*. [181,182] reported on the nature of basal texture and its effect on the fracture mechanism in cp-titanium. In cp-titanium, at low deformation rate a split-basal texture was observed (figure 2.41) which modified the fracture mechanism from dimple fracture in the transverse-directed specimen to intergranular fracture in the rolling-directed specimen as shown in figure 2.42 [181]. By increasing the deformation rate to 50% displayed a strong basal texture and decreased the tensile and tear properties of the sample. At high levels of deformation (>50%) the split distribution of basal texture redeveloped and anisotropy in the sample was observed again. Similarly, the phase transformation in cp-titanium was also observed by the same author. A randomly distributed widmannstatten microstructure was observed and the basal planes were alignedin the transverse direction [182]. This texture component changes the fracture mechanism from semi-ductile fracture to brittle intergranular fracture.

Several authors reported on the orientation dependent hardness of cp – titanium as well as for titanium alloys [183-187] and have found that hexagonal titanium holds the highest hardness in basal orientations as compared to non-basal orientations as shown in figure 2.43. Figure 2.44displays the variation of the hardness of Ti-6Al-4V as a function of orientation, the basal orientation shows highest hardness and the hardness value decreases with increase in deviation from the basalorientation. The elastic modulus is isotropic in the

basal plane, and it varies with the angle around an axis lying in the (0001) plane. It is already reportedthat the basal orientation has ~1.5 time higher directional modulus than the non-basal orientations.

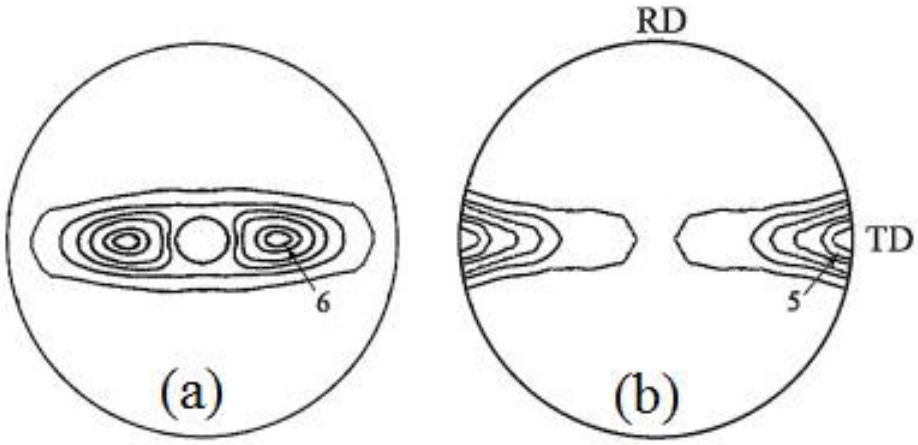

Figure 2.41: (0002) pole figure of (a) as received specimen and (b) annealed specimen [181].

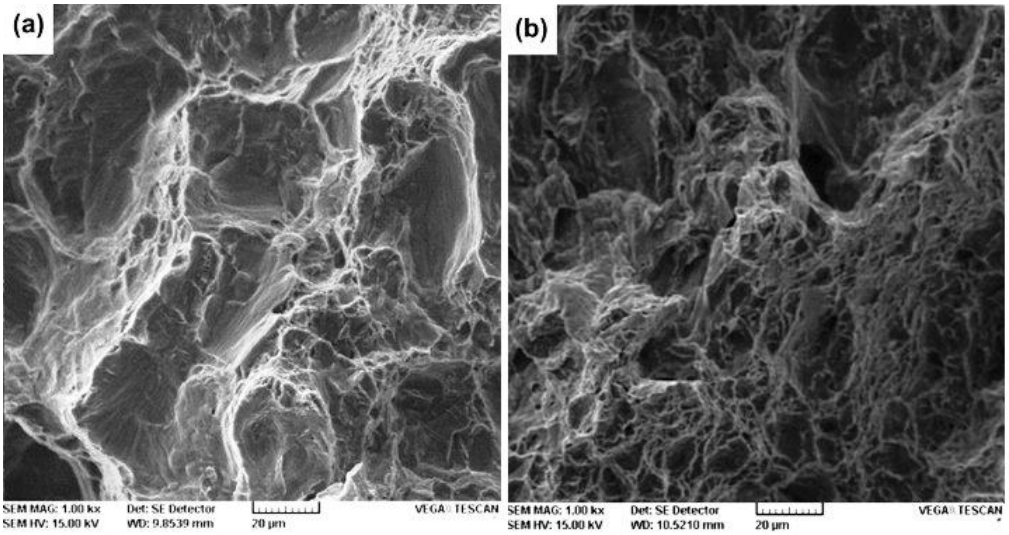

Figure 2.42: SEM micrographs of tear fracture surface (a) RD (rolling direction) sample, and (b) TD (transverse direction) sample [181].

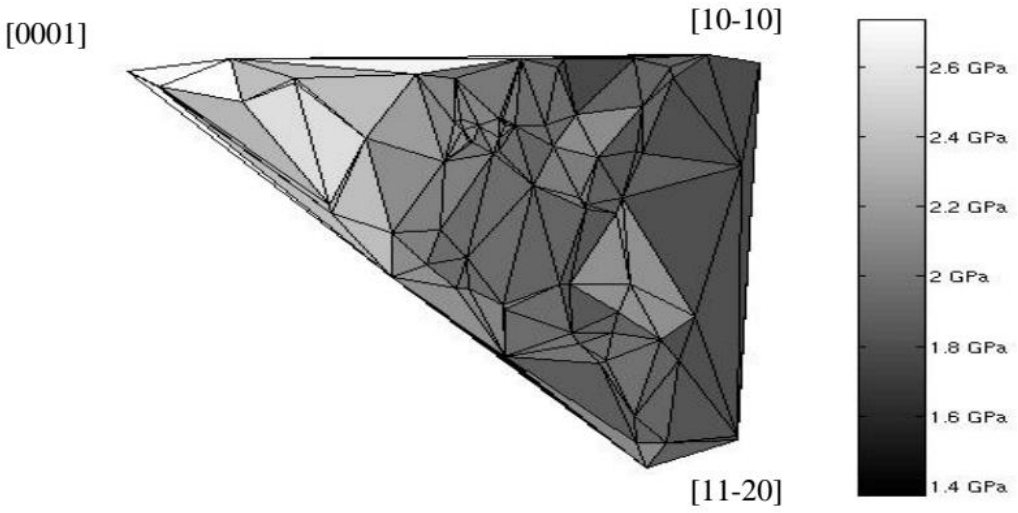

Figure 2.43: Inverse pole figure shows the orientation dependent hardness in commercially pure titanium sample. Hardness varies from 2.73 GPa for indentation parallel to basal plane (shown in white) to 1.34GPa for indents normal to basal plane (shown in black) [187].

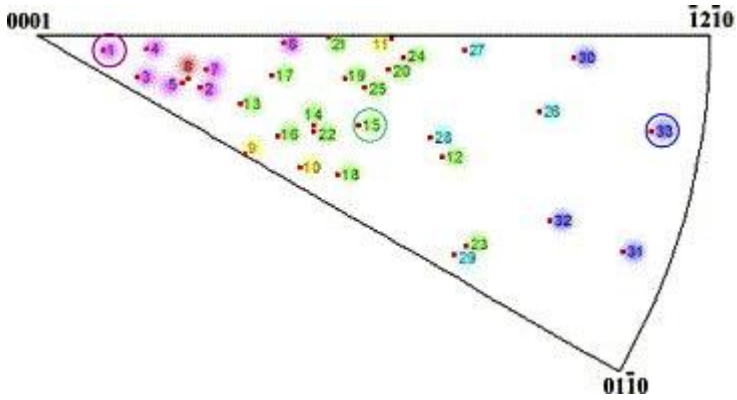

Figure 2.44: Inverse pole figure showing the hardness of individual grains/orientations in a decreasing order from basal to non-basal orientations [185].

Bache and Evans [188] reported that a highly textured unidirectional rolled Ti-6Al-4V sheet exhibits higher ultimate tensile strength and yield strength when loading in the transverse orientation i.e. loading perpendicular to the basal plane. However, the fatigue strength of Ti-6Al-4V sheets was greater when the load was applied to the longitudinal orientation i.e. loading parallel to the basal plane due to the stress relaxation is encouraged. Figure 2.45 and figure 2.46 shows the strength, ductility and the fracture strength of Ti-6Al-4V sheets in the transverse orientation loading and longitudinal orientation loading. The strength and ductility were improved due to the activation of slip systems on different orientations. The variation in fatigue strength was due to the change

of stress relaxation during cyclic loading parallel to the longitudinal direction as a result of the preferential arrangement of $\{10\bar{1}0\}$ prismatic planes.

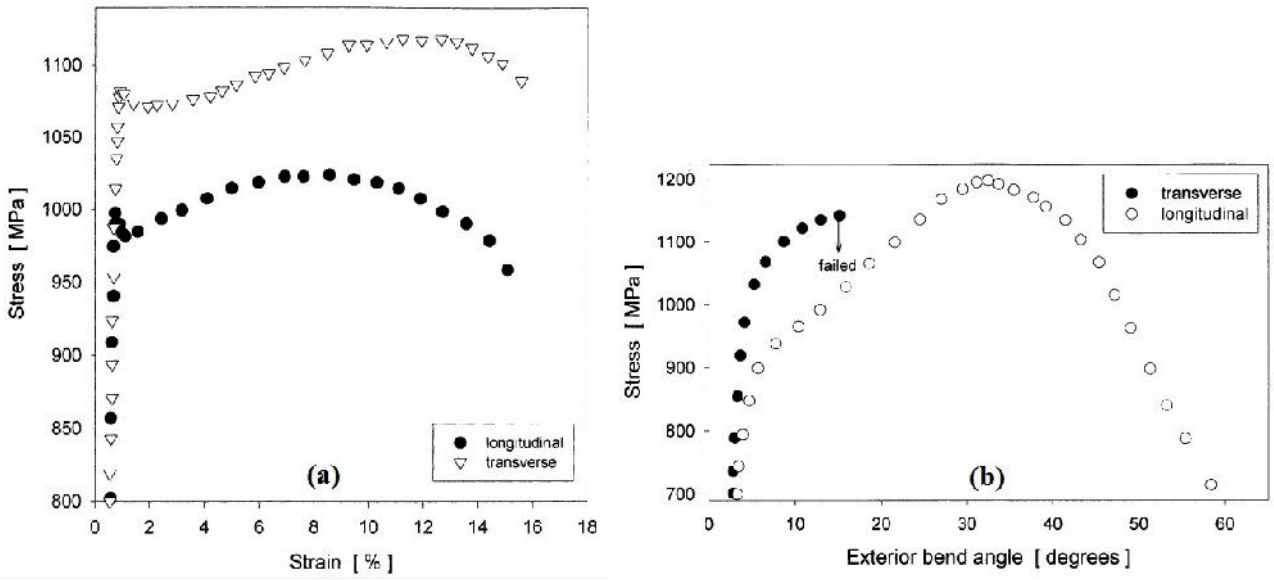

Figure 2.45: (a) Stress–strain curves for specimens orientated parallel to the longitudinal transverse plate rolling directions and (b) Ductility bend tests for specimens orientated parallel to the longitudinal and transverse plate rolling directions [188].

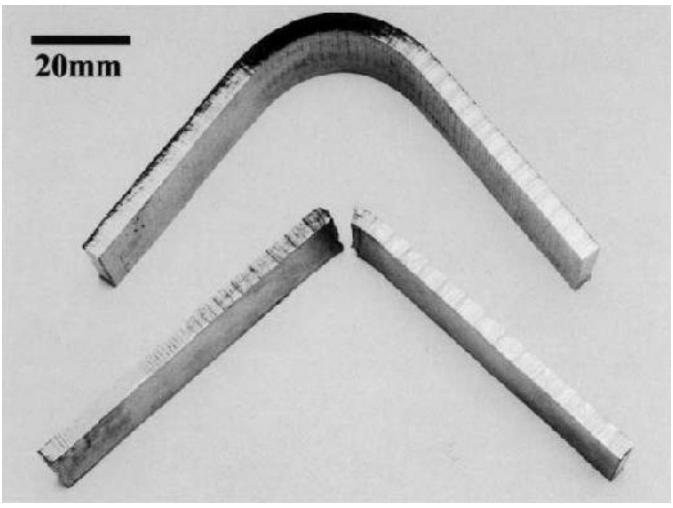

Figure 2.46: Longitudinal (top) and transverse (bottom) specimens after bend testing [188].

Magnesiumwas found to besoft when tested in tension along c-axis with twinning and hard in compression without twinning [189-191]. On the other hand, magnesium possess high strength when tensile force lying in the basal plane. So, the knowledge of active deformation modes allows us to determine the optimum conditions for texture strengthening in magnesium. For example in extruded magnesium alloys, the $<10\bar{1}0>$ directions are parallel to the extrusion direction (ED), and this deliberates high tensile strength along the ED although with low compressive strength [192].

Barnet *et.al*. [191] studied the evolution of hot-working flow stress of AZ31 magnesium alloy with strain during channel die compression. Three differently oriented channel die compression was done such as the "*c*-axis compression", "*c*-axis extension", and "*c*-axis constraint" conditions as shown in figure 2.47. The influence of orientation on the flow stress is shown in figure 2.48. The main difference of flow stress orientation at low strain is due to the restricted number of slip systems available in magnesium. At room temperature slip in magnesium occurs predominantly by basal slip, while prismatic and pyramidal slip becomes more noticeable with increase in temperature. Twinning also readily activated on $\{10\bar{1}2\}<10\bar{1}1>$ system. When deformation occurs in the condition of *c*-axis constraint, the prismatic <*a*> slip systems will be favourable in this orientation and results in the low flow stress and low strain hardening rate. When deformation happens in the condition of *c*-axis compression, the prismatic <*a*> slip systems will be difficult to activate in this orientation, and hence the deformation is mainly activated by the pyramidal $\{11\bar{2}2\}<11\bar{2}3>$ slip system and will result in the high flow stress and high strain hardening rate. When deformation occurs in the condition of *c*-axis extension, the prismatic <*a*> slip systems will be unfavourable to activate and the pyramidal $\{11\bar{2}2\}<11\bar{2}3>$ slip system and twinning on the $\{10\bar{1}2\}<10\bar{1}1>$ system plays the major role to bring the *c*-axis alignment with the plate normal and compression will then become the principal deformation mode, so moderate flow stress and strain hardening rate can be achieved.

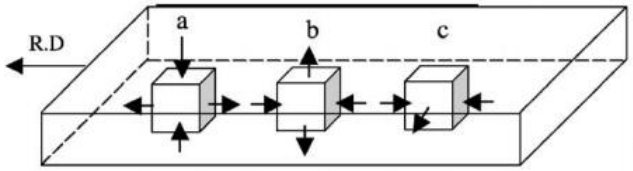

Figure 2.47: Orientation of the AZ31 Mg samples with texture reference frame under: (a) c- axis compression; (b) c-axis extension; and (c) c-axis constraint [189].

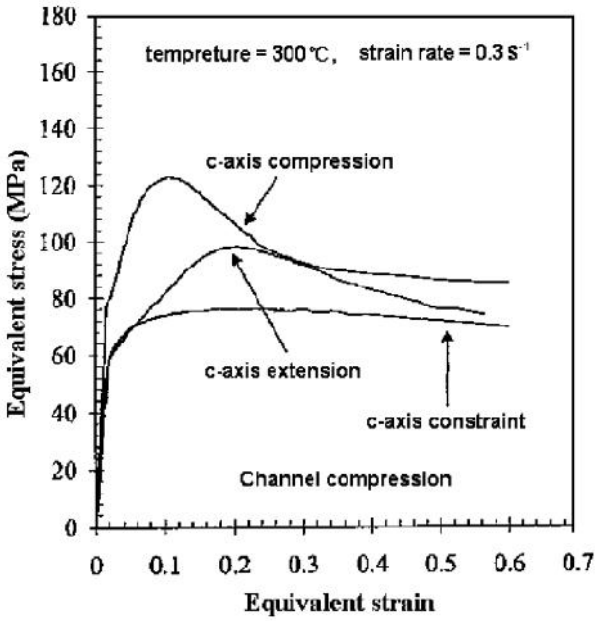

Figure 2.48: Flow stress–Equivalent strain curves of the AZ31 Mg alloy tensile tested at 300^{o}C and 0.3 s^{-1} [189].

Yuan *et. al*. [193] reported a strong crystallographic orientation along ED || $<10\bar{1}0>$ direction in the as-extruded Mg–5Zn–1Mn alloy. This shows higher yield strength and tensile strength in the ED and exhibits higher ductility and thermal conductivity in the transverse direction. The variation of mechanical response in ED is due to the orientation and activation of slip systems. As the spread of the basal orientation was observed towards ED and most of the grains parallel to ED and also the Schmidt factor of crystals in this direction is close to zero. As a result, the basal slip system is tough to activate for which the strength increases in this direction. In the TD, a prominent basal texture was observed.It decreases the ductility and the deformation turn out to be inhomogeneous and is ruled by the formation of shear bands.

Zhang *et. al*. [194] reported that with the weakening of the basal texture, the elongation was interestingly increased over 64% in Mg–Y–Nd–Zr alloy as shown in figure 2.49. Also in AZ31 alloy with the weakening of basal fibre texture the tensile strength and elongation increases [192] as shown in figure 2.50. Serebryany *et. al.* [195] reported on the correlation of crystallographic texture and strength of hot compressed Mg-Y-Gd-Zr alloy. With the weak basal and prismatic texture, the alloy possesses higher strength at room temperature and irregularity of the yield stress during tension and compression. Conventional wrought magnesium alloys also possess asymmetry in the yield strength of basal planes. The yield strength in tension is higher than that in compression [196]. However, ductility can be higher when the basal plane is oriented at 45° to the applied stress direction due to the easily activation of basal dislocations [190].

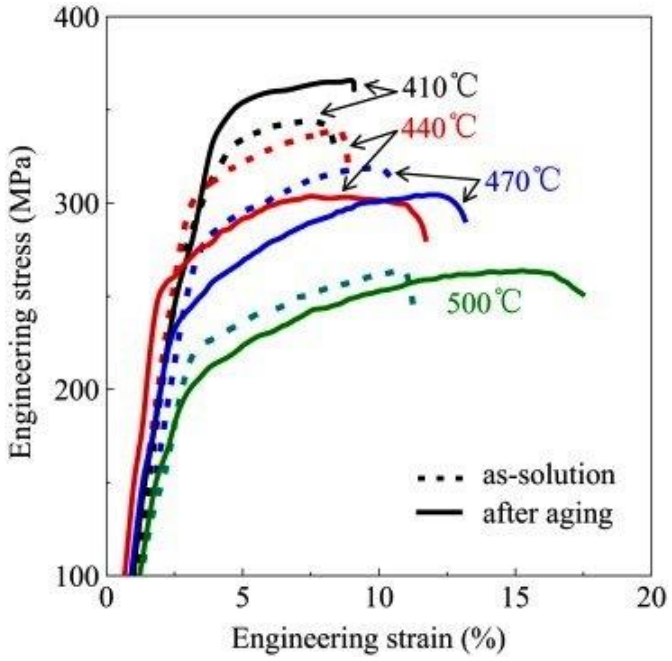

Figure 2.49: Effect of heat treatment on typical engineering stress–strain curves tensile tested at room temperature for Mg–Y–Nd–Zr alloy, after hot deformation to ε=1.5 at various temperatures from 410 to 500 ^{o}C [194].

Like hexagonal titanium, magnesium possesses high hardness at the basal orientation than compared to non-basal orientations and hardness also increases with increase in the rate of deformation (figures 2.51 and 2.52) [197]. Guang-sheng *et. al*. [198] proposed that the mechanical properties of the AZ31 magnesium alloy can be improved by

processing through repeatedly unidirectional bending (RUB) with the basal texture component. The AZ31 sheets experiencing RUB at room temperature and subsequent annealing at 533 K shows optimum mechanical properties. Whereas RUB at medium to high temperature and subsequent annealing at 533 K possess low yield strength and fracture elongation.

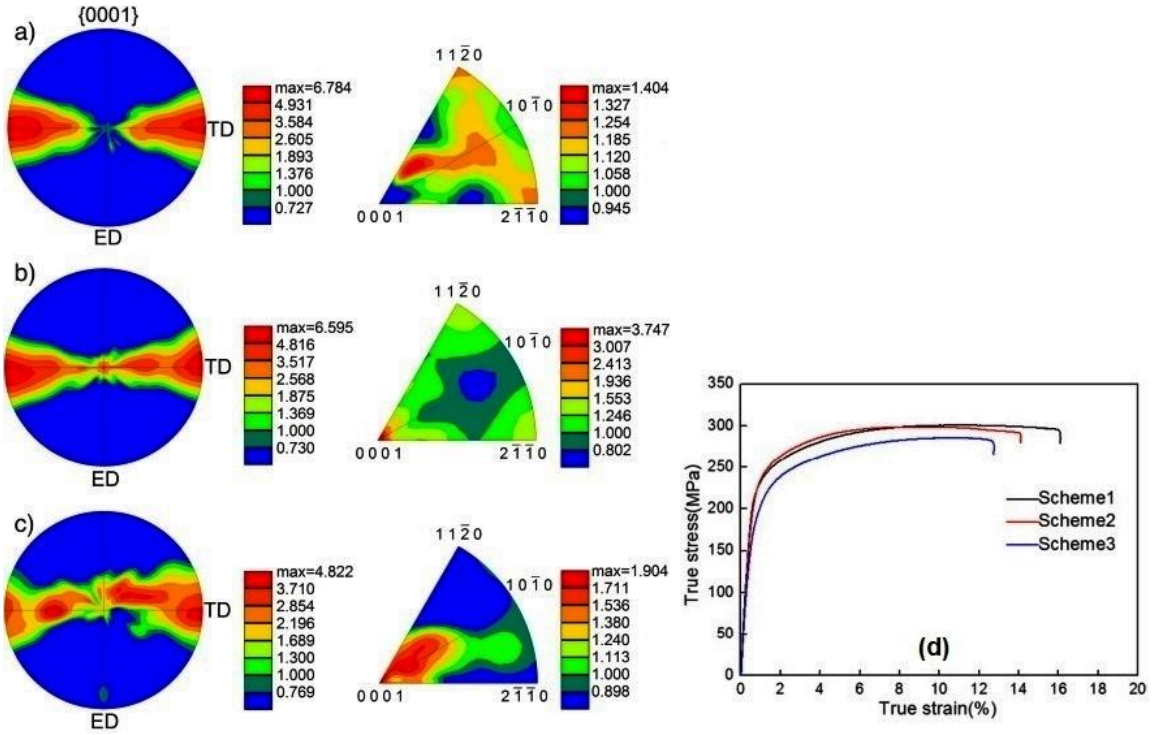

Figure 2.50: {0001} pole figure and inverse pole figures showing the orientation of differently strained samples, (a) Scheme1 (b) Scheme2 (c) Scheme3 and (d) Stress-Strain curves of three schemes [192].

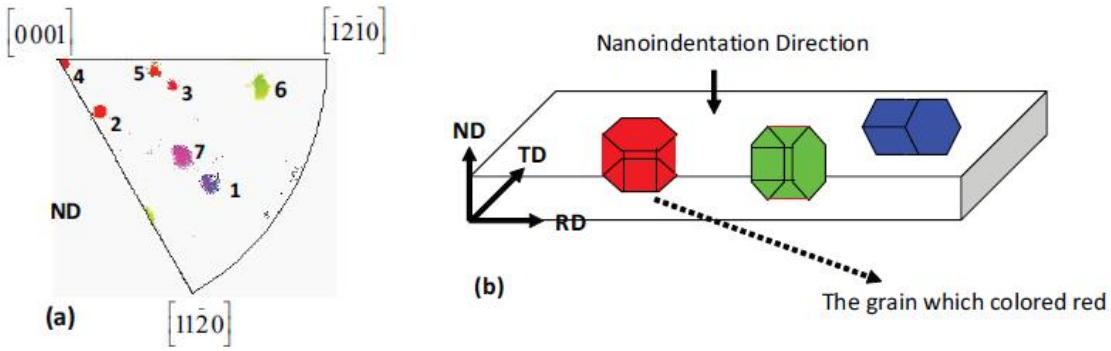

Figure 2.51: (a) Showing the hardness of individual grains/orientation in [0001] inverse pole figure, (b) orientations of the grains in hot rolled pure magnesium sheet [197].

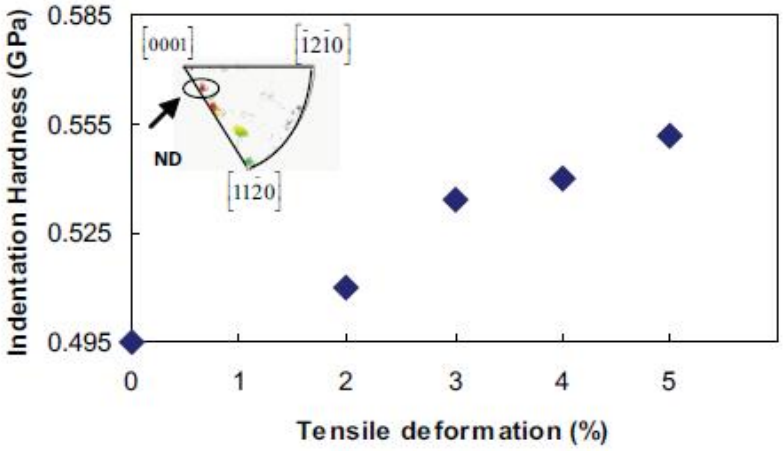

Figure 2.52: Showing indentation hardness as a function of tensile deformation [197].

Agnew *et. al*. [199] studied the relationship between mechanical properties and texture evolution of AZ31B alloy. The mechanical property such as ductility was increased with the rise in temperature and was accompanied by a decrease in the flow stress. Also, an increase in strain rate sensitivity and reduction in normal anisotropy was observed. This change in anisotropy was perceived due to activation of non-basal <c+a> slip and tensile twinning during deformation. The texture observed during this study was the basal component rotated away from the compression axis by ~20°, by which the compressive ductility dramatically increases over the tensile ductility. Foley *et. al.* [200] reported that by controlling the texture through step-down equal channel angular extrusion (ECAE) processing the mechanical properties can be modified as shown in figure 2.53. The result shows that the highest tensile strength is observed in the flow direction (FD) and lowest tensile strength in the longitudinal direction (LD).

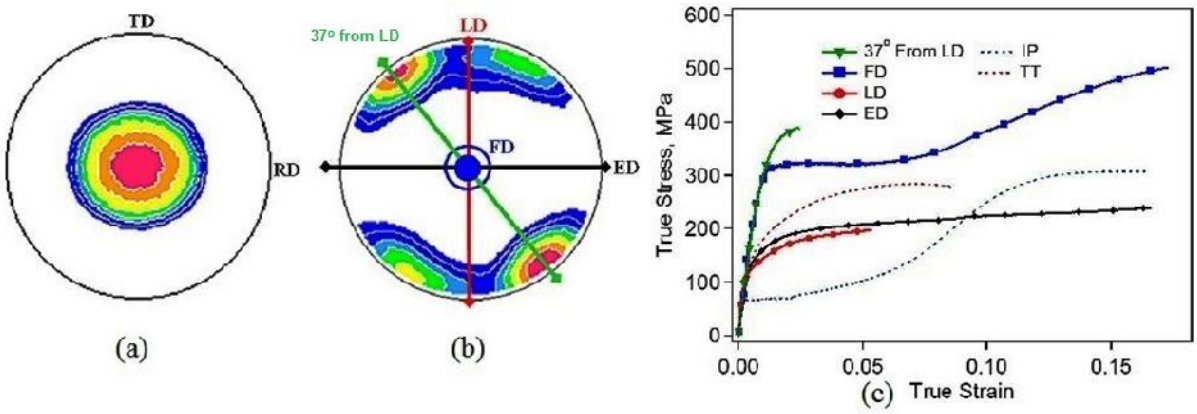

Figure 2.53: (0002) pole figures for (a) the hot-rolled and annealed AZ31B Mg alloy recorded on the rolling plane and (b) the ECAE processed sample taken on the flow plane. Directional arrow colours correspond with the different orientations and compression curves in (c) FD (flow direction); LD (longitudinal direction); ED (extrusion direction) [200].

The mechanical properties of zinc such as bendability, creep, hardness, and cracking are directly linked to the preferred orientation [162,165-167,170,201-203]. The rolled zinc sheets show excellent bendability and creep behaviour with the basal orientation deviate 20^{o} away from the ND towards RD [162,165,167,170,201]. Zhang *et. al*. [167] observed that in ZnCuTi alloy the mechanical properties such as the bendability behaviour at low temperature was improved by the evolution of favourable orientation when processed through asymmetric rolling. Vincent *et. al*. [201] reported that bendability and cracking behaviour can be enhanced by the asymmetric skin-pass rolling with the favourable orientation. The bendability and creep behaviour are improved by the evolution of the sharper basal texture 20^{o} away from the ND towards RD but at the same time, the yield strength can be decreased when processed through reverse shear loading [204]. Pure zinc processed through high-pressure torsion (HPT) displays very high strength and excellent ductility along the in-plane direction due to the activation of non-basal slip systems (figure 2.54) [166]. Several authors reported the effect of preferred orientation on the hardness of zinc deposits, and they investigated that prism texture component offers highest hardness [202-205]. Saber*et. al*. [202] proposed the highest hardness values of nanocrystalline zinc when the preferred orientation of the zinc deposits was the prismatic $(11\bar{2}0)$ texture.

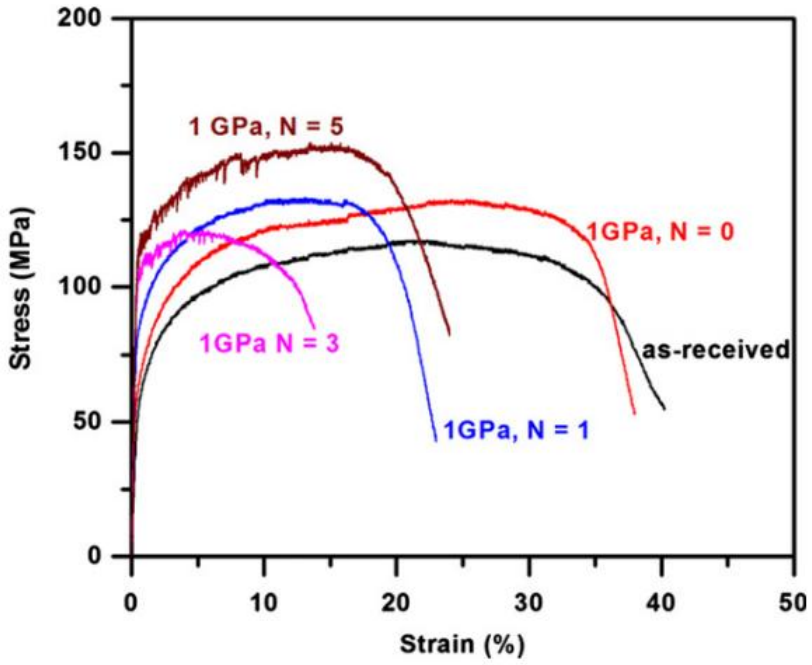

Figure 2.54: Stress–strain curves corresponding to pure Zn tested in tension at room temperature and $3X10^{-3}S^{-1}$before and after processing by HPT. In as-received material the tensile axis is perpendicular to the extrusion direction and in the HPT-processedspecimens, it is perpendicular to the disk normal [166].

References

[1] J. Barksdale, Titaniumin *The Encyclopedia of the Chemical Elements*, Reinhold Book Corporation, New York, 1968, p.732.

[2] R. Boyer, G. Welsch and E. W. Collings, *Materials properties handbook: Titanium alloys*, ASM International, Materials Park, OH, 1993.

[3] M. Hunter, Journal of American Chemical Society, 32 (1910) p.330.

[4] A. Zarkades and F. Larson, *The Science, Technology and Application of Titanium*, The Institute of Metals, Oxford, 1970.

[5] R. Boyer, Materials Science and Engineering A, 213 (1996) p.103.

[6] M. Peters, J. Hemptenmacher, J. Kumpfert and C. Leyens, Structure and Properties of Titanium and Titanium Alloys in *Titanium and Titanium Alloys:Fundamentals and Applications*, Wiley-VCH Verlag GmbH & Co. KGaA, Weinheim, 2003, p.1.

[7] M. Jackson and R. R. Boyer, Titanium and its Alloys: Processing, Fabrication and Mechanical Performance in *Encyclopedia of Aerospace Engineering*, John Wiley & Sons Ltd., Chichester, 2010.

[8] C. Leyens and M. Peters, *Titanium and Titanium Alloys: Fundamentals and Applications*, Wiley-VCH Verlag GmbH & Co. KGaA, Weinheim, 2003.

[9] S. Seong, O. Younossi, B.W. Goldsmith, T. Lang, and M. Neumann, *Titanium: industrial base, price trends, and technology initiatives,* Rand Corporatio,Santa Monica, CA, 2009, p.10.

[10] M. Yamada, Materials Science and Engineering A, 213 (1996) p.8.

[11] G. Lütjering and J. C. Williams, *Titanium*, Springer-Verlag, New York, 2003.

[12] J. Newkirk and A. Geisler, Acta Metallurgica, 1 (1953) p.370.

[13] J. Donachie, *Titanium: A technical Guide*, ASM International, Materials Park, OH, 1988.

[14] M. K. Mcquillan, *Titanium*, Butterworths Scientific, London, 1956.

[15] E. Collings, *The Physical Metallurgy of titanium Alloys*, American Society for Metals, Metals Park, OH, 1984.

[16] W. G. Burgers, *Rekristallisation, verformter Zustand und Erholung*, Akademischer

Verlagsgesellschaft, Leipzig, 1941.

[17] Y. N. Wang and J. C. Huang, Materials Chemistry and Physics, 81 (2003) p.11.

[18] M. Niewczas, Acta Materialia,58 (2010) p.5848.

[19] B. Lei, PhD Thesis,Universite Paul Verlaine-Metz, France, 2011.

[20] E. I. Galindo-Nava, Materials and Design, 83 (2015) p.327.

[21] J. W. Christian and S. Mahajan, Progress in Materials Science, 39 (1975) p.1.

[22] N. E. Paton and J. C. Williams, in *proceedings of 2nd International Conference on Strength of Metals and Alloys*, Metals Park, OH, 1970.

[23] M. Jackson and K. Dring, Materials Science and Technology, 22 (2013) p.881.

[24] I. Polmear, *Light Alloys-Metallurgy of the Light Metals*, John Wiley and Sons, New York, 1995.

[25] E. Kleefisch, *Industrial Application of Titanium and Zirconium*, ASTM International, West Conshohocken, PA, 1981.

[26] R. Abbaschian and R. Reed-Hill, *Physical Metallurgy Principals*, Cengage Learning India, New Delhi, 2008.

[27] L. M. Gammon, R. D. Briggs, J. M. Packard, K. W. Batson, R. R. Boyer and C. W. Domby, Metallography and Microstructures of Titanium and Its Alloys in *Metallography and Microstructures of Nonferrous Alloys*, ASM International, Metals Park, OH, 2004, p.899.

[28] J. Emsley, *Titanium, Nature's Building Blocks: An A-Z Guide to the Elements*, Oxford University Press, Oxford, 2001.

[29] P. E. Denney and D. E. A. Metzower, *Laser Beam Welding of Titanium*, Welding Research Suppliment, New York, 1989.

[30] K. Kubiak and J. Sieniawski, Journal of Materials Processing Technology, 78 (1998) p.117.

[31] V. Sevan, *Rosoboronexport controls titanium in Russia*, Sevanco Strategic Consulting, Norway, 2006.

[32] D. R. Lide, *CRC Handbook of Chemistry and Physics*, CRC Press, Boca Raton (FL) 2005.

[33] M. M. Avedesian and H. Baker, *ASM Specialty Handbook: Magnesium and Magnesium Alloys*, ASM International, Metals Park, OH, 1999.

[34] H. Davy, Philosophical Transactions of the Royal Society of London, 98 (1808) p.333.

[35] E. Aghion and B. Bronfin, Materials Science Forum, 350-351 (2000) p.19.

[36] H. Friedrich and B. L. Mordike, *Magnesium Technology: Metallurgy, Design Data, Applications*, Springer-Verlag, Berlin, Heidelberg, 2006.

[37] K. U. Kainer, *Magnesium alloys and their applications*, Wiley-VCH, Weinheim, 2008.

[38] B. L. Mordike and T. Ebert, Materials Science and Engineering A, 302 (2001) p.37.

[39] S. B. Yi, S. Zaefferer and H. Brokmeier, Materials Science and Engineering A, 424 (2006) p.275.

[40] M. R. Barnett, N. Stanford, P. Cizek, A. Beer, Z. Xuebin and Z. Keshavarz, Journal of The Minerals, Metals & Materials Society, 60 (2009) p.19.

[41] M. R. Barnett, Materials Science and Engineering A, 464 (2007) p.8.

[42] H. Fan and J. A. El-Awady, Journal of Applied Mechanics,82 (2015) p.101006(1).

[43] R. E. Reed-Hill and W. D. Robertson, Acta Metallurgica, 5 (1957) p.717.

[44] T. Obara, H. Yoshinga and S. Morozumi, Acta Metallurgica, 21 (1973) p.845.

[45] H. Yoshinga, T. Obara and S. Morozumi, Materials Science and Engineering, 12 (1973) p.255.

[46] J. T. Black and A. K. Ronald, *DeGarmo's Materials and Processes in Manufacturing*, Wiley, Hoboken, 2011.

[47] A. Lindemann, J. Schmidt, M. Todte and T. Zeuner, Thermochimica Acta, 382 (2002) p.269.

[48] L. Čížek, M. Greger, L. A. Dobrzański, I. Juřička, R. Kocich, L. Pawlica and T. Tański, Journal of Achievements in Materials and Manufacturing Engineering,18 (2013) p.203.

[49] C. Bettles and M. Gibson, Journal of the Minerals, Metals, and Materials Society, 57 (2005) p.46.

[50] M. Easton, A. Beer, M. R. Barnett, C. Davies, G. Dunlop, Y. Durandet, S. Blacket, T. Hilditch and P. Beggs, Journal of the Minerals, Metals, and Materials Society, 60 (2008) p.57.

[51] N. N. Greenwood and A. Earnshaw, *Chemistry of the Elements*, Butterworth-

Heinemann, Oxford, 1997.

[52] J. Emsley, *Zinc Nature's Building Blocks: An A-Z Guide to the Elements*, Oxford University Press, Oxford, 2001.

[53] M. Tisaz, *Physical Metallurgical for Engineers*, ASM Internal and Freund Publishing House Ltd., London - Tel Aviv, 2002, p.383.

[54] R. Bell and R. Cahn, Proceedings of the Royal Society A, 239 (1957) p.494.

[55] R. E. Cooper and J. Washburn, Acta Metallurgica, 15 (1967) p.639.

[56] P. T. Craddock, Journal of Archaeological Science, 5 (1978) p.1.

[57] R. N. Caron and J. T. Staley, Zinc and Zinc Alloys: Effects of composition, Processing and Structure on Properties of Nonferrous Alloys in *ASM Handbook Volume 20: Materials Selection and Design*, G. E. Dieter, ed., ASM International, Materials Park, OH, 1997.

[58] M. Bounoughaz, E. Salhi, K. Benzine, E. Ghali and F. Dalard, Journal of Materials Science,38 (2003) p.1139.

[59] A. Stwertka, *"Zinc". Guide to the Elements*, Oxford University Press, Oxford, 1998.

[60] Q. Ashton Acton, PhD, *Zinc Compounds—Advances in Research and Application*, Scholarly Editions, Atalanta, Georgia, 2013.

[61] X. G. Zhang, *Corrosion and Electrochemistry of Zinc*, Springer Science & Business Media, Berlin, 1996.

[62] R. D. Doherty, Progress in Materials Science, 42 (1997) p.39.

[63] A. D. Rollett, F. J. Humphreys, G. S. Rohrer and M. Hatherly, *Recrystallization and Related Annealing Phenomena*, Elsevier Ltd., Amsterdam, 2004.

[64] R. D. Doherty, Scripta Metallurgica, 19 (1985) p.927.

[65] R. H. Hobrock, Journal of the Aeronautical Sciences, 3 (1936) p.191.

[66] F. Haessner, *Recrystallization of Metallic Materials*, Rieder-Verlag, Stuttgart, 1978.

[67] F. J. Humphreys, Acta Materialia, 45 (1997) p.4231.

[68] P. P. Bhattacharjee, N. Tsuji and R. K. Ray, Metallurgical and Materials Transactions A, 42 (2011) p.2769.

[69] J. P. Sah, G. J. Richardson and C. M. Sellars, Metal Science, 8 (1974) p.325.

[70] O. Daaland and E. Nes, Acta Materialia, 44 (1996) p.1415.

[71] N. N. Stanford and M. R. Barnett, Scripta Materialia, 58 (2008) p.179.

[72] L. Mackenzie and M. Pekguleryuz, Scripta Materialia, 59 (2008) p.665.

[73] K. Hantzsche, J. Bohlen, J. Wendt, K. Kainer, S. Yi and D. Letzig, Scripta Materialia, 63 (2010) p.725.

[74] F. J. Humphreys, Acta Materialia, 45 (1997) p.5031.

[75] E. Hornbogen and U. Köster, *Recrystallization of Metallic Materials*, Riederer Verlag GmbH, Stuttgart, 1978, p.159.

[76] J.H. Ryu, Y.S. Lee and D. N. Lee, Metals and Materials International, 7 (2001) p.251.

[77] K. Kashihara and H. Inagaki, Materials Transactions, 3 (2009) p.528.

[78] M. Wrobel and S. Dymek, Archives of Metallurgy,42 (1997) p.151.

[79] A. Bhattacharyya, D. Rittel and G. Ravichandran, Metallurgical and Materials Transactions A, 37A (2006) p.1137.

[80] I. Ulacia, N. Dudamell, F. Gálvez, S. Yi, M. Pérez-Prado and I. Hurtado, Acta Materialia, 58 (2010) p.2988.

[81] D. N. Lee and S. H. Hong, Recrystallization textures of plane strain rolled polycrystalline aluminum alloys and copper in *Recrystallization and Grain Growth*, Springer-Verlag, Berlin, 2001.

[82] A. Etter, M. Mathon, T. Baudin, V. Branger and R. Penelle, Scripta Materialia, 46 (2002) p.311.

[83] S.-H. Hong and D. N. Lee, Journal of Engineering Materials and Technology, 124 (2002) p.13.

[84] N. Rajmohan, Y. Hayakawa, J. A. Szpunarl and J. Root, International Centre for Diffraction Data, Advances in X-ray Analysis, 42 (2000) p.460.

[85] G. Mohamed and B. Bacroix, Acta Materialia, 48 (2000) p.3295.

[86] G. Guiglionda, A. Borbély and J. Driver, Acta Materialia,52 (2004) p.3413.

[87] G. L. Ferran, R. D. Doherty and R. W. Cahn, Acta Metallurgica, 19 (1971) p.1019.

[88] L. M. Clarebrough, M. E. Hargreaves and G. W. West,Proceedings of The Royal Society A, 232 (1955) p.252.

[89] B. J. Duggan and W. B. Lee, *in Proceedings of the 8th International Conference on Textures of Materials*, J. S. Kallend and G. Gottstein, eds., TMS Mechanical

Metallurgy Committee, Warrendale, 1988, p.625.

[90] C. S. Barrett and T. Massalski, *Structure of Metals*, Pergamon Press, Oxford, 1980.

[91] P. J. Appsa, J. R. Bowenb and P.B. Prangnell, Acta Materialia, 51 (2003) p. 2811.

[92] S. S. Gorelik, *Recrystallization in Metals and Alloys,* MIR Publishers, Moscow, 1981.

[93] K. Lucke, Zeitschrift für Metallkunde, 52 (1961) p.1.

[94] M. O. Dimitrov, Comptes Rendus de l'Académie des Sciences, 247 (1958) p.25.

[95] H. R. Wenk and P. V. Houtte, Reports on Progress in Physics, 67 (2004) p.1367.

[96] O. Engler, Acta Materialia, 48 (2000) p.4827.

[97] O. Engler, Acta Materialia, 49 (2001) p.1237.

[98] O. Engler, X. W. Kong and K. Lücke, Acta Materialia, 49 (2001) p.1701.

[99] G. Gottstein, *Physicalische Grundlagen der Materialkunde*, Springer-Verlag, Berlin-Heidelberg, 2001.

[100] R. Higginson, C. Pinna, J. Beynon and B. Wynne, Materials Science and Technology, 19(4) (2003) p.477.

[101] J. Nah, H. Kang, M. Huh and O. Engler, Scripta Materialia, 58 (2008) p.500.

[102] R. Higginson, A. MacGregor and E. Palmiere, Materials Science Forum, 396-402(1) (2002) p.303.

[103] I. A. Ginden, Y. D. Starodubov and V. I. Khotkevich, Fizika Metallov I Metallovedenie, 24 (1967) p.149.

[104] W. M. Williams and R. Eborall, Journal of the Institute of Metals, 81 (1953) p.501.

[105] R. J. Garbor, I. A. Ginden, B. G. Lazerew and Y. D. Starodubov, Soviet physics, Solid state, 2 (1960) p.991.

[106] S. H. Hong and D. N. Lee, Materials Science and Engineering A, 351 (2003) p.133.

[107] H.-J. Shin, H.T. Jeong and D. N. Lee, Materials Science and Engineering A, 279 (2000) p.244.

[108] S. H. Hong and D. N. Lee, ISIJ International, 42 (2002) p.1278.

[109] I. L. Dillamore, C. J. E. Smith and T. W. Watson, Material Science and Technology,1 (1967) p.49.

[110] N. Rajmohan, J. A. Szpunar, Y. Hayakawa, Textures and Microstractures 32 (1999)

p.153.

[111] Y. Hayakawa, J. A Szpunar, Acta Materialia, 45 (1997) p.3721.

[112] Y. Hayakawa, L. A. Szpunar, Acta Materialia, 45 (1997) p.4713.

[113] P. A. Beck and P. R. Sperry, Journal of Applied Physics,21 (1950) p.150.

[114] J. E. Bailey, Philosophical Magazine, 5 (1960) p.485.

[115] J. E. Bailey, Electron microscope observations on recovery and recrystallization processes in cold worked metals in *Electron Microscopy and Strength of Crystals*, Interscience, New York, 1963, p.535.

[116] J. E. Bailey and P. B. Hirsch, Proceedings of the Royal Society of London, 267 (1962) p.11.

[117] P. Cotterill and P. R. Mould, *Recrystallization and grain growth in metals*, Surrey University, London, 1976, p.85.

[118] P. A. Beck and H. Hu, *Recrystallization, grain growth, and textures*, American Society for Metals, Materials Park, OH, 1966.

[119] K. Lucke, The Canadian Journal of Metallurgy and Materials Science, 13 (1974) p.261.

[120] W-M. Mao and P. Yang, Transactions of Nonferrous Metals of Society of China, 24 (2014) p.1635.

[121] P. Mukhopadhyay and A. K. Verma, Defence Science Journal, 60 (2010) p.330.

[122] K. Lücke, Le Journal de Physique Colloques, 36 C4 (1975) p.C4-339.

[123] K. Lücke, Le Journal de Physique Colloques, 36 C4 (1975) p.C4-339.

[124] A. W. Bowen, Materials Science and Engineering, 29 (1977) p.19.

[125] N. Bozzolo, N. Dewobroto, T. Grosdidier and F. Wagner, Materials Science and Engineering A, 397 (2005) p.346.

[126] N. Bozzolo, N. Dewobroto, H. R. Wenk and F. Wagner, Journal of Materials Science, 42 (2007) p.2405.

[127] R. J. Contieri, M. Zanotello and R. Caram, Materials Science and Engineering A, 527 (2010) p.3994.

[128] A. Hayama and H. Sandim, Materials Science and Engineering A, 418 (2006) p.182.

[129] M. Hayashi, H. Yoshimura, M. Ishii and H. Harada, Nippon Steel Techinical

Report, 62 (1994) p.64.

[130] H. Jiang, J. Liu, Z. Mi, A. Zhao and Y. Bi, International Journal of Minerals, Metallurgy and Materials, 19 (2012) p.530.

[131] S. Nourbakhsh and T. O'Brien, Materials Science and Engineering, 100 (1988) p.109.

[132] B. Sander and D. Raabe, Materials Science and Engineering A, 479 (2008) p.236.

[133] A. K. Singh and R. A. Schwarzer, Transactions of the Indian Institute of Metals, 61 (2008) p.371.

[134] Z. P. Zeng, S. Jonsson and H. J. Roven, Acta Materialia, 57 (2009) p.5822.

[135] Z. Zeng, Y. Zhang and S. Jonsson, Materials Science and Engineering A, 513-514 (2009) p.83.

[136] Z. S. Zhu, J. L. Gu and N. P. Chen, Scripta Metallurgica, 30 (1994) p.605.

[137] Z. S. Zhu, J. L. Gu and N. P. Chen, Scripta Materialia, 34 (1996) p.1281.

[138] Z. Zhu, R. Liu, M. Yan, C. Cao and J. Gu, Journal of Materials, 2 (1997) p.5163.

[139] G. A. C. Branco, Ph.D Thesis, The Florida State University, US, 2005.

[140] F. Wagner, N. Bozzolo, O. Van Landuyt and T. Grosdidier, Acta Materialia, 50 (2002) p.1245.

[141] H. Inoue and N. Inakazu, *Recrystallisation 90,* The Minerals, Metals and Materials Society, Warrendale, PA, 1990.

[142] C. Vanitha, M. Kiran Kumar, G. K. Dey, D. Srivastava, R. Tewari and S. Banerjee, Materials Science and Engineering A, 519 (2009) p.51.

[143] F. Gerspach, N. Bozzolo and F. Wagner, Scripta Materialia, 60 (2009) p.203.

[144] N. Dewobroto, N. Bozzolo, P. Barbéris and F. Wagner, Materials Science Forum, 467-470 (2004) p.453.

[145] L. Yanzhang, H.-gil. Kim and J. Y. Park, Rare Metal Materials and Engineering, 42 (2013) p.667.

[146] K. Y. Zhu, B. Bacroix, T. Chauveau, D. Chaubet and O. Castelnau, Metallurgical and Materials Transactions A, 40 (2009) p.2423.

[147] Y. Perlovich, Development of strain hardening inhomogeneity during texture formation under rolling of bcc-metals in *Numerical Prediction of Deformation Processes and the Behavior of Real Materials*, Riso National Laboratory, Roskilde,

Denmark, 15th Riso International Symposium on Material Science, 5-9 September 1994, p.445.

[148] V. D. Hiwarkar, S. K. Sahoo, I. Samajdar, A. Satapathy, K. V. M. Krishna, G. K. Dey, D. Srivastav, R. Tewari and S. Banarjee, Journal of Nuclear Materials, 412 (2011) p.287.

[149] A. Styczynski, C. Hartig, J. Bohlen and D. Letzig, Scripta Materialia, 50 (2004) p.943.

[150] M. T. Pérez-Prado and O. Ruano, Scripta Materialia, 46 (2002) p.149.

[151] X. P. Chen, L. X. Wang, R. Xiao, X. Y. Zhong, G. J. Huang and Q. Liu, Journal of Alloys and Compounds, 604 (2014) p.112.

[152] L. L. Chang, E. F. Shang, Y. N. Wang, X. Zhao and M. Qi, Materials Characterization, 60 (2009) p.487.

[153] B. Beausir, S. Biswas, D. I. Kim, L. S. Tóth and S. Suwas, Acta Materialia, 57 (2009) p.5061.

[154] G.-j Huang, Q. Liu, L. Wang, R. Xin, X. Chen and F. Pan, Transactions of Nonferrous Metals Society of China, 18 (2008) p.s170.

[155] M. R. Barnett, M. D. Nave and C. J. Bettles, Materials Science and Engineering A, 386 (2004) p.205.

[156] Y. Qiao, X. Wang, Z. Liu and E. Wang, Materials Science & Engineering A, 568 (2013) p.202.

[157] R. E. Bauer, H. Mecking and K. Lücke, Materials Science and Engineering, 27 (1977) p.163.

[158] X. Yang, Z. Ji, H. Miura and T. Sakai, Transactions of Nonferrous Metals Society of China, 19 (2009) p.55.

[159] H. Sun, S. Liang and E. Wang, Transactions of Nonferrous Metals Society of China, 19 (2009) p.349.

[160] H. Y. Chao, H. F. Sun, W. Z. Chen and E. D. Wang, Materials Characterization, 62 (2011) p.312.

[161] X. Li and W. Qia, Materials Science and Engineering A, 560 (2013) p.321.

[162] M. J. Philippe, F. Wagner, F. Mellab, C. Esling and J. Wegria, Acta Metallurgica, 42 (1994) p.239.

[163] D. Solas, C. Tomé, O. Engler and H. Wenk, Acta Materialia, 49 (2001) p.3791.

[164] A. Sheikh-Ali, D. Molodov and H. Garmestani, Scripta Materialia, 46 (2002) p.857.

[165] M. Diot, J. J. Fundenberger, M. J. Philippe, J. Wegria and C. Esling, Scripta Materialia, 39 (1998) p.1623.

[166] B. Srinivasarao, A. Zhilyaev, T. Langdon and M. Perez-Prado, Materials Science & Engineering A, 562 (2013) p.196.

[167] F. Zhanga, G. Vincent, Y. Sha, L. Zuo, J. J. Funderberg and C. Esling, Scripta Materialia, 50 (2004) p.1011.

[168] U. F. Kocks, C. N. Tomé and H. R. Wenk, *Texture and Anisotropy: Preferred Orientations in Polycrystals and Their Effect on Materials Properties*, Cambridge University Press, Cambridge, 2000.

[169] B. Verlinden, J. Driver, I. Samajdar and R. D. Doherty, *Thermo-Mechanical Processing of Metallic Materials*, Elsevier Ltd., Amsterdam, 2007.

[170] J. J. Fundenberger, M. J. Phillipe, F. Wagner and C. Esling, Acta Materialia, 45 (1997) p.4041.

[171] H. R. Wenk, T. Takeshita, R. Jeanloz and G. C. Johnson, Geophysical Research Letter, 15 (1988) p.76.

[172] B. Hutchinson, Materials Science and Technology, 31 (2015) p.1393.

[173] A. Oppedal, H. Kadiri, C. Tomé, S. Vogel and M. Horstemeyer, Philosophical Magazine, 93 (2013) p.4311.

[174] E. Tenckhoff, *Deformation mechanisms, texture and anisotropy in zirconium and zircaloy*, ASTM International, Philadelphia, 1988.

[175] K. L. Murty, Materials Forum, 15 (1991) p.217.

[176] C. WenFang, G. AiHong, Z. Lian and L. ChunMing, Science China Technological Sciences, 53 (201) p.1513.

[177] D. McDarmaid, A. Bowen and P. Partridge, Materials Science and Engineering, 64 (1984) p.105.

[178] Z. S. Zhu, R. Y. Liu, M. G. Yan and C. X. Cao, Journal of Materials Science, 32 (1997) p.5163.

[179] J. C. Earthman, K. L. Murty, B. V. Tanikella and J. C. Britt, Journal of the Minerals, Metals, and Materials Society, 46 (1994) p.48.

[180] R. M. Tchorzewski and W. B. Hutchinson, Metallurgical Transactions A, 9 (1978) p.1113.

[181] H. Nasiri-Abarbekoh, A. Ekrami and A. Ziaei-Moayyed, Materials and Design, 34 (2012) p.268.

[182] H. Nasiri-Abarbekoh, A. Ekrami and A. Ziaei-Moayyed, Materials and Design, 37 (2012) p.223.

[183] J. Kwon, M. Brandes, P. Phani, A. Pilchak, Y. Gao and M. Mills, Acta Materialia, 61 (2013) p.4743.

[184] F. K. Mante, G. Baran and B. Lucas, Biometerials, 20 (1999) p.1051.

[185] G. B. Viswanathan, E. Lee, D. Maher, S. Banerjee and H. Fraser, Acta Materialia, 53 (2005) p.5101.

[186] T. Britton, H. Liang, F. Dunne and A. Wilkinso, Proceedings of the Royal Society A, 466 (2010) p.695.

[187] E. Merson, R. Brydson and A. Brown, Journal of Physics: Conference Series, 126 (2008) p.12.

[188] M. Bache and W. Evans, Materials Science and Engineering A, 319–321 (2001) p.409.

[189] K. Liu, C. Sun, Z. Wang, S. Li, Q. Wang and W. Du, Journal of Alloys and Compounds, 665 (2016) p.76.

[190] M. R. Barnett, Journal of Light Metals, 1 (2001) p.167.

[191] J. Koike, Metallurgical and Materials Transactions A, 36 (2005) p.1689.

[192] F. Li , X. Zeng, Q. Chenb and G. Caoa, Materials and Design, 85 (2015) p.389.

[193] J. Yuan, K. Zhang, T. Li, X. Li, Y. Li, M. Ma, P. Luo, G. Luo and Y. Hao, Materials and Design, 40 (2012) p.257.

[194] D. Zhang, Z. Yang, H. Sun, Y. Li, J. Wang, Z. Zhang, Y. Ye and T. Sakai, Materials Science and Engineering A, 640 (2015) p.51.

[195] V. N. Serebryany, L. L. Rokhlin and A. N. Monina, Inorganic Materials: Applied Research, 5 (2014) p.116.

[196] C. S. Roberts, *Magnesium and its Alloys*,John Wiley, New York, 1960.

[197] G. Nayyeri, W. Poole and C. Sinclair, Investigation Of The Local Mechanical Properties in Pure Mg Using Nanoindentation in *Mg2012: 9th International*

Conference on Magnesium Alloys and their Applications, Vancouver, 2012, P.1325.

[198] H. Guang-sheng, S. Bo, X. Wei and Z. Lei, Transactions of Nonferrous Metals Society of China, 20 (2010) p.1815.

[199] S. Agnew, M. Yoo and C. Tome, Acta Materialia, 49 (2001) p.4277.

[200] D. Foley, M. Al-Maharbi, K. Hartwig, I. Karaman, L. Kecskesc and S. Mathaudhu, Scripta Materialia, 64 (2011) p.193.

[201] G. Vincent, F. Zhang, J. J. Fundenberger and C. Esling, Scripta Materialia, 53 (2005) p.775.

[202] Kh. Saber, C. Koch and P. Fedkiw, Materials Science and Engineering A, 341 (2003) p.174.

[203] Z. Mei and J. Morris Jr., Cracking of textured zinc coating during forming process in *The Physical Metallurgy of Zinc Coated Steel*, The Minerals, Metals & Materials Society, Warrendale, 1994.

[204] M. Borodachenkova, W. Wen, F. Barlat, A. Pereira and J. Grácio, Journal of Materials Processing Technology, 224 (2015) p.143.

[205] S. Shaffer, Ph.D Thesis, University of California, Berkeley, US, 1990.

Chapter 3

Experimental Details

3.1 Commercially Pure Titanium

3.1.1 Material and Sample Preparation

CP-titanium (grade-2) plates of 5 mm thickness were used as the starting material for the present investigation. The composition (in wt. %) of these plates is as follows: Fe = 0.034, C = 0.004, N = 0.004, H = 0.004, O = 0.134 and Ti = 99.82.These plates were subjected to rolling, ARB and cross-rolling respectively in a laboratory rolling mill. Both rolling and cross-rolling were carried out up to 90% reduction in thickness at a true strain of 5% in each pass. Some rolled sheets were annealed at 700^{o}C for subsequent ARB processing. The ARB process consists of cutting, stacking and rolling of sheets [1, 2]. The annealed sheet was first cut into two-halves, and then wire-brushed and cleaned with acetone and finally tied to the other by a metallic wire. The tied bunch of plates was then cold rolled to 50% reduction in thickness. In the present investigation, the ARB processing was repeated for six times[1].

Samples of 10 mm length × 5 mm width were prepared from different sheets. The samples were annealed at 600ºC for different soaking time (0.17 min (10 sec), 0.33 min (20 sec), 0.50 min (30 sec), 1 min, 1.5 min, 2 min, 5 min, 10 min and 30 min) followed by air cooling. The temperature of annealing was decided from an isochronal annealing, which was carried out at 500, 600 and 700^{o}C for 1hr, on different cold rolled (i.e. rolled, ARB processed and cross-rolled) cp-titanium plates. It was observed that the samples are fully recrystallized at 600^{o}C of annealing.

From the cold rolled and annealed sheets, tensile specimens were prepared w.r.to different sample orientations – along rolling direction, along 45^{o} to the rolling direction and along 90^{o} to the rolling direction. The sample along the rolling direction was subjected to tensile deformation beyond yield point, till ultimate tensile strength and till fracture respectively.

[1] The equivalent strain for ARB processing of six passes is equal to 4.8.

The samples were metallographic polished, and then electro-polished before subsequent textural and microstructural characterization. Standard procedure was followed for metallographic polishing, whereas electro-polishing was carried out in a Struers polisher, LectroPol-5, at 25V for 20 sec. The electrolyte used was methanol and perchloric acid (80:20) at a temperature of -20°C.

3.1.2 Characterization Techniques

X-ray diffraction (XRD) was carried out in a Panalytical MRD system whereas EBSD was carried out in a FEI Quanta-FEG scanning electron microscope using a TSL-OIM (Tex. SEM. Ltd. – Orientation Imaging Microscope) EBSD package. For XRD texture five poles, $(0002), (01\bar{1}1), (01\bar{1}2), (01\bar{1}3)$ and $(11\bar{2}4)$, were measured and subsequently ODF (Orientation Distribution Function) was calculated using a commercial software Labotex 3.0 [29]. Stored energy values of some orientations/XRD peaks, $(01\bar{1}1)$, $(01\bar{1}2), (01\bar{1}3)$ and $(11\bar{2}4)$, were estimated from peak broadening analysis using Stibitz formula [4,5,6]. According to the formula [6]:

$$\overline{E_j}\ \alpha,\beta\ = \frac{3}{2}\gamma_{hkl}\frac{(\Delta d/d)^2}{(1+\ 2\vartheta_{hkl}{}^2)} \tag{3.1}$$

where, $\bar{E}_j(\sim,\ )$ is the stored energy and Y_{hkl}&ν_{hkl} are the directionally dependent values of Young's modulus and Poisson's ratio respectively. $\frac{\Delta d}{d}$ can be obtained from the peak profiles as,

$$\frac{\Delta d}{d} = \frac{B}{2\tan\theta} \tag{3.2}$$

and $B^2 = B_r{}^2 - B_a{}^2$ (3.3)

where, B_r and B_a are the measured values of FWHM (full width half maximum) of the rolled and annealed samples (30 min. of annealing time) respectively.

An approximate area of 1 mm × 1 mm was scanned by the EBSD in each sample. Beam and video conditions were kept identical between the scans using a step size of

0.2μm. In EBSD analyses, grains were identified based on 15º misorientation criterions - i.e. continuous presence of more than 15º boundary. Twin boundaries were identified through appropriate axis angle relationship, 94.8º<$\bar{1}2\bar{1}0$> for tensile twins & 64.3º<$\bar{1}100$> for compressive twins, in hcp (hexagonal close packed) titanium. Once the axis-angle relationship was frozen, twin fractions (5º deviation) could be estimated from the EBSD software. Misorientations in a grain were represented by grain average misorientation (GAM), grain orientation spread (GOS) and misorientation angle. GAM is defined as the average misorientation between each neighbouring points in a grain while GOS is the misorientation between all measurement points in a grain and the grain average orientation. Misorientation angle is the grain boundary misorientation between two grains. Orientation estimated elastic stiffness of different grains was estimated using the procedure explained elsewhere [7]. To evaluate the active slip systems in different grains/orientations, Schmid factor value was estimated from the EBSD scans. Different slip systems for room temperature deformation of cp-titanium are considered: basal, (0001)<$11\bar{2}0$>, prismatic, ($10\bar{1}0$)<$11\bar{2}0$>, pyramidal, ($10\bar{1}1$)<$11\bar{2}0$>, first-order pyramidal, ($10\bar{1}1$)<$11\bar{2}3$>, and second-order pyramidal, ($11\bar{2}2$)<$11\bar{2}3$>, slips [8,9,10].For estimating the Taylor factor values, of different grains/orientations, full constraint Taylor model is used with appropriate slip systems and uni-axial tension as the strain tensor.

Tensile testing was carried out in an Instron-1195 in accordance with the ASTM E8M-03 standard. Tensile testing was performed respectively in the rolling direction, 45º to the rolling direction and 90º to the rolling direction of the cold rolled and annealed sheets. Three sets of tensile testing were carried out and the average value is being reported.

Nanoindentation tests are carried out using a nano-mechanical testing instrument, HysitronTriboindenter (TI 900). A Berkovich diamond indenter is used for indentation. Hardness of more than 300 grains is measured using a load of 9000 μN. The load is being decided based on the indentation depth [11].

3.2Pure Magnesium

3.2.1 Material and Sample Preparation

Pure magnesium, obtained from General Motors, USA, was subjected to cold rolling of 90% reduction in thickness in a laboratory rolling mill. Such an unusually high reduction percentage in cold rolling of magnesium was achieved through multistep cross rolling (MSCR) [12]. During MSCR, the direction of rolling was changed by 90°in each step of rolling till 90% reduction in thickness was achieved.Improvements in formability of magnesium alloys (as opposed to the unalloyed magnesium considered here) through cross-rolling have also been observed by some researchers [13-15]. The rolled samples were then subjected to annealing at 200 °C for 10 s, 30 s, 1 min, 2 min, 5 min, 10 min and 30 min of soaking times respectively. The magnesium plate was also subjected to hot rolling at 200 °C to 90 % reduction in thickness. The samples, i.e. cold rolled, annealed and hot rolled, were metallographic polished and electro-polished for subsequent textural and microstructural characterizations. Standard methods were adopted for metallographic polishing whereas electro-polishing was carried out using an electrolyte containing mixture of ethanol to ortho-phosphoric acid by 3:5 ratio (by volume) at 0 °C. Electro-polishing was carried out at 3 V for 30 sec and subsequently at 1.5 V for 2 minutes.

3.2.2 Characterization Techniques

XRD is carried out in a Bruker D8-Discover system using CuK_{α}radiation for both deformed and annealed samples. Six poles, (0002), $(10\bar{1}0)$, $(10\bar{1}1)$, $(10\bar{1}2)$, $(10\bar{1}3)$ and $(11\bar{2}0)$, are measured. Texture is measured on the ND plane containing RD-TD direction. Orientation distribution functions (ODFs) were calculated using the Labotex 3.0 software [3]. Sections through the 3-dimensional ODFs were plotted using a commercial graphics program, Slicer Dicer. Using the Labotex software, volume fractions of different fibres/orientations were estimated through integration method [3] with a 10° tolerance on the deviation from the ideal orientation(s).

Dislocation density of the basal, (0002), and off-basal, $(01\bar{1}3)$, orientations is estimated through the methodology described in [16]. Stored energy values, for the basal and off-basal orientations i.e. (0002) and $(01\bar{1}3)$ respectively, is estimated using Stibitz formula [6].

EBSD, on the ND plane of the magnesium samples, is carried out on a FEI-Quanta 200-HV SEM (scanning electron microscope). Data acquisition and analyses are performed using the TSL-OIM version 6.0 software. Beam and video conditions are kept identical between the scans and a step size of 0.2 μm is used. Misorientation in a grain is represented by grain orientation spread (GOS) and it is defined as the misorientation between all measurement points of a grain and the grain average orientation. Orientation estimated elastic stiffness of different grains is estimated using the procedure explained elsewhere [7]. Based on the known single-crystal elastic constants of hexagonal titanium, orientation information and appropriate strain tensor, average polycrystalline elastic stiffness values are estimated using the Voight and Reussaveragingscheme [17] using TSL-OIM software. The deformation (strain) gradient used for the present study is: $\begin{matrix} -0.5 & 0 & 0 \\ 0 & -0.5 & 0 \\ 0 & 0 & 1 \end{matrix}$. Schmid factor [8] of different grains/orientations is determined using the basal slip system and the stress state as: $\begin{matrix} -0.5 & 0 & 0 \\ 0 & -0.5 & 0 \\ 0 & 0 & 1 \end{matrix}$.

Nanoindentationis carried out using a nano-mechanical testing instrument, HysitronTriboindenter (TI 900). A Berkovich diamond indenter is used for indentation. Hardness of approximately 50 grains on the ND plane is measured using a load of 11000 μN.

Vickers hardness is measured on the ND plane in a LECO Micro-hardness tester LM 248AT using 0.1 kgf load and a dwell time of 15 sec. Average hardness of 10 indentations at different regions of the sample is estimated.

3.3 Pure Zinc

3.3.1 Material and Sample Preparation

As-cast pure Zn was used as the starting material for the present study. It was subjected to cryo-rolling (rolling with liquid Nitrogen) in a laboratory rolling mill through MSCR to impart 90% reduction in thickness at a true strain of 5% in each step of rolling. In cryo-rolling process the sample was dipped in liquid nitrogen (-196 ^{o}C) for 5 min before each roll pass. Cryo-rolling was performed to avoid the recrystallization of the samples.The cryo-rolled samples were then subjected to annealing at 50 ^{o}C for 5 min, 10

min, 20 min and 30 min of soaking times respectively. For subsequent characterizations, specimens are prepared by mechanical polishing up to 2500 grit SiC papers followed by diamond polishing and colloidal silica polishing. The final step of polishing is completed with etching the sample with a solution containing 90 ml H_2O, 9 ml HNO_3 and 1 ml C_2H_5OH for few seconds.

3.3.2 Characterization Techniques

XRD was carried out in a Panalytical MRD system using CuK_α radiation for both rolled and annealed samples. Five poles namely, (0002), $(10\bar{1}0)$, $(10\bar{1}1)$, $(10\bar{1}2)$ and $(11\bar{2}2)$, were measured. Orientation distribution functions (ODFs) were estimated using Labotex 3.0 software [3]. Texture was measured on the ND plane containing RD-TD direction.

EBSD was carried out on a FEI-Quanta 3D FEG scanning electron microscope. Data acquisition and analyses were performed using the TSL-OIM version 6.0 software. Beam and video conditions were kept identical between the scans and a step size of 0.2 μm was used. Twin boundaries were identified through appropriate axis-angle relationships, $85.59^o < 2\bar{1}\bar{1}0 >$ for $\{10\bar{1}2\} < 11\bar{2}0 >$ type compressive twins [18-20]. Once the axis-angle relationship was frozen, twinfractions (at 5° deviation) were estimated using the TSL software. It may be noted that only $\{10\bar{1}2\} < 11\bar{2}0 >$ type compressive twins were observed in the present study.

Vickers hardness of all the samples was measured in a LECO micro-hardness tester at a load of 5 gf for dwelling time of 15 sec. Vickers hardness at 12 different locations of each sample was measured and the mean hardness value is reported.

References

[1] Y. Saito, H. Utsunomiya, N. Tsuji and T. Sakai, Acta Materialia, 47 (1999) p.579.

[2] D. Terada, S. Inoue and N. Tsuji, Journal of Materials Science, 42 (2007) p.1673.

[3] K. Pawlik and P. Ozga, *LaboTex: The Texture Analysis Software,* Göttinger Arbeiten zur Geologie und Paläontologie, SB4, 1999.

[4] G. Stibitz, Physical Review, 49 (1937) p.862.

[5] G. Stibitz, Physical Review, 8 (1947) p.147.

[6] N. Rajmohan, Y. Hayakawa, J. A. Szpunar and J. H. Root, Acta Materialia, 45 (1997) p.2485.

[7] S. K. Sahoo, V. D. Hiwarkar, I. Samajdar, G. K. Dey, D. Srivastav, R. Tiwari and S. Banerjee, Scripta Materialia, 56 (2007) p.963.

[8] Z. Zeng, Y. Zhang and S. Jonsson, Materials Science and Engineering A, 513-514 (2009) p.83.

[9] S. Nemat-Nasser, W.G. Guo and J.Y. Cheng, Acta Materialia, 47 (1999) p.3705.

[10] F. Bridier, P. Villechaise and J. Mendez, Acta Materialia, 53 (2005) p.555.

[11] G. Viswanathan, E. Lee, D. Maher, S. Banerjee and H. Fraser, Acta Materialia, 53 (2005) p.5101.

[12] S. Suwas and N. P. Gurao, Development of Microstructures and Textures by Cross Rolling in *Comprehensive Materials Process*, Elsevier Ltd., Amsterdam, 2014, p.81.

[13] X. Li, T. Al-Samman and G Gottstein, Materials and Design, 32 (2011) p.4385.

[14] Y. Chino, K. Sassa, A. Kamiya and M. Mabuchi, Materials Science and Engineering A, 441 (2006) p.349.

[15] Y. Chino, K. Sassa, A. Kamiya and M. Mabuchi, Materials Letters, 61 (2007) p.1504.

[16] I. Groma and F. Szekely, Journal of Applied Crystallography, 33 (2000) p.1329.

[17] T. Mura, *Micromechanics of Defects in Solids,* Matrinus Nijhoff, Dordrecht, 1987, p.421.

[18] J. G. Antonopoulos, Th. Karakostas, Ph. Komninou and P. Delavignette, Acta Metallurgica, 36 (1988) p.2493.

[19] C. Chyung and C. Wei, Philosophical Magazine, 15 (1967) p.161.

[20] R. L. Bell and R. W. Cahn, Proceedings of the Royal Society A, 239 (1957) p.494.

Chapter 4

Recrystallization Texture in CommerciallyPure Titanium

This chapter is intentionally kept blank.

Chapter 5

Recrystallization Texture in Pure Magnesium

This chapter is intentionally kept blank.

Chapter 6

Recrystallization Texture in Pure Zinc

This chapter is intentionally kept blank.

Chapter 7

Orientation Dependent Mechanical Properties of Commercially Pure Titanium and Pure Magnesium

This chapter is intentionally kept blank.

Chapter 8

Summary

In the present thesis, the recrystallization textures in HCP metals such as cp-titanium, pure magnesium and pure zinc has been investigated. Subsequently, the hardness of different orientations has been measured and it was correlated with the bulk mechanical property of cp-titanium and pure magnesium respectively. However, due to experimental difficulties and keeping in mind that structural application of pure zinc is limited; the orientation dependent hardness of pure zinc has not been carried out in the present study. The study can be summarized in the following four sections such as: (1) Recrystallization texture in cp-titanium; (2) Recrystallization texture in pure magnesium; (3) Recrystallization texture in pure zinc; (4) Orientation dependent mechanical properties of cp-titanium and pure magnesium.

8.1 Recrystallization Texture in CP-Titanium

It was observed that cp-titanium had a strong $[11\bar{2}5]$ *fibre texture after annealing irrespective of the pre-annealing strains/strain-paths.* CP-titanium plates were subjected to unidirectional-rolling (rolling), accumulative roll bonding (ARB) and cross-rolling followed by annealing at 600 ^{o}C for a large range of soaking time starting from 10 s to 30 min. The samples were fully recrystallized after 5 min of annealing and the samples were seen to develop almost similar texture when annealing was carried out beyond 5 min of annealing time. However, before annealing the texture development was seen to be different in the respective samples subjected to different rolling processes. The initial $(11\bar{2}5)<1\bar{1}00>$ texture present in the deformed structure got strengthened during annealing of the samples and finally the samples had a strong $[11\bar{2}5]$ fibre texture after annealing.

8.2 Recrystallization Texture in Pure Magnesium

A dominant basal (fibre) texture was observed in pure magnesium after annealing. Pure magnesium was subjected to cold (cross-) rolling and hot rolling of 90% reduction in

thickness. Cold rolled samples were then subjected to annealing at 200 °C for a range of soaking times staring from 10 s to 30 min. The texture developments in cold rolled, annealed and hot rolled samples were observed to be identical. However, the volume fraction of basal orientations ($<0001>$ fibre and $<01\bar{1}7>$ fibre) decreased with increasing annealing time up to 5 min,beyond which it was increased with further increasing the annealing time until 30 min. While the volume fraction of orientations away from basal orientation ($<01\bar{1}3>$ fibre) increased initially at 10 sofannealingtime and remain constant on further increasing theannealingtime. The hot rolled sample exhibited astronger basal texturealong with a larger fraction of low angle grain boundaries and coarser grain size compared to cold rolled and annealed samples.

8.3 Recrystallization Texture in Pure Zinc

A dominant $<11\bar{2}0>$ fibre texture was observed in pure zinc after annealing. As-cast pure zinc was subjected to cryo-rolling of 90% reduction in thickness. The rolled samples were then annealed at 50 ^{o}C for different soaking times of 5 min, 10 min, 20 min and 30 min respectively. Texture was observed to be similar in both the rolled and annealed samples. However, the texture intensity was increased till 10 min of soaking time and it was then decreased on further increasing the soaking time. Only $\{10\bar{1}2\}$ type compressive twins were observed in the samples and these twinning was found to be significant in all the samples. The Vickers hardness of the samples was increased till 10 min of annealing time followed by decreased in hardness on further increasing the annealing time.

8.4 Orientation Dependent Mechanical Properties of CP-Titanium and Pure Magnesium

*It was observed that the hardness of the grains close to basal orientation was higher compared to non-basal orientations of cp-titanium. It was further observed that the estimated bulk mechanical properties of cp-titanium had a direct relationship with the volume fraction of basal grains/orientations.*Annealed cp-titanium sheets were subjected to tensile deformation along the rolling direction, along 45^{o} to the rolling direction and along 90^{o} to the rolling direction respectively. Crystallographic textures and mechanical

properties of these cp-titanium samples were measured to find out the correlation between the textures with mechanical properties of the samples. The hardness of different grains/orientations was estimated through nanoindentation. It was observed that the hardness of the grains close to basal orientation was higher compared to that of non-basal orientations and the sample with higher volume fraction of basal orientations had higher mechanical properties.

In pure magnesium also the basal orientations were found to be higher and an increase in deviation from basal orientation the hardness of an orientation was decreased. However, the difference in hardness between basal orientations and the orientations away from basal was not significant like cp-titanium. Annealed pure magnesium sample was subjected to nanoindentation and then electron backscattered diffraction to characterize the hardness of different grains/orientations in pure magnesium. It was observed that orientations < 14^{o} from basal orientation had higher hardness compared to orientations at 14-28^{o} from basal orientations. Subsequently, a direct relationship of bulk Vickers hardness with the volume fraction of basal orientations was observed.

Scope for Further Research

The following works are proposed to be investigated that has not been carried out in the present thesis:

1) Because of the lack of expertise in mathematical modelling, the present work has been purely based on the experimental results and the theoretical understanding. So the use of simulation packages or mathematical modelling may be tried out.

2) In pure magnesium, the orientation dependent mechanical property investigated in the present thesis was based on the hardness values only. However, this can be extended to the tensile properties.

3) Deformation texture developments in pure zinc will be an interesting subject of research as this has not been exploited in the literature. Also as zinc is widely used as a corrosion resistant material, investigation of the orientation dependent corrosion properties of pure zinc can also be useful from the application point of view.

Dissemination

Journal Articles

[1] S. Panda, S.K. Sahoo, A. Dash, M. Bagwan, G. Kumar, S. C. Mishra and S. Suwas, Orientation dependent mechanical properties of commercially pure (cp) titanium, **Materials Characterization,** 98 (2014)pp. 93–101.

[2] S.K. Sahoo, S. Panda, R.K. Sabat, G. Kumar, S.C. Mishra, U. K. Mohanty and S. Suwas, Effect of pre-annealing strains on annealing texture developments in commercially pure (CP) titanium, **Philosophical Magazine**, 95(2015)pp.1105-1124.

[3] S.K. Sahoo, R.K. Sabat, S. Panda, S.C. Mishra and S. Suwas, Mechanical Property of Pure Magnesium: From Orientation Perspective Pertaining to Deviation from Basal Orientation, **Journal of Materials Engineering and Performance**, 24 (2015) pp. 2346-2353.

[4] S. K. Sahoo, R. K. Sabat, S. Panda, S. C. Mishra and S.Suwas, Texture and Microstructure Evolution of Pure Zinc duringRolling at Liquid Nitrogen Temperature and Subsequent Annealing,**Materials Characterization**,*(In press).*

[5] S. K. Sahoo, R. K. Sabat, S. Panda, S. C. Mishra, S. Suwas and A. D. Rollett, Texture and Microstructure Evolution in Pure Magnesium Subjected to Cold Rolling, Annealing, and Hot Rolling, (Under Preparation).

Conference Presentations

[1] S. Panda, S. K. Sahoo and S. C. Mishra (2013),Annealing Texture in CommerciallyPure Titanium, **NCPCM 2013**, NIT, Rourkela.

[2] S. Panda, S. K. Sahoo and S. C. Mishra (2013),Annealing Texture in CommerciallyPure Titanium, **IUMRS-ICA 2013**, IISc. Bangalore.

[3] S. Panda, S. K. Sahoo and S. C. Mishra (2014),Nanoindentation Study of Pure Magnesium, **ISRS 2014**, IIT, Chennai.